A tsunami forecast model for San Juan, Puerto Rico

Yong Wei

Abstract

As part of NOAA's tsunami forecast, this study addresses the development, validation, and stability tests of the tsunami forecast model for San Juan, Puerto Rico. Based on the Method of Splitting Tsunami (MOST), the tsunami forecast model is constructed at a spatial resolution of 2 arc sec (~ 60 m) in the finest grid to accomplish 4-hour simulation of wave inundation onto dry land within 11 minutes of computing time. A reference inundation model is developed in parallel using grids of higher resolution of 1/3 arc sec (~ 10 m) to provide high-resolution reference for the forecast model. The present study also conducted sensitivity tests to optimize grid coverage and grid resolution by comparing results between the forecast model and the reference model. The San Juan forecast model was validated using the August 8, 1946 Dominican Republic (M7.4) tsunami, and the modeling results agree well with the recorded data. Model results were also evaluated using the August 4, 1946 (M7.8) event and the November 1, 1755 Lisbon event based on historical accounts. The model results show good agreement between the forecast model and reference model except for the first two waves, meaning the forecast model is qualified to provide quantitative estimation of the inundation, runup and computed maximum values for potential threats of future tsunamis. The stability of the forecast model is further evaluated based on eight synthetic scenarios generated in Puerto Rico Trench, Hispaniola Trench, Cayman Trough, Los Muertos Trough and South Sandwich Island at different levels of M_w 9.3, M_w 7.5 and M_w 6.4.

1. Background and Objectives

The National Oceanic and Atmospheric Administration (NOAA) Center for Tsunami Research (NCTR) at the NOAA Pacific Marine Environmental Laboratory (PMEL) has developed a tsunami forecasting capability for operational use by NOAA's two Tsunami Warning Centers located in Hawaii and Alaska (Titov *et al.*, 2005). The system is designed to provide basin-wide warning of approaching tsunami waves accurately and quickly. The system, termed Short-term Inundation Forecast of Tsunamis (SIFT), combines real-time tsunami event data with numerical models to produce estimates of tsunami wave arrival times and amplitudes for coastal communities at risk. The SIFT system integrates several key components: deep-ocean observations of tsunamis in real time, a basin-wide pre-computed propagation database of water level and flow velocities based on potential seismic unit sources, an inversion algorithm to refine the tsunami source based on deep-ocean observations during an event, and high-resolution tsunami forecast models.

The objective of this present work is to develop an operational forecast model to be used in near real time to protect the community of San Juan, Puerto Rico, from the potential impact posed by a tsunami. San Juan is the capital and most populous municipality in Puerto Rico, an unincorporated territory of the United States. Being the most important

city of Puerto Rico, San Juan is the center of finance, manufacture, culture and tourism of Puerto Rico. San Juan Port is one of the busiest in the Caribbean; the city has nearly 400,000 population, and nearly two million inhabitants in the Metropolitan Statistical Area, which includes San Juan and other municipalities. The area of the Caribbean Sea is geologically active. Caribbean Islands are known to be prone to tsunami hazards caused by distant, local and regional earthquakes, landslides and volcanic eruptions. The increasing population, development and tourism in the coastal area makes the Caribbean Islands more vulnerable today than they were when the last major tsunami occurred in this area on August 8, 1946 due to a M7.4 earthquake off the Dominican Republic (Lander et al., 2002). What's more, San Juan is not one of the ten Tsunami Ready communities in Puerto Rico/U.S. Virgin Islands announced in 2010. All these facts make the development of a tsunami forecast model for San Juan, Puerto Rico an urgent need within the U.S. tsunami warning system to more effectively and efficiently warn and protect San Juan from catastrophic tsunami attack in the future.

2. Forecast Methodology

A high-resolution inundation model was used as the basis for development of a tsunami forecast model to operationally provide an estimate of wave arrival time, wave height, and inundation at San Juan, Puerto Rico following tsunami generation. All tsunami forecast models are run in real time while a tsunami is propagating across the open ocean. The San Juan model was designed and tested to perform under stringent time constraints given that time is generally the single limiting factor in saving lives and property. The goal of this work is to maximize the length of time that the community of San Juan has to react to a tsunami threat by providing accurate information quickly to emergency managers and other officials responsible for the community and infrastructure.

The general tsunami forecast model, based on the Method of Splitting Tsunami (MOST), is used in the tsunami inundation and forecasting system to provide real-time tsunami forecasts at selected coastal communities. The model runs in minutes while employing high-resolution grids constructed by the National Geophysical Data Center. MOST is a suite of numerical simulation codes capable of simulating three processes of tsunami evolution: earthquake, transoceanic propagation, and inundation of dry land. The MOST model has been extensively tested against a number of laboratory experiments and benchmarks (Synolakis *et al.*, 2008) and was successfully used for simulations of many historical tsunami events. The main objective of a forecast model is to provide an accurate, yet rapid, estimate of wave arrival time, wave height, and inundation in the minutes following a tsunami event. Titov and González (1997) describe the technical aspects of forecast model development, stability, testing, and robustness, and Tang *et al.* (2009) provide detailed forecast methodology.

A basin-wide database of pre-computed water elevations and flow velocities for unit sources covering worldwide subduction zones has been generated to expedite forecasts (Gica *et al.*, 2008). As the tsunami wave propagates across the ocean and successively reaches tsunameter observation sites, recorded sea level is ingested into the tsunami forecast application in near real-time and incorporated into an inversion algorithm to produce an improved estimate of the tsunami source. A linear combination of the pre-computed database is then performed based on this tsunami source, now reflecting the

transfer of energy to the fluid body, to produce synthetic boundary conditions of water elevation and flow velocities to initiate the forecast model computation.

Accurate forecasting of the tsunami impact on a coastal community largely relies on the accuracies of bathymetry and topography and the numerical computation. The high spatial and temporal grid resolution necessary for modeling accuracy poses a challenge in the run-time requirement for real-time forecasts. Each forecast model consists of three telescoped grids with increasing spatial resolution in the finest grid, and temporal resolution for simulation of wave inundation onto dry land. The forecast model utilizes the most recent bathymetry and topography available to reproduce the correct wave dynamics during the inundation computation. Forecast models, including the San Juan model, are constructed for at-risk populous coastal communities in the Pacific and Atlantic Oceans. Previous and present development of forecast models in the Pacific (Titov *et al*., 2005; Titov, 2009; Tang *et al*., 2008; Wei *et al*., 2008; Tang *et al*., 2012; Wei *et al.*, 2012) have validated the accuracy and efficiency of each forecast model currently implemented in the real-time tsunami forecast system. Models are tested when the opportunity arises and are used for scientific research. Tang *et al*. (2009) provide forecast methodology details.

3. Model development

The general methodology for modeling at-risk coastal communities is to develop a set of three nested grids, referred to as A, B, and C-grids, each of which becomes successively finer in resolution as they telescope in to the population and economic center of the community of interest. The offshore area is covered by the largest and lowest resolution A-grid while the near-shore details are resolved within the finest scale C-grid to the point that tide gauge observations recorded during historical tsunamis are resolved within expected accuracy limits. The procedure is to begin development with large spatial extent merged bathymetric topographic grids at high resolution, and then optimize these grids by sub sampling to coarsen the resolution and shrink the overall grid dimensions to achieve a 4-hr simulation of modeled tsunami waves within the desired time period of 10 min of wall-clock time. The basis for these grids is a high-resolution digital elevation model constructed by the National Geophysical Data Center and NCTR using all available bathymetric, topographic, and shoreline data to allow accurate representation of the wave dynamics during the inundation computation for an at-risk community. For each community, data are compiled from a variety of sources to produce a digital elevation model referenced to Mean High Water in the vertical and to the World Geodetic System 1984 in the horizontal (http://ngdc.noaa.gov/mgg/inundation/tsunami/inundation.html). From these digital elevation models, a set of three high-resolution, "reference" elevation grids are constructed for development of a high-resolution reference model from which an 'optimized' model is constructed to run in an operationally specified period of time. The operationally developed model is referred to as the optimized tsunami forecast model or forecast model for brevity.

3.1 Forecast area

Located on the north shore of Puerto Rico Island, San Juan is subject to tsunami attack originated in the Atlantic Ocean and Caribbean Sea. The main tsunami source

regions in the Atlantic Ocean are at the boundary between North America plate and Caribbean Plate, where lies the Hispaniola Trench, Puerto Rico Trench, and Lesser Antilles Subduction Zone from west to east (Figure 1a and 1c). Another potential sources zone is the Gulf of Cadiz as part of the Azores-Gibraltar plate boundary (Figure 1a and 1b), where the 1755 Lisbon earthquake generated the most severe tsunami across the Atlantic Ocean. A third source region is the South Sandwich subduction zone in the South Atlantic Ocean, which were not detailed in Figure 1 but shown in Figure 18 when addressing the synthetic scenarios for forecast model testing.

The Caribbean is one of the smaller surface plates of the earth. This plate remains at a fixed spot relative to the deep earth, while the North American plate is being shoved westward. The subduction is ongoing; its rate constrained by GPS is 19.7±0.4 mm/y at an azimuth of 255.6±0.9° (DeMets et al., 2007). The westward-moving North American plate is being driven under the Antilles Arc where volcanism is active. On the north side of the plate corner, the North American plate slides past the Caribbean, but irregularities of in the plate boundaries causes stresses that result in a complicated underthrusting of plate fragments. The interaction of plates causes the volcanism of the Antilles Arc on the eastern boundary of the Caribbean plate and creates major stresses all along the northern boundary (Nealon and Dillon, 2001).

The Puerto Rico/Virgin Islands region is located at the northeastern corner of the Caribbean plate where the seismic motions are complex (Figure 1c). This region's documented history includes no candidate for a great earthquake along the Puerto Rico Trench. This abyss, as much as 8 km deep, extends 800 km around the northeast corner of the Caribbean plate at its boundary with the subducting North America plate.

Around Puerto Rico, the narrow island shelf exist in the north, south and west provinces (Figure 1d). The north is the narrowest and is characterized by high wave energy and terrigenous sediments. Insular shelf and slope morphology varies greatly in Puerto Rico with differences in shelf width, shelf and slope inclination, shelf break depth, and the extent of natural barriers. The shelf has inclinations ranging from 0.1 to 3.0 degrees and widths ranging from 0.3 to 21 km. The insular shelf is extremely narrow in comparison to continental shelves. On the west coast, moderate shelf inclination varies from 0.1 to 0.5 degrees with shelf widths ranging from 0.4 to 6.6 km. On the north coast, the shelf inclination varies from 0.22 to 11 degree. The shelf width ranges from 0.3 to 3.2 km. The flattest shelves were found on the east and south coasts, where the platform is inclined from 0.1 to 0.7 degrees. On the east, shelf inclination varies from 0.1 to 0.3 degrees. On the south, shelf inclination is from 0.1 to 0.7 degrees. The south coast has a wider insular shelf ranging from 5 to 21 km. The shelf break is at depths of 10 to 40 meters around the Island.

3.2 Historical events and data

The greatest of the northeast Caribbean's documented tsunamis originated on the other side of the Atlantic Ocean, during the 1755 Lisbon earthquake. It had peak amplitudes estimated as 4.5 m in St. Martin, up to 7 m in Saba, 3.6 m in Antigua and Dominica, >2 m in Martinique, and 1.5-1.8 m in Barbados (Zahibo and Pelinovsky, 2001; Barkan et al., 2009).

Among historical tsunamis originating within the northeast Caribbean (Figure 2), perhaps the largest was generated by the ~M7.2 1867 Virgin Islands earthquake. Reid and Taber (1920) and Barkan and ten Brink (2010) reported that this tsunami did not affect the northern and eastern coasts of the islands facing the Atlantic Ocean because the tsunami source was a fault or faults in Anegada Passage, south of St. Thomas. However, Lander et al. (2002) described the tsunami waves caused by this earthquake were 1 to 6 m depending on the orientation of the particular coast of Puerto Rico. At San Juan and Arroyo, water rose to 0.9 and 1.5 m, and high waves were observed at the Vieques Island. At Fajardo, a very small wave was reported, and at Yabucoa the sea retreated and inundated 137 m on its return.

Since 1867, the maximum reported tsunami water level in San Juan, 66 cm, was resulted from the 1918 Mona Passage M7.3 earthquake (Table 1).

The 4 August 1946 M7.8 earthquake in Dominican Republic was one of the strongest earthquakes ever reported in the Caribbean. This earthquake and tsunami did not cause serious damage in Puerto Rico, although they resulted in severe damage and loss of life at Matancitas and nearby coastal towns of the Dominican Republic.

A strong aftershock of the 4 August 1946 earthquake occurred four days later, and the tsunami it generated caused 75 fatalities and left 20,000 homeless in Puerto Rico. The sea withdrew at Aguadilla and Mayaguez and Lander et al. (2002) reported some damage at San Juan on the west coast of Puerto Rico. However, it was not clear whether the damage was due to the earthquake or the tsunami waves that followed. A maximum water level of 60 cm was reorted at San Juan 35 min after the M7.4 earthquake. However, the marigram archived at NGDC (http://www.ngdc.noaa.gov/hazard/data/marigrams/1766/sjpr_19460808.jpg) indicates that the 60 cm water level included the tidal level. The actual tsunami wave amplitude was only about 4 cm maximum after removing the tidal level.

Large landslide escarpments have been mapped on the seafloor north of Puerto Rico (Grindlay, 1998; Schwab et al., 1991). Studies have shown that a repetition of these landslide failures, even lesser ones could be catastrophic for San Juan and Puerto Rico (Mercado et al., 2002). ten Brink et al. (2004 and 2006) uses multibeam bathymetry and re-processed seismic reflection profiles to describe and quantify slope failures and to identify sites of potential future failures. Their data indicate that slope failure is likely an incremental process even within the amphitheater of the slope. Their numerical simulation indicates a runup height only 1/3 of previous estimate. Although modeling landslide-generated tsunamis are beyond the scope of this study, the developed forecast and reference models are useful for assessment of these hazards in real time and in long-term applications.

3.3 San Juan tide gauge

The NOS San Juan tide gauge is located at the southern tip of U.S. Coast Guard compound to the west of Old San Juan harbor (Figure 3 and 4). It was established in 1962, and the present installation dates from 1989. The Mean High Water datum is 1.432 m above the station datum. The mean tidal range is only 0.34 m, and the diurnal tidal range is slightly larger, 0.48 m. The tidal records since 1962 indicates an increasing rate of sea level change at about 1.65 ± 0.52 mm/yr, which is equivalent to a change of 16 cm in 100 years.

3.4 Model setup

3.4.1 Versions of MOST

The MOST model has had different versions since its initial development by Titov and Synolakis (1995 & 1998) that solves the tsunami wave dynamics with a finite-difference numerical scheme based on characteristic form of nonlinear shallow water equations. For propagation, MOST uses the shallow water wave equations in spherical coordinates with numerical dispersion to account for different propagation wave speeds at different frequencies. As stated in Burwell et al. (2007), the physical process of frequency dispersion can be approximated by numerical dispersion.

For flooding forecast, high-resolution inundation models are optimized for most vulnerable communities. This version of MOST (MOST Version 2) uses nested computational grids to telescope down to the high-resolution area of interest for inundation computation. Nested grids are used to generate a sufficient number of nodes per wavelength to enable solution of the equations with minimum error. The numerical coupling between all nested grids in MOST Version 2 is unidirectional from the outer grid. That is, the inner grid has no effect on the outer grid, and the outer grid provides the inner grid with computed wave amplitudes and flow velocities at all four boundaries by linear interpolation from coarser resolution. The downstream boundary conditions from outer grid require no overlapped marginal areas between grids. In this study, the forecast model for San Juan is developed using MOST Version 2.

The latest version of MOST (MOST Version 4) performs computations in a single grid (referred to as Master grid) with different types of input specified below, and computes boundary time-series input into enclosed grids, if any, for further refinement of the solution. It is characterized by an ability to nest grids given by polar/azimuth angle pairs in spherical coordinate systems arbitrary rotated with respect to the Geophysical system based on latitude and longitude) and each other, which allows for the use of grids adapted to local bathymetric features at each grid scale. Another important feature of MOST Version 4 is that the model computation has been parallelized, which allows the model tasks to be distributed to multiple computational CPUs for speedy computation. In this study, the reference model for San Juan is developed using MOST Version 4. The different versions of the model

require different forms of input specification, as seen in Appendix A where the files employed for the forecast and reference models are listed.

3.4.2 Grid boundary and resolution

Burwell et al. (2007) studied the diffusion and dispersion characterization of MOST model, and concluded that the nature of the scheme at all resolvable wave numbers is that the scheme is diffusive and dispersive for $\beta = (gd)^{1/2}\Delta t/\Delta x \neq 1$, where Δt is the temporal step, d is the water depth, and Δx is the space step. Diffusive effects are stronger for poorly resolved waves (large space step compared to wave length), while diffusive effects go down but dispersive effects continue to increase as β reduces. Thus, numerical dispersion can be an issue closer to shore, but can be controlled to some level by the choice of β, in other words, the ratio between Δt and Δx. The tsunami propagation database (Gica et al., 2008) was developed at a grid spacing of 4-arc-minute (about 7.2 km at the equator) and saved at 16-arc-minute (about 28.8 km at the equator) resolution. This resolution may introduce excessive model diffusion effects if applied directly to the continental shelf where water depth is generally less than 100 m. The telescoped grids adopted in MOST model are thus critical for wave transformation over the continental shelf, and eventually critical for the inundation modeling at the coastline. Ideally, manipulation of β value will reduce the effects of diffusion and mimic the real-world dispersion through numerical dispersion.

3.4.3 Digital Elevation Model (DEM) of San Juan, Puerto Rico

The bathymetry and topography used in the development of this forecast model was based on a digital elevation model provided by the National Geophysical Data Center and the author considers it to be an adequate representation of the local topography and bathymetry. As new digital elevation models become available, forecast models will be updated and report updates will be posted at http://nctr.pmel.noaa.gov/forecast_reports/.

Taylor et al. (2008) described the development of a 1-arc-sec DEM for Puerto Rico and 1/3-arc-sec DEMs for six communities along Puerto Rico's coastline, including San Juan. This work by NGDC was an update and extension of their previous development of DEMs specifically for San Juan and Mayaguez, Puerto Rico (Taylor et al., 2006). The updated DEM uses bathymetric datasets from seven different surveys (Figure 5), including lidar surveys done for coastal areas near San Juan by NOS and U.S. Army Corps of Engineers through the Scanning Hydrographic Operational Airborne Lidar Survey (SHOALS). The topographic datasets used to derive the DEM were primarily obtained from the Puerto Rico Office of Management and Budget (PROMB) at a spatial resolution of 10 m and Budget and the U.S. Geological Survey at a spatial resolution of 1/3 arc sec. San Juan topography was primarily provided by the PROMB data, which covers entire Puerto Rico, Culebra islands and the western half of Vieques. All the bathymetric and topographic data are transformed to a vertical datum of MHW, and to a horizontal datum of WGS 84.

According to Taylor et al. (2008), the Puerto Rico DEMs have an estimated horizontal accuracy of 10 m for topographic features, a few hundred meters for deep-water bathymetry, while the shallow, near-coastal regions have an accuracy

approaching that of subaerial topographic features. The vertical accuracy of topography is estimated to be 0.5 m for the PROMB DEMs. Bathymetric areas have an estimated accuracy of between 0.1 m and ~2% of water depth.

However, a careful inspection to the 1/3-arc-sec San Juan DEM indicates the bathymetry in some of the lagoons and channels was set to a constant value, probably due to lack of data there. Also, some of the bridges were not removed from the DEM for modeling purpose in this study. These are improved in this study (details are discussed in section 3.4.3), although some caveats may still exist in the developed grids. They are subject to further improvement wherever new data becomes available.

3.4.4 Development of model grids

Development of an optimized tsunami forecast model for San Juan began with the merged bathymetric/topographic grids shown in **Figure 6 to 11**. Grid dimension extension and additional information were updated as needed and appropriate. **Table 2** provides specific details of both reference and tsunami forecast model grids, including extents and complete input parameter information for the model runs is provided in **Appendix A**.

Figures 6 and 7 show the coverage of the A grid with a spatial resolution of 20 arc sec (~ 600 m) for the reference model, and 47.24 arc sec (~ 1,460 m) for the forecast model. Both grids are obtained from a 9-arc-sec intermediate dataset developed by NGDC in 2005 for Caribbean and Gulf of Mexico. The drawback of the 9-arc-sec dataset is that it contains no topography, which does not affect the model computation in A grid as no tsunami inundation computation is engaged at this level. The reference model A grid covers the region between 69.9°W and 60.504014°W in longitudinal direction, and between 16.05°N and 18.95°N in latitudinal direction. This grid represents the northeast Caribbean region from southeast of Dominican Republic to Guadeloupe in the Lesser Antilles. The forecast model A grid covers slightly smaller area, between 69.0°W and 61.008115°W in longitudinal direction, and between 16.5°N and 18.95°N in latitudinal direction, to gain more efficiency in computing time. Puerto Rico and the Virgin Islands are included in both A grids, although the northern boundary does not completely extend to the Puerto Rico trench. It is important that the shallow reef and shelf around Puerto Rico and those in the Virgin Islands and Lesser Antilles are included in the A grid. This setup ensures the tsunami waves dynamics in the deep ocean are properly extended from the propagation database to the inundation models before they reach the shallow coastal regions. Figures 6-9 clearly show the shallow shelf areas are along the east, south and southwest of Puerto Rico. The north shore of Puerto Rico, including San Juan, is particularly vulnerable to tsunami waves striking from the north, where the Puerto Rico Trench and the Hispaniola Trench are the potential source regions that may generate catastrophic tsunamis.

Figures 8 and 9 show the coverage of B grid with a spatial resolution of 6 arc sec (~ 180 m) for the reference model, and 12 arc sec (~ 360 m) for the forecast model.

Both grids were obtained from the San Juan 1/3-arc-sec DEM developed by NGDC. The reference model B grid covers the region between 67.4°W and 65.2°W in longitude, and between 17.8°N and 18.6°N in latitude. The forecast model B grid covers a slightly smaller area: 67.35°W to 65.55°W in longitude and 17.8°N to 18.6°N in latitude, to gain efficiency in computing time. Both grids cover the entire island of Puerto Rico. In the north and south, the boundary of these B grids reaches depths of 1,000 m to provide more accurate modeling results of the waves over the shelf using finer grid resolution, especially in the north shore of Puerto Rico. The B grids are not fully extended to deep water in the east and west in order to reduce the computing time.

Figures 10 and 11 show the coverage of C grid with a spatial resolution of 1/3 arc sec (~ 9 m) for the reference model, and 2 arc sec (~ 60 m) for the forecast model. Both grids were obtained from the San Juan 1/3 sec DEM developed by NGDC. The reference model C grid covers the region between 66.1888889°W and 65.975°W in longitude, and between 18.375°N and 18.5°N in latitude. The forecast model C grid covers slightly smaller area, between 66.2°W and 65.975°W in longitude, and between 18.4°N and 18.5°N in latitude. Both grids cover the most populated coastline of San Juan from Ensenada de Boca Vieja in the west to Laguna La Torrecilla in the east, about 25 km in east-west direction. Just west of Laguna La Torrecilla, the main runway of the San Juan International Airport lies very close to the coastline with an elevation between 2 to 2.5 m above MHW. The water depth at the north boundary of C grid is about 100 m. The SHOALs data provides many details of the nearshore bathymetric features. The water depth in most of the bays near San Juan, including the main harbor, is less than 10 m and do not change much. The ship channels in San Juan Harbor (Bahia de San Juan) are dredged to 11 to 12 m deep. What make San Juan difficult for tsunami inundation modeling are the canals, lagoons and marshes that connect to the ocean through small entrances. Due to lack of survey data, a routine that NGDC employs is to assign a constant depth value in these inland water bodies, such as 0.4 m in the San Juan 1/3-arc-sec DEM. Ellis (1976) reported the history of dredging and filling of lagoons in the San Juan area, and pointed out that the average water depth in Laguna Torrecilla and Laguna San Jose is about 2.4 m. Therefore, a water depth of 2.4 m was used to replace the original 0.4 m in these lagoons. It is worth noting that the water depth in the lagoons is kept constant in the developed models as no detailed survey data was available at the time when the models were developed. When available, improved bathymetry will be incorporated in future model grids.

4. Results and Discussions

4.1 Model validation

Lack of tsunami measurements in the Atlantic has been a major issue of model validation for the tsunami forecast models developed for U.S. East Coast and Caribbean. The present San Juan tide gage was established in 1962, and since then it has not registered

any significant tsunami event, except for a 2-cm wave for the 2004 Indian Ocean tsunami (Table 1). Following the August 4, 1946 Dominican Republic M7.8 earthquake, a small tsunami was reported along the western and northern coasts of Puerto Rico, and the San Juan tide gage recorded a 66-cm wave (O'Loughlin and Lander, 2003). However, the location of the tide gage that observed the 66-cm tsunami is unknown to the author of this report, and it is also unclear that whether the recorded water level had included the tidal level. On August 8, 1946, another strong earthquake (M7.4), located 100 km northwest of the one four days earlier, brought tsunami once again to San Juan. A marigram documented by NGDC recorded the water level at a tide gage of Arsenal, San Juan during this tsunami (Figure 12). This marigram is probably the only time series record of tsunami water level near San Juan, and thus a valuable dataset to validate the San Juan forecast model. In this study, we use both events, the August 4, 1946 Dominican Republic and the 1755 Lisbon, for model validation, even though the tsunami sources of these two events were not well defined.

A simple source model was used for tsunami generation due to the August 8, 1946 Dominican Republic M7.4 earthquake: 0.71 m slip on a 100 km × 50 km fault (ATSZ b54). As the coordinates (66.11583°W, 18.46306°N) provided on Figure 12 are not accurate enough to pinpoint the exact location of the Arsenal tide gage, a point (66.115142°W, 18.462738°N) in water close to (66.11583°W, 18.46306°N) was chosen for model/data comparison. Figure 13e and 13f show that the model results agree well with the recorded data, although the model underestimates the first wave. The reference model results show excellent agreement with the forecast model for the first couple of waves, but the model starts to produces numerical noise at a level of cm. One can see that the model cannot reproduce the high-frequency components on the observation. It is unclear what the causes of these high-frequency waves are, and a most possible explanation could be the instrumental response to local wave conditions.

As the source location and magnitude (between M7.8 – 8.1) of the 1946 Dominican Republic earthquake are still in debate, two simple model sources were used as model inputs: one is a M7.8 source with 2.81-m slip on a 100 km by 50 km unit source, and the other one is a M8.1 source with 8-m slip on a 100 km by 50 km unit source. The model results shown in Figure 12 indicate that the M7.8 source could only generate about 8 cm wave amplitude at the current tide gage location, and the maximum wave amplitude is about 30 cm along the coastline of Bahia de San Juan and the Old San Juan. These wave amplitudes suggest that a M7.8 source for the Dominican Republic earthquake may be an underestimate of this event. The computational results from the M8.1 source give a maximum wave amplitude of 0.2 m at the present tide gage location, but indicate a general 0.6 to 0.8 m along the coastline of Bahia de San Juan and the Old San Juan (Figure 13), which fits better with the historical description. We note here that we consider the uncertainty of source mechanism, including its magnitude and source area, as the main difficulty for a quantitative model validation of the August 4, 1946 earthquake and tsunami. Once again, the historical description of the tsunami wave amplitude of 66 cm at San Juan tide gage may have included both the tidal level and the tsunami waves.

The earthquake source of the 1755 Lisbon tsunami has not been fully understood. Previous studies have proposed a few source mechanisms that may have potentially produced this basin-wide tsunami. The magnitude of the proposed earthquake ranges from 8.0 to 9.0 (Barkan et al., 2009; Muir-Wood and Mignan, 2009; Titov et al., 2009; Roger et al., 2010), while the rupture area varies between 6,000 km^2 and 480,000 km^2. Titov et al. (2009) have compared five tsunami scenarios due to different earthquake sources and they all indicated that the tsunami impact on U.S. East Coast was minor, as a tsunami was not reported or documented anywhere in United States. The preferred scenario of Barkan et al. (2009) reported very similar results after comparing the tsunami records at many places in the Atlantic, particularly in the Caribbean (**Figure 1b**). This report uses the 1755 Lisbon tsunami as a "validation" case study, for which we adopted earthquake rupture parameters from Barkan et al. (2009), and an earthquake magnitude 9.0 from Muir-Wood and Mignan (2009) (Figure 1b). This scenario represents a "worst case" scenario of the 1755 Lisbon tsunami, which can explain the tsunami runup heights and overwash observed in the British Virgin Islands and Lesser Antilles (Wei et al., 2011). **Figure 16** shows the maximum wave amplitude in the Atlantic Ocean resulted from the M9.0 1755 Lisbon scenario. **Figure 17e and 17f** shows the computed time series at the tide gage location of San Juan. One can see that the maximum wave amplitude is smaller than 0.5 m, and the maximum wave height is about 0.9 m. The forecast model indicates some minor flooding along the bank at the entrance of the San Antonio canal (**Figure 17**), while the reference model shows no flooding at the same location. When looking at the time series comparison between the two models (**Figure 17e and 17f**), one can observe that, when comparing to the reference model, the forecast model gives larger wave amplitudes for the first two waves, but shows excellent match for the following 10 waves. The discrepancy of the wave amplitude on the first wave can be largely attributed to use of different versions of MOST in the forecast model (MOST version 2) and reference model (MOST version 4). The difference in the modeling results by these two versions is currently being investigated and probably will be reported in a different study. The computational results show high-speed current up to 1 to 3 m/s (about 4 to 6 knots) along the coastline, and the most rapid currents, 3 to 4 m/s, occur offshore where the bathymetry changes abruptly (Figure 17). The flow speed at the entrance and in the ship channel of Bahia de San Juan is also up to 3 m/s, which may pose danger to ships maneuvering in the harbor during a tsunami event. In San Antonio Canal, a narrow navigable section in Bahia de San Juan lying south of Old San Juan and San Juan Island, the water level is 0.6 to 0.8 m above MHW, and the flow speed is between 0.4 to 0.7 m/s. As no major tsunami flooding or impact were reported in San Juan during the 1755 Lisbon tsunami, the model results representing an upper limit of the Lisbon tsunami that fits the historical records.

For a near field source, such as 1946 Dominican Republic events, the forecast model and reference model both show excellent agreement. Except for the amplitude of the first two waves for the 1755 Lisbon event, the computational results from the forecast model and the reference model show close agreement in wave period, arrival time, and current speed in both validation cases. It indicates that the forecast model developed at 2 arc sec is able to achieve the similar computational accuracy as the reference model, but can save computational resources by nearly 500 times. This makes the forecast model a very

powerful tool to provide rapid and accurate tsunami forecast in real time.

4.2 Model stability testing using synthetic scenarios

Model stability testing using synthetic scenarios provides important case studies to test the robustness and durability of the developed models from different perspectives:

1. Synthetic scenarios examine the developed models with mega tsunamis to guarantee model stability. These model tests ensure the stability of the forecast model during a catastrophic event.
2. Synthetic scenarios also examine the developed models with medium tsunamis to guarantee model stability under smaller wave conditions. These model tests ensure the efficiency of the forecast model during a moderate event.
3. Synthetic scenarios examine the developed models with negligible tsunami waves to guarantee the modeling results are not influenced by the numerical noise.
4. The synthetic scenarios were selected in such way that at least one from each potential tsunami source zone is tested. These cases are used to examine the reliability of the developed models for all directions of the incoming tsunami waves.

Table 3 summarized all the synthetic scenarios (plotted in Figure 18) used in the present model testing. Except for the 1755 Lisbon (used as a model validation in section 4.1), other scenarios were artificially constructed from the combination of the unit sources, shown as black boxes. Table 3 gives the details of unit source and the coefficients for a total of eight scenarios, six with magnitude 9.3, one with magnitude 7.5 and one micro-wave test. Two of the magnitude-9.3 cases were selected in the Puerto Rico Trench and Hispaniola Trench since they are considered as the most dangerous tsunamigenic earthquake zones in the Atlantic (ten Brink et al., 2004). The earthquake zones between the Caribbean plate and South America have been relatively inactive, and the tsunami waves generated there have minor impacts on the U.S. East Coast based on the tsunami hazard assessment study by Titov et al. (2009, Chapter 2). Therefore, no synthetic scenarios were selected from this area. The magnitude-9.3 scenario from South Sandwich source zone was used for modeling stability test in response to different tsunami directionalities.

The synthetic scenario ATSZ 48-57, generated by a 2004-Indian-Ocean-type magnitude 9.3 earthquake from Puerto Rico Trench, causes the most catastrophic impact to San Juan and its vicinity. The modeling results in **Figure 19** show that such an event, if arriving at high tide, would penetrate inland by 4 to 5 km at least and destroy much of the waterfront at Toa Baja, Old San Juan, San Juan, and Carolina (including the entire San Juan International Airport) with waves up to 21 m above MHW along the shoreline. The water level on land is generally greater than 10 m, and becomes especially high (up to 17 m above MHW) between Old San Juan and San Juan International Airport, which is highly populated by tourists. The water elevation at the airport may also reach 18 m above MHW, and cause significant damage to the main infrastructure. The only place that may be able to avoid flooding is the high ground of Old San Juan. What can also lead to devastation is the accompanied tsunami flow, which is generally between 8 to 12 m/s along the shoreline when flooding on land. These high-speed flows will gradually slow down to 4 to 5 m/s until they reach 2 km inland, and then to 1 m/s or less until they reach

the inundation limit at a distance about 4 to 5 km from the shoreline. It is also worth noting the flow speed offshore may reach 33 m/s when the bathymetry changes abruptly. These offshore currents probably will prevent any ships or boats from evacuating the harbor to deep water. The time series in **Figure 19e and 19f** indicates a dominant first wave up to 3 m above mean high water at the tide gage followed by a few waves with a maximum amplitude of 2.5 m. The time series computed by the reference model and forecast model are nearly identical, which reflects the accuracy of forecast model under extreme wave conditions. The time series at the tide gauge also indicates that the waves arriving two hours after the earthquake have longer wave period than the leading waves. The 24-hour run of forecast model shows no instability, meaning the model will stay stable under large waves. The inundated area computed by the forecast model (color coded area in Figure 20) is larger than that predicted by the reference model (magenta line in Figure 20), mostly in the flat area in the south of the International Airport. This is attributed to different grid resolution implemented in the two models, where the reference model at 1/3 arc sec can describe the ocean-front topography better than forecast model at 2 arc sec. These fine features are mostly smoothed into coarser grids employed in the forecast model, and therefore create a smoother land elevation in the forecast model for the waves to overflow more easily.

A tsunami source with same magnitude from the synthetic scenario ATSZ 38-47, in Lesser Antilles, causes much smaller flooding along the coastline of San Juan with maximum wave amplitude of up to 3.5 m (Figure 21). Similar to scenario ATSZ 48-57, the highest water elevation occurs along at the waterfront, particularly along the coastline between Old San Juan and San Juan International Airport. Flooding also occurs at the low land area in San Juan, especially the San Juan International Airport, and along the east shoreline of Ensenada de Boca Vieja. The flow speed at the entrance of San Juan harbor is up to 2.5 m/s, but is reduced to smaller than 0.5 m/s inside the harbor. Similar to synthetic event ATSZ 48-57, the fastest tsunami flow occurs offshore forming a band of high-speed zone between 3 to 6 m/s along the abrupt bathymetric change. The computed time series at the tide gauge have nearly identical waveforms, indicating that the forecast model and reference model agree well with each other. The 24-hour run of forecast model illustrates long-lasting wave activities inside San Juan harbor. The waves arriving after 12 hours of the tsunami generation still have amplitudes comparable to the first two hours. These late waves are probably due to reflection from the continent of Africa.

The synthetic scenarios ATSZ 58-67 and ATSZ 82-91 give similar computational results at San Juan. With the forecast model, both scenarios showed minor inundation along the canals, while the reference model indicates no flooding. The color pattern in **Figures 22a-d and 23a-d** shows that, in both scenarios, wave amplitudes are up to 1 m in Ensenada de Boca Vieja and 0.3 to 0.9 m/s in Bahia de San Juan, where the current speed reaches 2.5 m/s at the entrance of San Juan Harbor. Inside the harbor, although the wave amplitude is still 0.7 to 0.8 m, the flow speed is reduced to smaller than 0.3 m/s. The computed time series at tide gauges are highly consistent in both scenarios. Unlike scenarios ATSZ 48-57 and 38-47, the largest wave amplitude at tide gauge occurs on the second wave, about 0.5 m in amplitude. The wave period is about 1 hour for ATSZ 58-67, but only about 30 min for the ATSZ 82-91 for the first eight waves within 4 hours of

the event. A notable feature of the time series at the tide gage, in both scenarios (**Figure 22e and 22f** and **Figure 23e and 23f**), is the leading depression N-waves (Tadepalli and Synolakis, 1994), which was propagating from the tsunami source. Different than the Puerto Rico Trench and the Hispaniola Trench, where the North America plate is subducting southwesterly beneath the Caribbean plate, the geological setting at ATSZ 58-67 and ATSZ 82-91 is has strong features of submarine troughs – Cayman Trough at ATSZ 58-67 and Los Muertos Trough at ATSZ 82-91. The Cayman Trough is a complex transform fault zone bounded by strike-slip faults, while Los Muertos trough is an indication of northerly dipping Caribbean Plate and associated seismic zones, in contrast to the south-dipping Puerto Rico – Lesser Antilles subduction zone (LaForge and McCann, 2005). The northerly dip of the Los Muertos Trough results in an uplift at its southern extent but a subsidence at the north that generates the leading depression when the tsunami waves propagate.

The synthetic scenario of ATSZ 68-77 produces negligible impact along San Juan's coastline with wave amplitude up to 0.2 m. However, it is a special case that highlights two important characteristics of tsunami waves: wave period and late waves. The computed time series at the San Juan tide gage shows that the wave period of the ATSZ 68-77 scenario, about one to two hours, is unusually long. The wave amplitude did not reach its maximum until almost 9 hours after the tsunami was generated, while the first notable peak arrived about at three hours. The modeling results between the forecast model and the reference model (for the first eight hours) show excellent agreement in computed wave amplitude, flow speed, and time series at the tide gage (**Figure 24)**. The synthetic scenario of ATSZ 68-77 stresses the need of retaining tsunami warning or watch for more than 24 hours for San Juan during a real tsunami event.

Excellent agreement was also found between the forecast model and reference model for the synthetic scenario of SSSZ 1-10 (**Figure 25)** that represents M_w 9.3 earthquake-generated tsunami waves from the South Sandwich source zone. The model results show that maximal water elevation of 0.5 m is along the coastline of Ensenada de Boca Vieja and 0.4 m to the east of San Juan. The flow speed at the entrance of San Juan harbor is about 0.2 to 0.3 m/s, and less than 0.1 m/s in the harbor. Similar to ATSZ 68-77, the largest wave arrives about seven hours later than the first wave probably due to reflected waves from Africa.

The synthetic scenario of magnitude 7.5, ATSZ b52, introduces up to 0.4 m wave amplitude along the shoreline of San Juan, but only 0.04 m at the tide gage. Both the forecast model and reference model show good consistency and stability in terms of maximum wave amplitudes, flow speed (**Figure 26a-d**) and the time series at the tide gage (**Figure 26e-f**), although the time series at the tide gauge starts to show discrepancies after four hours into the event. The micro scenario SSSZ b11 is useful in testing the model stability under the conditions of negligible wave. From the computed maximum wave amplitude (**Figure 27a-d**), one can see that the water elevation at the oceanfront is only on the order of 10^{-4} m. The reference model C grid introduces some numerical abnormality during the model run, while the forecast model gives stable results up to 24 hours of computation. The issue with the reference model is being further

investigated.

5. Sensitivity test of friction factor

Most of the tsunami models use a constant friction factor throughout the computational domain. The most commonly-used friction factor for coastal water nearshore is a Manning' coefficient n = 0.03. However, it is known that the friction factor has a main influence on tsunami wave dynamics nearshore and onshore, specially over shallow and wide shelves, and ultimately affect the computational results for tsunami inundation and runup.

Four different friction factors, n^2 = 0.0001, 0.0004, 0.0009, and 0.0016, are tested for San Juan forecast model to examine the influence on computational results of wave amplitude, flow speed, and inundation extent. The synthetic scenario ATSZ 48-57 is used for these tests as it causes most extensive flooding in San Juan. Figure 28 indicate that the inundation extent along San Juan's coastline is not very sensitive to the friction factor – all four test cases show similar inundation limit. The lower panels of Figure 28 show the influence of friction on wave amplitude and flow speed at the tide gage. In addition to the actual tide gage site, time series are extracted for synthetic "gages" representing conditions outside and in the middle of San Juan Harbor (see Figure 28a). The wave-amplitude time series at the offshore gage are almost identical for all friction factors. The flow speed comparison shows smaller maximum flow speed corresponding to larger friction factor at all three gages. In this case, the flow speed drops about 40% when the friction is two times larger (n^2 increases from 0.0001 to 0.0004), and n^2 = 0.0004, 0.0009, and 0.0016 give similar results. However, the difference of maximum wave amplitude is large inside Bahia de San Juan, especially after the first wave. The time series of wave amplitude at the bay center gage shows that the water level was as low as 4 m below the MHW for n^2 = 0.0001, and n^2 = 0.0016 gives much higher water level, up to 8 m above MHW, in the Bahia de San Juan. The effect of friction on flow speed at the center of the bay is similar to that at offshore gage – smaller friction results in larger flow speed. At the tide gage location, it is worth noting that smallest friction (n^2 = 0.0001) leads to a leading depression as large as 3 m below MHW for half an hour, while the largest friction (n^2 = 0.0016) gives a contrasting result with positive water elevation as high as 4 m above MHW. The flow speed at the tide gage has the same tendency as that at offshore gage – larger friction cause smaller flow speed, which is halved between friction factors of n^2 = 0.0001 and 0.0016.

It is obvious that different friction factor implemented in the model largely affects the tsunami wave dynamics near shore and along the coastline, especially in an enclosed water body, such as a bay or a harbor. Friction factor affects the water level less than the current velocities in the open ocean. The uncertainty of friction factor needs to be accounted in tsunami hazard assessment.

6. Summary and conclusions

San Juan is the most important coastal community in Puerto Rico, and a popular tourist destination attracting tourists from all over the world. San Juan is exposed to potential coastal hazards such as storm surge and tsunamis. These pose challenging, yet long-

standing, questions for the coastal communities on how to protect lives and property. Tsunami forecast and hazard assessment in San Juan remains significantly understudied, probably due to the minor impact and infrequent occurrence of tsunamis in San Juan's history, as well as in the Atlantic.

In this study, a tsunami forecast model is developed for the community of San Juan, Puerto Rico. The developed model is being implemented in NOAA's Short-term Inundation Forecast of Tsunamis (SIFT) to provide real-time modeling forecasts of tsunami wave characteristics, runup and inundation along San Juan's coastline. Discussion of the details of each individual components of the forecast model, including the bathymetry and topography, the basic model setup, and the model parameters are provided in the report. The forecast model employs grids as fine as 2 arc sec (~ 60 m) and can accomplish a four-hour simulation, in 12 minutes of computer CPU time. In parallel, a reference model using MOST version 4 was also developed, using grids as fine as 9 m, to provide reference results basis for performance evaluation of the forecast model.

Two historical events, August 4, 1946 Dominican Republic and 1755 Lisbon tsunamis were used as an approximate check; a full model validation could not be carried due to lack of historical tsunami records for these events. The model results indicate that the 1946 Dominican Republic tsunami generated from a M8.1 earthquake fits better with historical description of the maximum wave. The 1755 Lisbon tsunami is used as a model validation case to show the San Juan models did not produce "surprising" results. Based on Barkan et al. (2009) and Muir-Wood and Mignan (2009) sources of the 1755 tsunami, the modeling results showed 2-m maximum wave amplitude along the coastline of San Juan and 0.5 m at the tide gage. Minor tsunami inundation was shown at the west and southeast of Ensenada de Boca Vieja, and a maximum current speed of 2 m/sec at the entrance of San Juan Harbor. It is worth noting that the modeling of 1755 Lisbon tsunami in San Juan was based on its present bathymetric and topographic features. The results from both the forecast model and the reference model showed good agreement in arrival time and wave period. The forecast model gives larger wave amplitude for the first two waves.

A total of nine synthetic scenarios, including six catastrophic, one small-size, and one micro-size earthquake-generated, were used to examine the stability of the developed forecast model and reference model for San Juan. The synthetic scenarios were selected in such a way that at least one from each of the Puerto Rico Trench, Hispaniola Trench and South Sandwich source zone is tested. Both the forecast model and reference model give stable and consistent results for most of the synthetic scenarios representing tsunami waves from different source locations and different directionalities.

1. A magnitude of 9.3 earthquake in the Puerto Rico Trench, represented by ATSZ 48- 57 in this report, may generate a catastrophic tsunami for San Juan, Puerto. The modeling results show such a tsunami may flood San Juan and its vicinity as far as 5 km inland with approximately 21 m wave amplitude along the coastline and 12 m/s flow current on land.

2. Scenarios ATSZ 38-47 caused minor flooding at the waterfront of San Juan with wave amplitude up to 3.5 m above MHW, and current speed up to 2.5 m/s at the entrance of San Juan Harbor. Other scenarios are considered as less threatening, but may still cause damage to the harbor facilities and vessels moored in the harbor with high-speed currents in San Juan Harbor.

3. Tsunamis generated from the submarine trough are featured with a leading depression when propagating into San Juan. The northerly dip of the Los Muertos Trough (scenario ATSZ 82-91) results in an uplift at its south, but a subsidence at the north that result in a leading depression when the tsunami waves propagate into the Atlantic. The faults in Cayman Trough (scenario ATSZ 68-77) were simulated using a subducting mechanism rather than a strike-slip mechanism.

4. For tsunamis generated in the Cayman trough or in South Sandwich source zone, the model simulations show the late waves are higher than the first. Along with these waves are longer wave period up to one to two hours. This lays emphasis on the need of retaining the tsunami warning or watch for more than 24 hours for the coasts of San Juan during a real tsunami event.

All model validation and stability tests demonstrated that the developed tsunami forecast model and reference model for San Juan, Puerto Rico, are robust and efficient for their implementation into both the short-term real-time tsunami forecast system and long-term tsunami inundation investigations, although the model accuracy still requires validation through real events in future. The forecast model developed for San Juan provides a four-hour forecast of first wave arrival, amplitudes, and inundation within 12 minutes based on testing with available historical and synthetic events as presented in this report.

7. Acknowledgement
The author wish to thank Edison Gica and Jean Newman for their work in the propagation database, Burak Uslu for providing propagation database tabular unit source information and graphics, and the entire modeling group of NCTR for helpful suggestions and discussion. The author especially acknowledges and thanks Marie C. Eble and Sandra Bigley for providing invaluable technical assistance and for editorial review. Collaborative contribution of the National Weather Service, the National Geophysical Data Center, and the National Data Buoy Center was invaluable. Funding for this publication and all work leading to development of a tsunami forecast model for San Juan, Puerto Rico was provided by the National Oceanic and Atmospheric Administration. This publication was partially funded by the Joint Institute for the Study of the Atmosphere and Ocean (JISAO) under NOAA Cooperative Agreement NO. NA17RJ1232, JISAO Contribution No. ****. This is PMEL Contribution No. ****.

References

Barkan R., and ten Brink, U.S. (2010): Tsunami simulations of the 1867 Virgin Islands earthquake: Constraints on epicenter location and fault parameters, Bulletin of the Seismological Society of America, 100, 995-1009.

Barkan, R., U.S. ten Brink, J. Lin, (2009), Far field tsunami simulations of the 1755 Lisbon earthquake: implications for tsunami hazard to the U.S. East Coast and the Caribbean, *Marine Geology*, 264, 109-122.

Burwell, D., E. Tolkova, and A. Chawla (2007): Diffusion and dispersion characterization of a numerical tsunami model. *Ocean Modelling*, *19*(1–2), 10–30.

DeMets, C., Mattioli, G., Jansma, P., Rogers, R. D., and Tenorio, C. (2007): Present motion and deformation of the Caribbean plate: constraints from new GPS geodetic measurements, from Honduras and Nicaragua, in: Geologic and Tectonic Development of the Caribbean Plate in Northern Central America, edited by: Mann, P., Special Paper, Geol. Soc. Am., 428, 21–36, doi:10.1130/2007.2428(02).

Ellis, S. R. (1976): History of dredging and filling of lagoons in the San Juan area, Puerto Rico, U.S. Geological Survey Water-Resources Investigations 38-76, p25.

Gica, E., M. Spillane, V.V. Titov, C. Chamberlin, and J.C. Newman (2008): Development of the forecast propagation database for NOAA's Short-term Inundation Forecast for Tsunamis (SIFT). NOAA Tech. Memo. OAR PMEL-139, 89 pp.

Grindlay, N.R. (1998): Volume and density approximations of material involved in debris avalanche on the south slope of the Puerto Rico Trench, *A report to the Puerto Rico Civil Defense and the University of Puerto Rico Sea Grant College Program*, 9 pp.

LaForge, R.C. and W.R. McCann (2005). A seismic source model for Puerto Rico, for use in probabilistic ground motion hazard analyses. *Active Tectonics and Seismic Hazards of Puerto Rico, the Virgin Islands, and Offshore Areas*, edited by P. Mann, The Geological Society of America special Paper 385, 223-248.

Lander, J.F., L.S. Whiteside, P.A. Lockridge (2002). A brief history of tsunamis in the Caribbean Sea. *Science of Tsunami Hazards*, 20(1), 57-94.

Mercado, A., N.R.Grindlay, P.Lynett, and P.L.-F.Liu (2002). Investigation of the potential tsunami hazard on the north coast of Puerto Rico due to submarine landslides along the Puerto Rico Trench, report, 432 pp., Puerto Rico State Emergency Manage.Agency, San Juan.

Muir-Wood, R. and A. Mignan (2009), A phenomenological reconstruction of the M_w 9 November 1st 1755 earthquake source, *The 1755 Lisbon Earthquake: Revisited*, *Geotechnical, Geological, and Earthquake Engineering*, 7, Part III, 121-146, doi: 10.1007/978-1-4020-8609-0_8.

Nealon, J.W. and W.P. Dillon (2001). Earthquakes and tsunamis in Puerto Rico and the U.S. Virgin Islands. U.S. Geological Survey Fact Sheet 141-00 online version 1.0 (http://pubs.usgs.gov/fs/fs141-00/fs141-00.pdf).

O'Laughlin, K.F. and J.F. Lander (2003). Caribbean tsunamis – a 500-year history from 1498-1998. *Kluwer Academic Publishers*, p263.

Reid, H. F., and S. Taber (1920). The Virgin Islands earthquakes of 1867–1868, *Bull. Seismol. Soc. Am.* 10, 9–30.

Roger, J., S. Allgeyer, H. Hebert, M.A. Baptista, A. Loevenbruck, F. Schindele (2010), The 1755 Lisbon tsunami in Guadeloupe Archipelago: source sensitivity and investigation of resonance effects, *The Open Oceanography Journal*, 4, 58-70.

Schwab, W.C., W.W. Danforth, K.M. Scanlon, and D.G. Masson (1991): A giant submarine slope failure on the northern insular slope of Puerto Rico, *Marine Geology*, *96*, 237-246.

Synolakis, C.E., E.N. Bernard, V.V. Titov, U. Kânoğlu, and F.I. González (2008): Validation and verification of tsunami numerical models. *Pure Appl. Geophys.*, *165*(11–12), 2197–2228.

Tadepalli, S. and C.E. Synolakis (1994). The run-up of N-waves on sloping beaches. *Proc. R. Soc.* A 445, 99-112.

Tang, L., V.V. Titov, E. Bernard, Y. Wei, C. Chamberlin, J.C. Newman, H. Mofjeld, D. Arcas, M. Eble, C. Moore, B. Uslu, C. Pells, M.C. Spillane, L.M. Wright, and E. Gica (2012): Direct energy estimation of the 2011 Japan tsunami using deep-ocean pressure measurements. J. *Geophys. Res.,* 117, C08008, doi: 10.1029/2011JC007635.

Tang, L., V. V. Titov, and C. D. Chamberlin (2009), Development, testing, and applications of site-specific tsunami inundation models for real-time forecasting, *J. Geophys. Res.*, 114, C12025, doi:10.1029/2009JC005476.

Tang, L., V.V. Titov, Y. Wei, H.O. Mofjeld, M. Spillane, D. Arcas, E.N. Bernard, C. Chamberlin, E. Gica, and J. Newman (2008): Tsunami forecast analysis for the May 2006 Tonga tsunami. *J. Geophys. Res.*, *113*, C12015, doi: 10.1029/2008JC004922.

Taylor, L.A., B.W. Eakins, R.R. Warnken, K.S. Carignan, G.F. Sharman and P.W. Sloss, (2006): Digital Elevation Models for San Juan and Mayaguez, Puerto Rico: Procedures, Data Sources and Analysis, NOAA National Geophysical Data Center technical report, Boulder, CO, 35 pp.

Taylor, L.A., B.W. Eakins, K.S. Carignan, R.R. Warnken, T. Sazonova, D.C. Schoolcraft (2008): Digital Elevation Models of Puerto Rico: Procedures, Data Sources and Analysis, *NOAA Technical Memorandum NESDIS NGDC-13, National Geophysical Data Center*, Boulder, CO, 27 pp.

ten Brink, U.S., W.W. Danforth, C. Polloni, B. Andrews, P. Lianes, S.V. Smith, E. Parker, and T. Uozumi (2004), New sea floor map of the Puerto Rico trench helps assess earthquake and tsunami hazards, *EOS*, 85, 349, 354.

ten Brink, U. S., E. L. Geist, P. Lynett, and B. Andrews (2006), Submarine slides north of Puerto Rico and their tsunami potential, in Caribbean Tsunami Hazard, edited by A. Mercado, and P. L.-F. Liu, World Sci., Hackensack, N. J.

Titov, V.V. (2009): Tsunami forecasting. Chapter 12 in *The Sea, Volume 15: Tsunamis*, Harvard University Press, Cambridge, MA and London, England, 371–400.

Titov, V.V, E. Gica, M. Spillane, Y. Wei, C. Moore, H. Zhou and R. Weiss (2009), Tsunami hazard assessment for the U.S. East Coast based on generation, propagation and inundation modeling, *NCTR Letter Report to the Nuclear Regulatory Commission*, 117pp.

Titov, V., and F.I. González (1997): Implementation and testing of the Method of Splitting Tsunami (MOST) model. NOAA Tech. Memo. ERL PMEL-112 (PB98-122773), NOAA/Pacific Marine Environmental Laboratory, Seattle, WA, 11 pp.

Titov, V.V., F.I. González, E.N. Bernard, M.C. Eble, H.O. Mofjeld, J.C. Newman, and A.J. Venturato (2005): Real-time tsunami forecasting: Challenges and solutions. Nat. Hazards, 35(1), Special Issue, U.S. National Tsunami Hazard Mitigation Program, 41–58.

Titov, V.V., and C.E. Synolakis (1995): Modeling of breaking and nonbreaking long-wave evolution and runup using VTCS-2, *J. Waterw. Port Coastal Ocean Eng.,* 121(6), 308-316.

Titov, V.V., and C.E. Synolakis (1998): Numerical modeling of tidal wave runup. *J. Waterw. Port Coastal Ocean Eng., 124*(4), 157–171.

Wei, Y., E. Bernard, L. Tang, R. Weiss, V. Titov, C. Moore, M. Spillane, M. Hopkins, and U. Kânoğlu (2008): Real-time experimental forecast of the Peruvian tsunami of August 2007 for U.S. coastlines. *Geophys. Res. Lett.*, *35*, L04609, doi: 10.1029/2007GL032250.

Wei, Y., C. Chamberlin, V. Titov, and L. Tang (2012): Modeling of the 2011 Japan tsunami - Lessons for near-field forecast. *Pure Appl. Geophys.*, doi: 10.1007/s00024-012-0519-z.

Wei, Y., U.S. ten Brink, and B. Atwater (2013): Tsunami sources that might explain the catastrophic overwash of Anegada, British Virgin Islands, between 1650 and 1800. *Journal of Geophysical Research*, in preparation.

Zahibo, N. and Pelinovsky, E. (2001): Evaluation of tsunami risk in the Lesser Antilles, *Natural Hazard and Earth Sciences*, 3, 221–231.

Figures

a

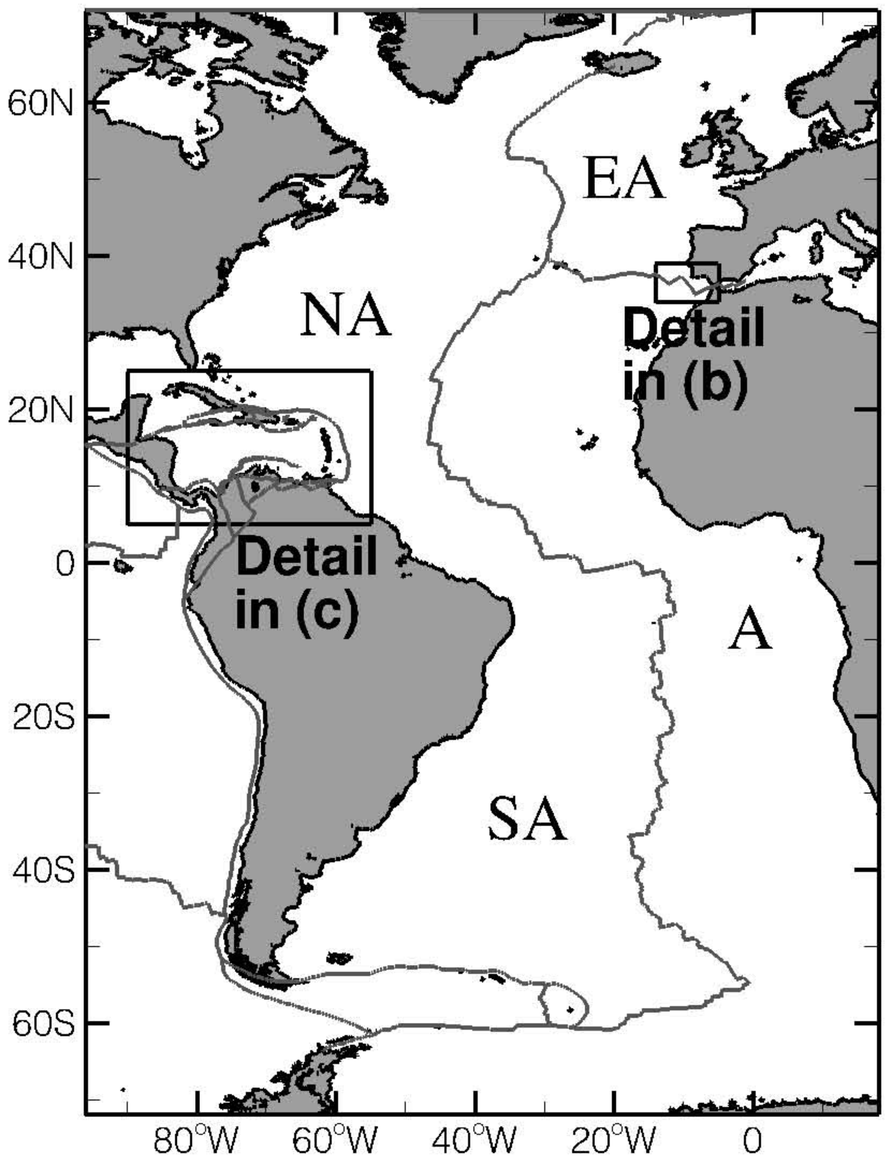
60N
40N
20N
0
20S
40S
60S
80°W
60°W
40°W
20°W
0
EA
NA
A
SA
Detail in (b)
Detail in (c)

b

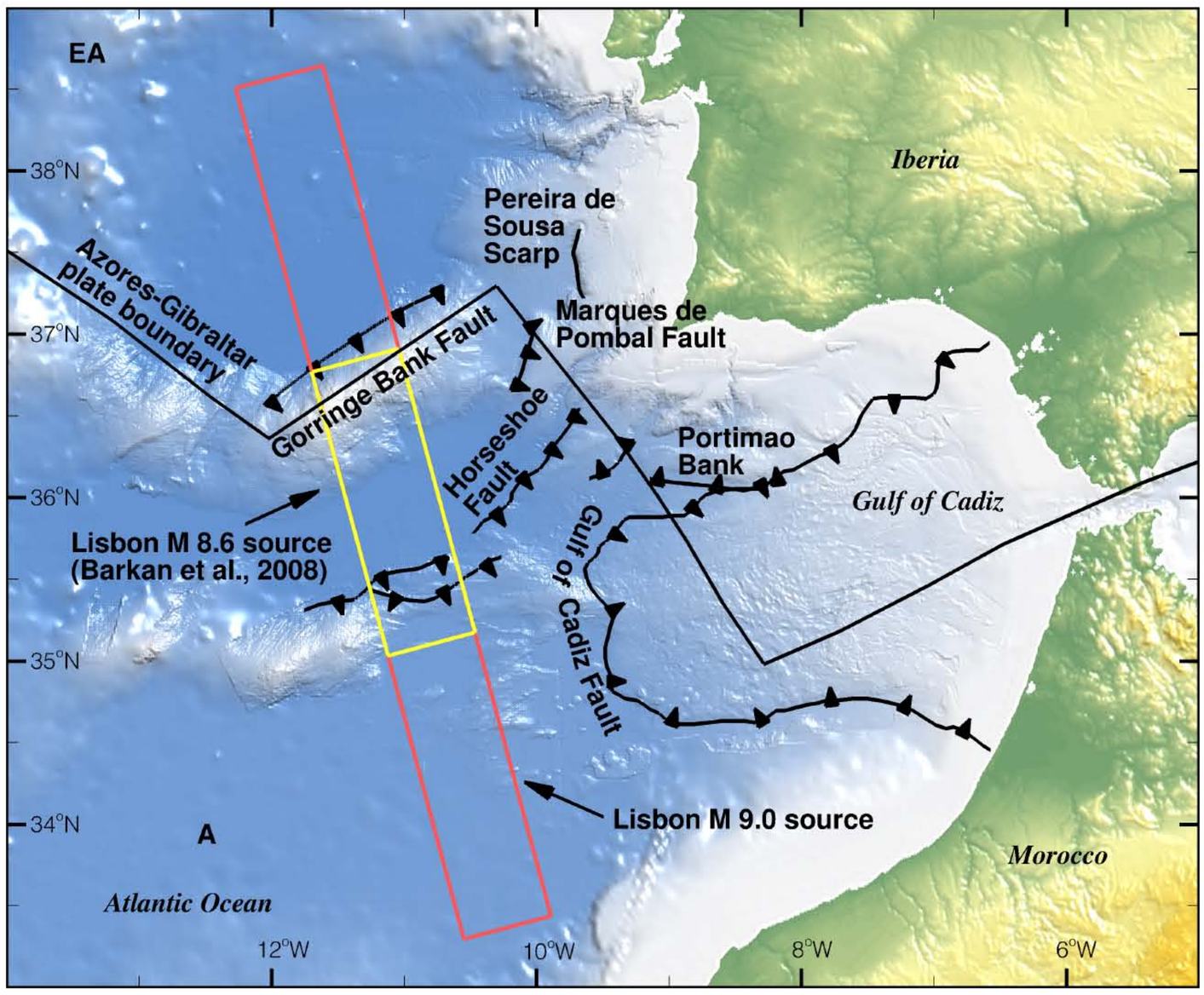
EA
38°N
37°N
36°N
35°N
34°N
12°W
10°W
8°W
6°W
Iberia
Azores-Gibraltar plate boundary
Gorringe Bank Fault
Pereira de Sousa Scarp
Marques de Pombal Fault
Horseshoe Fault
Portimao Bank
Gulf of Cadiz
Gulf of Cadiz Fault
Lisbon M 8.6 source (Barkan et al., 2008)
Lisbon M 9.0 source
A
Atlantic Ocean
Morocco

c

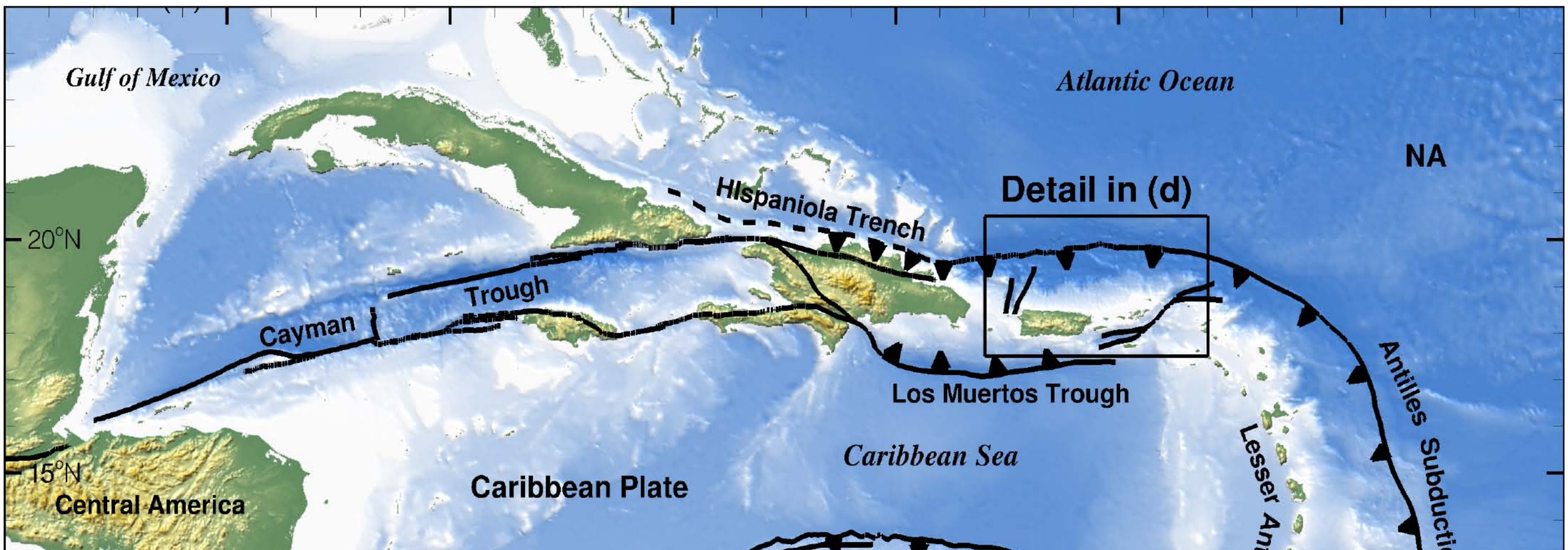
Gulf of Mexico
Atlantic Ocean
NA
Detail in (d)
Hispaniola Trench
20°N
15°N
10°N
Cayman Trough
Los Muertos Trough
Caribbean Sea
Caribbean Plate
Central America
Lesser Antilles
Antilles Subduction zone
Middle America Trench
Cocos Plate
Nazca Plate
SA
Pacific Ocean
85°W
80°W
75°W
70°W
65°W
60°W

d

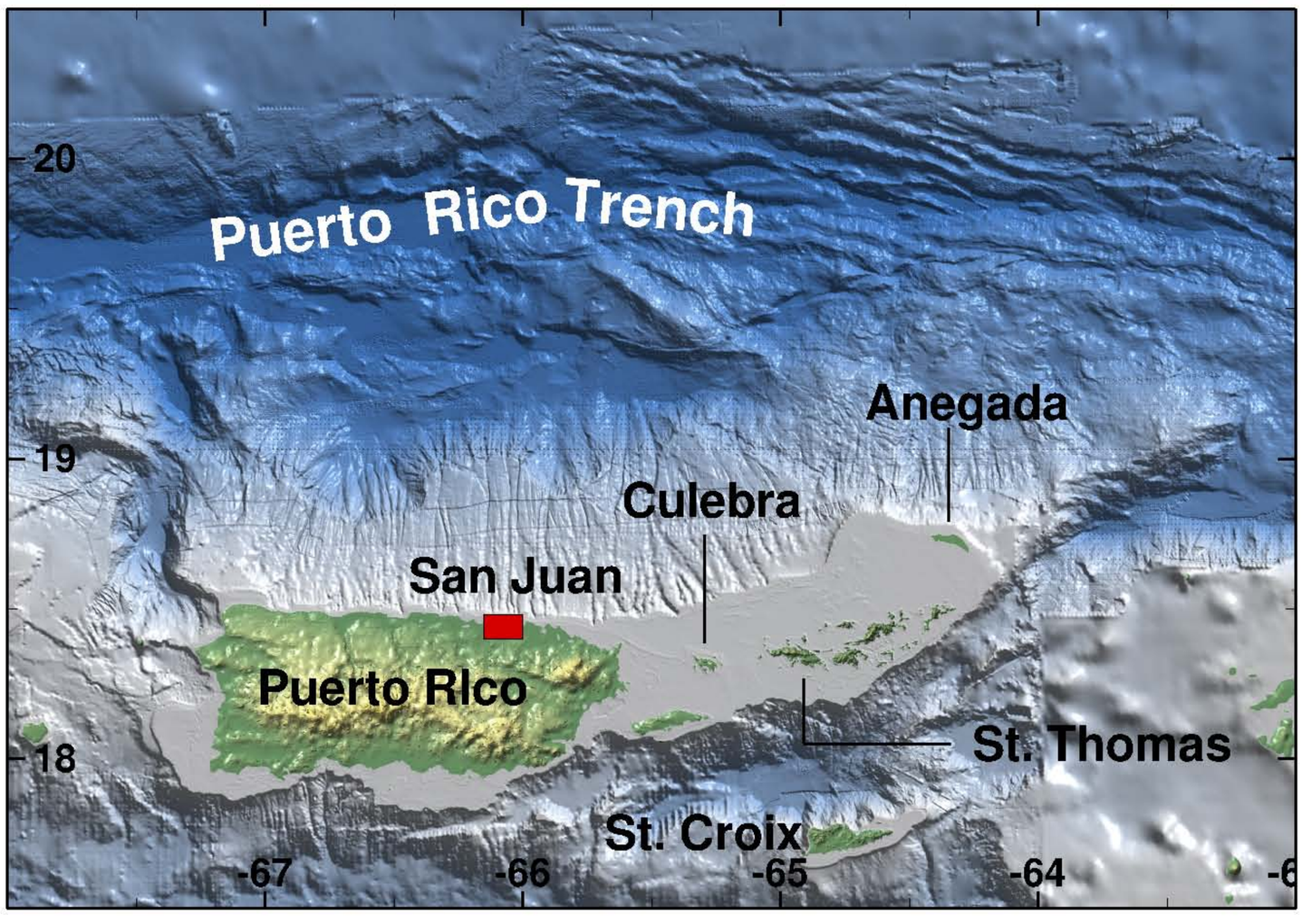
20
19
18
-67
-66
-65
-64
Puerto Rico Trench
Anegada
Culebra
San Juan
Puerto Rico
St. Thomas
St. Croix

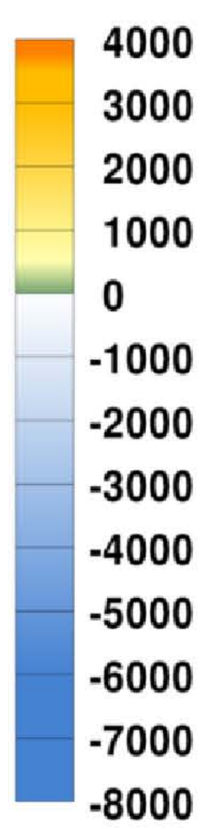
Depth (-) /Elevation (+)
in b, c and d (m)
4000
3000
2000
1000
0
-1000
-2000
-3000
-4000
-5000
-6000
-7000
-8000

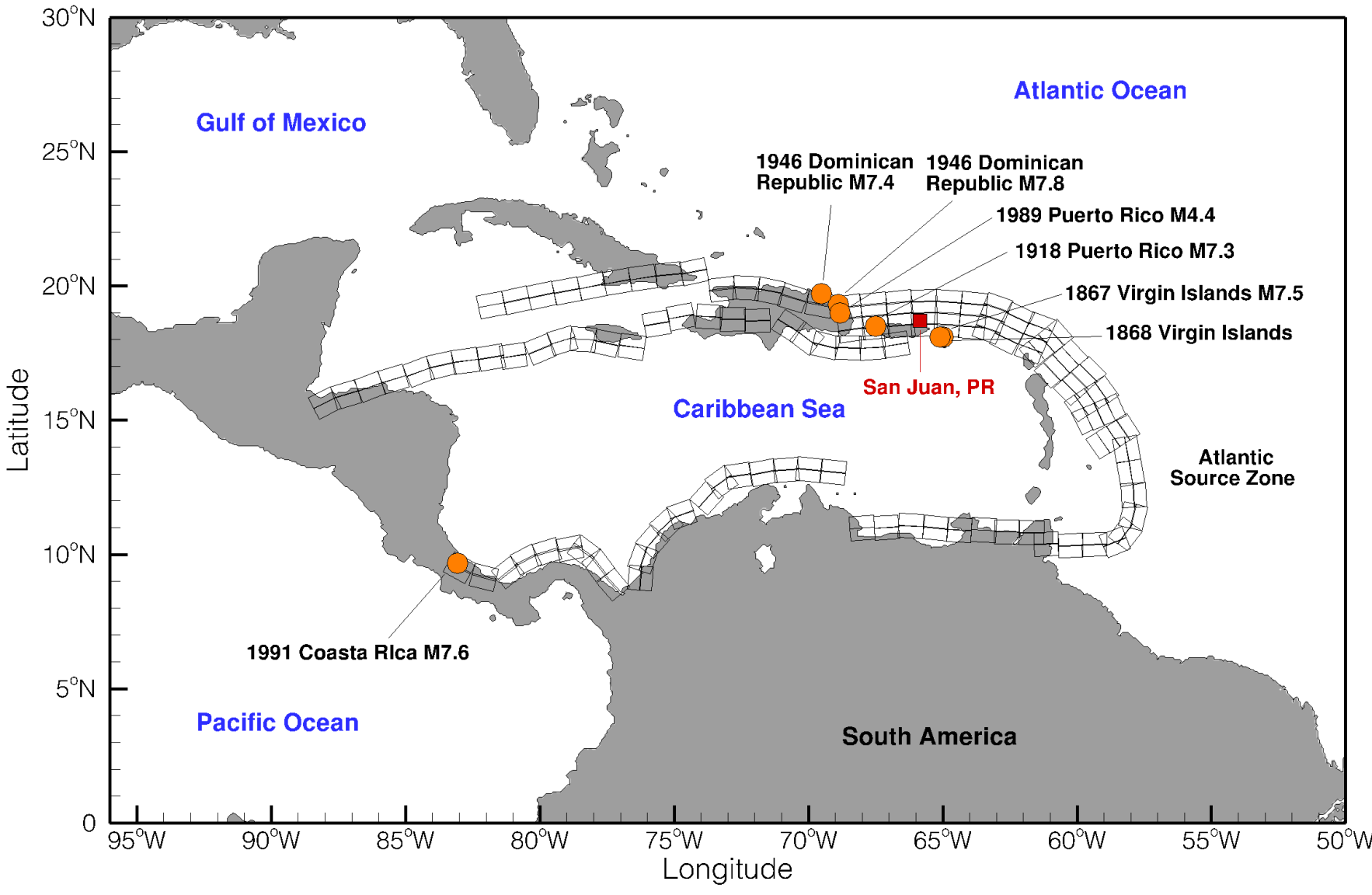
Gulf of Mexico
Atlantic Ocean
1946 Dominican Republic M7.4
1946 Dominican Republic M7.8
1989 Puerto Rico M4.4
1918 Puerto Rico M7.3
1867 Virgin Islands M7.5
1868 Virgin Islands
San Juan, PR
Caribbean Sea
Atlantic Source Zone
1991 Coasta RIca M7.6
Pacific Ocean
South America
30°N
25°N
20°N
15°N
10°N
5°N
0
95°W
90°W
85°W
80°W
75°W
70°W
65°W
60°W
55°W
50°W
Latitude
Longitude


4/1/2013
San Juan, Puerto Rico
San Juan
Palo Seco
El Boquerón
Laguna del Condado
NOS tide gauge
Bahía de San Juan
N18.45°
Cataño Pueblo
Cataño
Palmas
Bahía de Puerto Nuevo
Image © 2013 DigitalGlobe
1640 m
Google earth
Imagery Date: 2/16/2013 lat 18.454185° lon -66.106799° elev 0 m eye alt 7.37 km

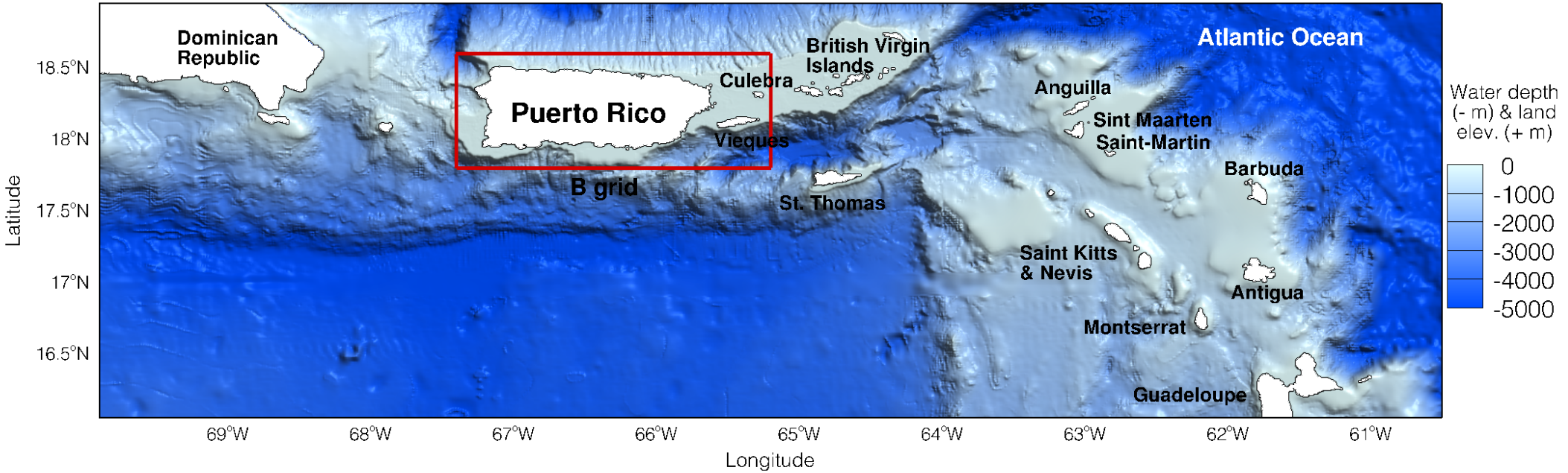
Dominican Republic
Puerto Rico
Culebra
Vieques
B grid
British Virgin Islands
St. Thomas
Atlantic Ocean
Anguilla
Sint Maarten
Saint-Martin
Barbuda
Saint Kitts & Nevis
Antigua
Montserrat
Guadeloupe
Water depth (- m) & land elev. (+ m)
0
-1000
-2000
-3000
-4000
-5000
18.5°N
18°N
17.5°N
17°N
16.5°N
Latitude
69°W
68°W
67°W
66°W
65°W
64°W
63°W
62°W
61°W
Longitude

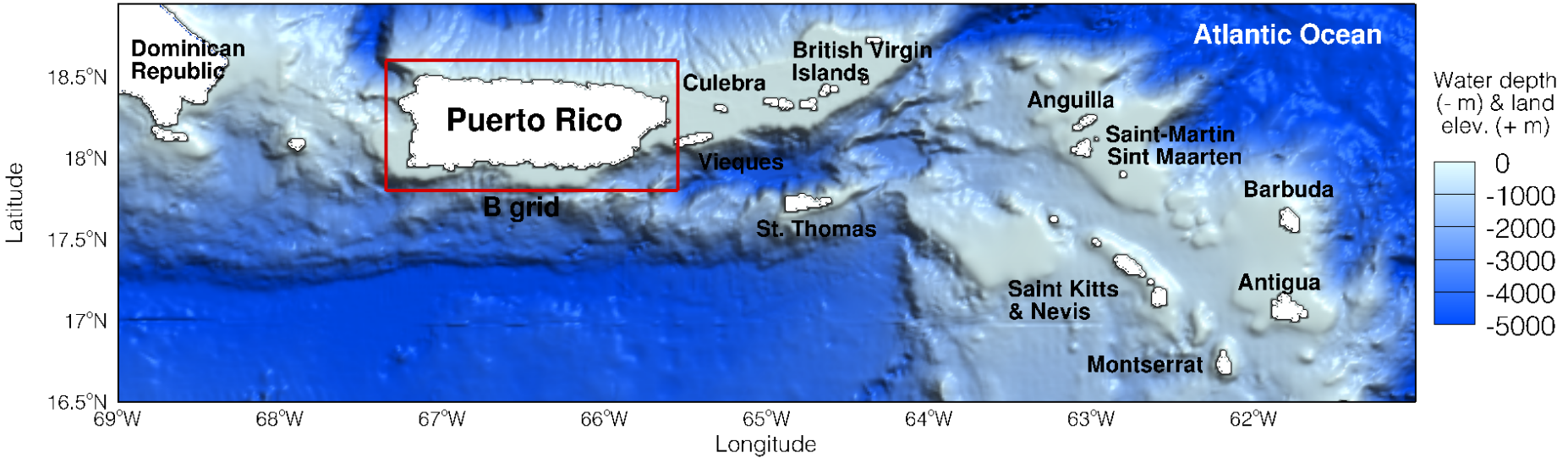
Dominican Republic
Puerto Rico
B grid
Culebra
British Virgin Islands
Vieques
St. Thomas
Anguilla
Saint-Martin
Sint Maarten
Barbuda
Antigua
Saint Kitts
& Nevis
Montserrat
Atlantic Ocean
Water depth
(- m) & land
elev. (+ m)
0
-1000
-2000
-3000
-4000
-5000
Latitude
18.5°N
18°N
17.5°N
17°N
16.5°N
69°W
68°W
67°W
66°W
65°W
64°W
63°W
62°W
Longitude

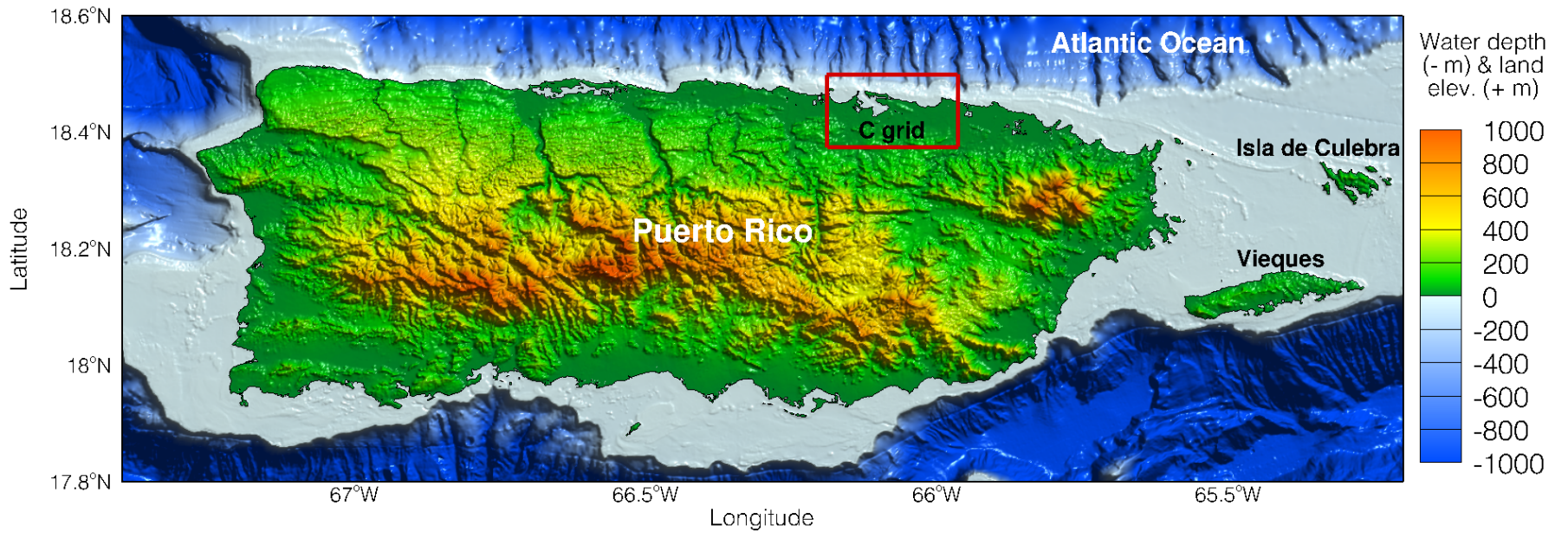
Atlantic Ocean
C grid
Isla de Culebra
Puerto Rico
Vieques
Water depth
(- m) & land
elev. (+ m)
1000
800
600
400
200
0
-200
-400
-600
-800
-1000
18.6°N
18.4°N
18.2°N
18°N
17.8°N
Latitude
67°W
66.5°W
66°W
65.5°W
Longitude

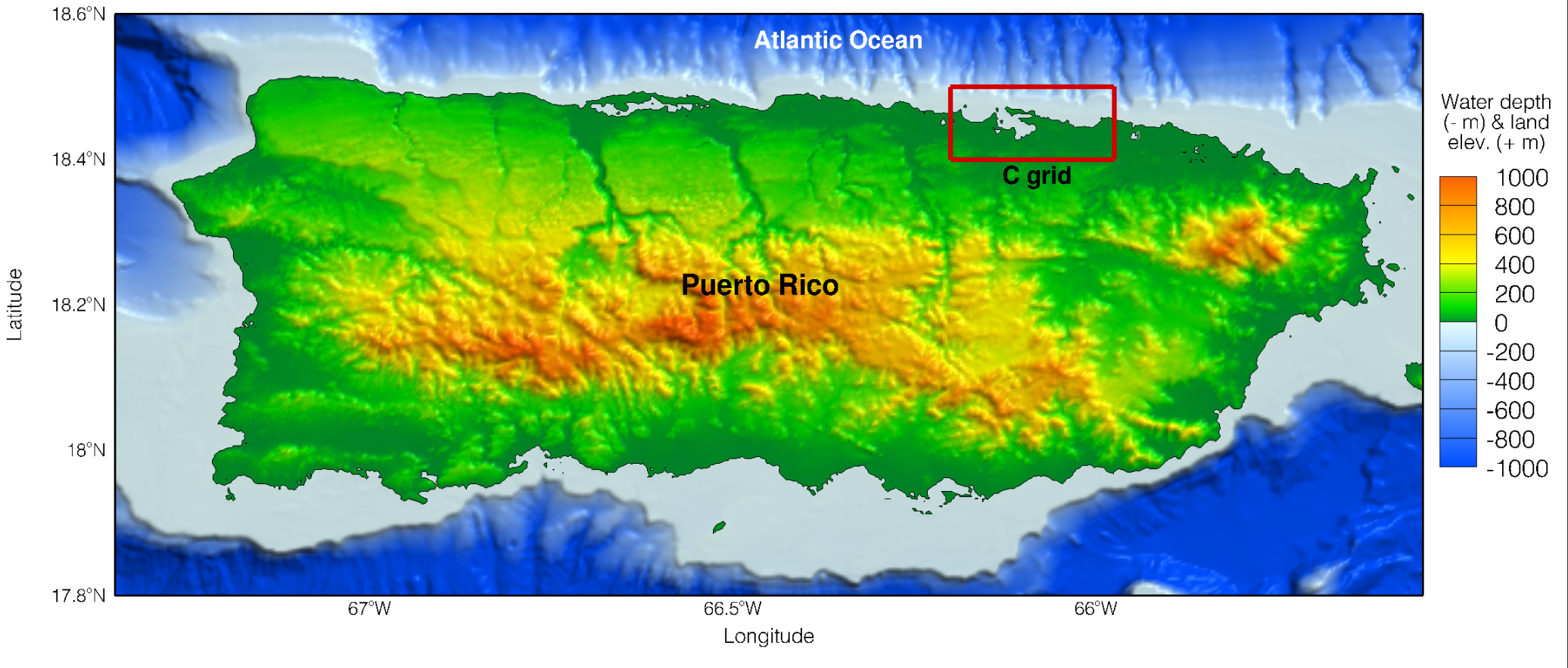
Atlantic Ocean
C grid
Puerto Rico
18.6°N
18.4°N
18.2°N
18°N
17.8°N
Latitude
67°W
66.5°W
66°W
Longitude
Water depth
(- m) & land
elev. (+ m)
1000
800
600
400
200
0
-200
-400
-600
-800
-1000

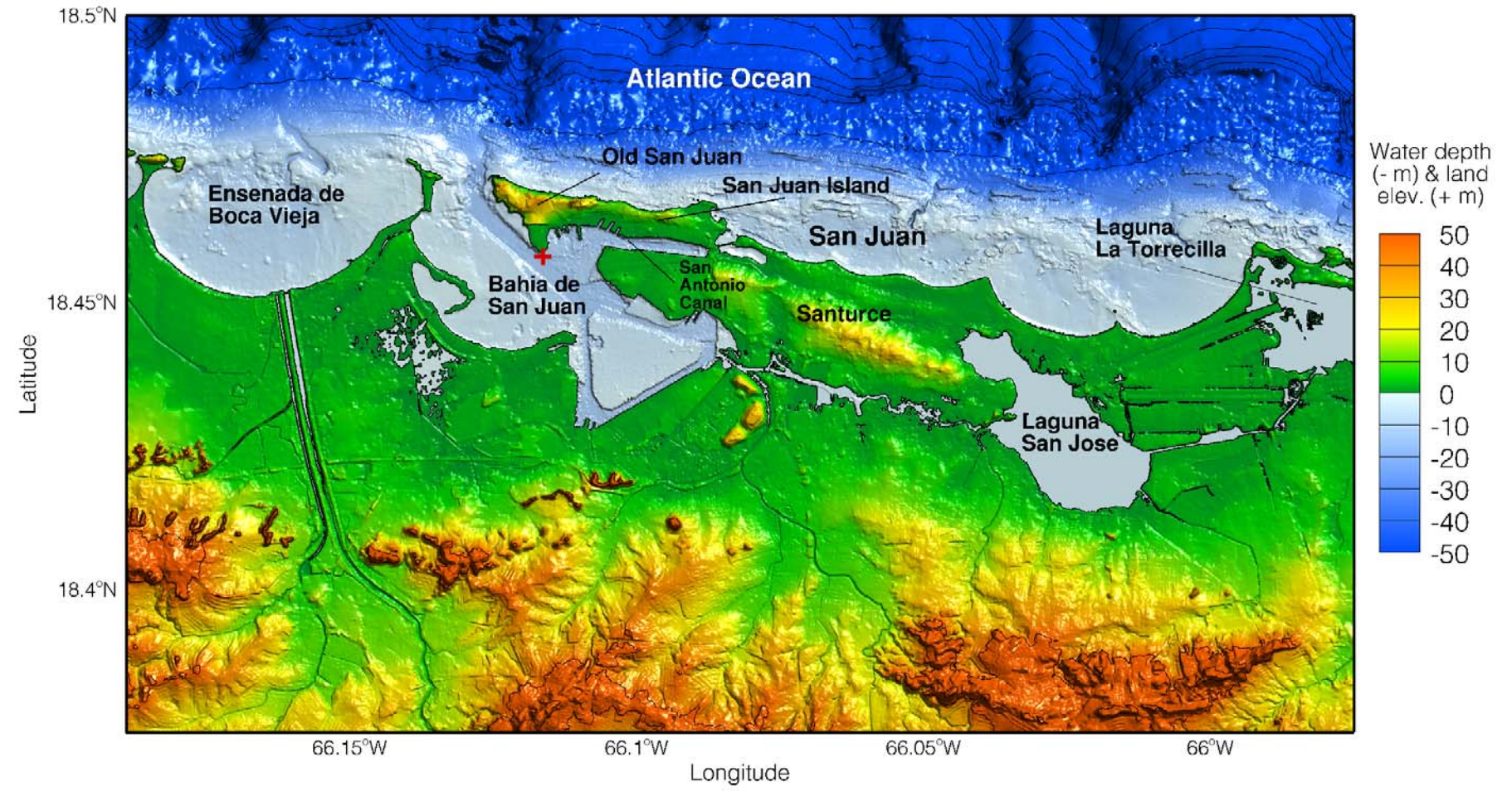
Atlantic Ocean
Old San Juan
San Juan Island
Ensenada de
Boca Vieja
San Juan
Laguna
La Torrecilla
Bahia de
San Juan
San
Antonio
Canal
Santurce
Laguna
San Jose
Water depth
(- m) & land
elev. (+ m)
50
40
30
20
10
0
-10
-20
-30
-40
-50
18.5°N
18.45°N
18.4°N
Latitude
66.15°W
66.1°W
66.05°W
66°W
Longitude

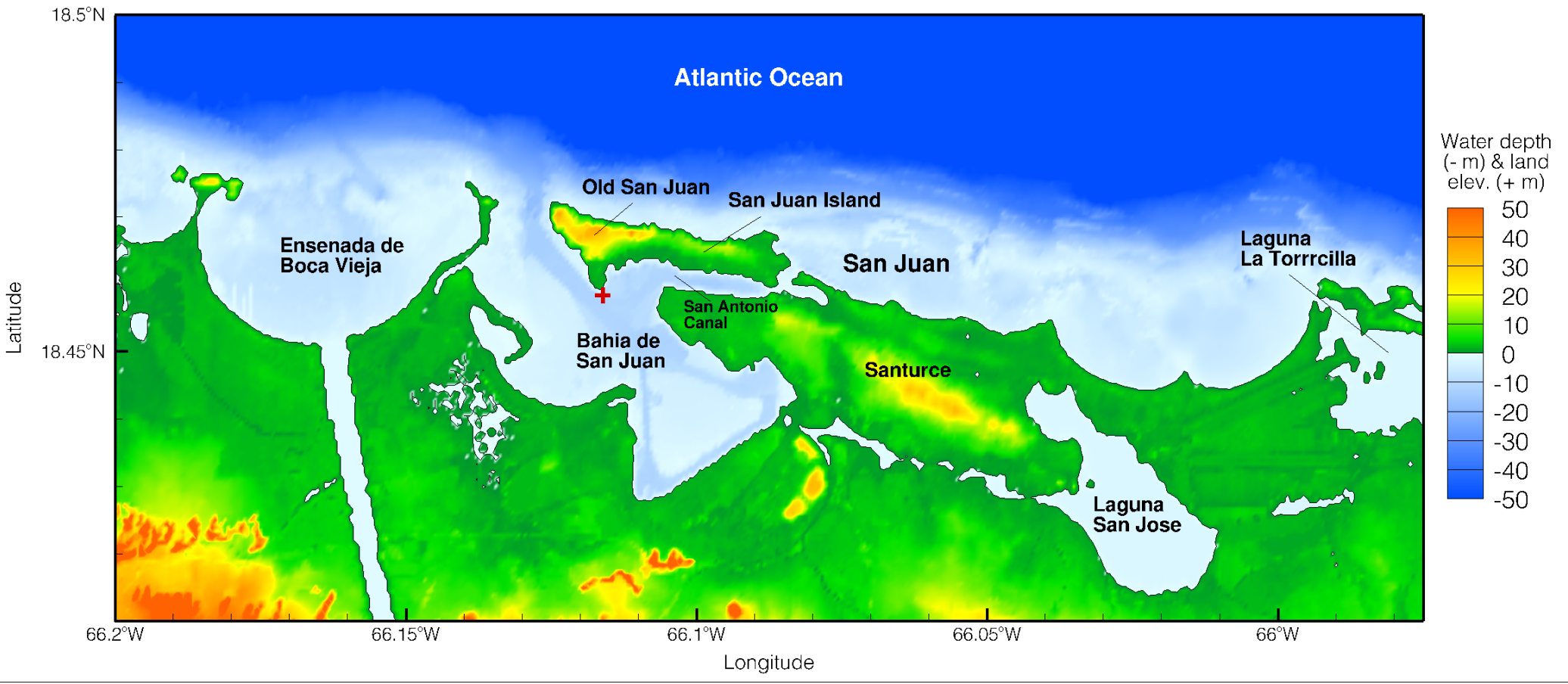
18.5°N
18.45°N
Latitude
66.2°W
66.15°W
66.1°W
66.05°W
66°W
Longitude
Atlantic Ocean
Old San Juan
San Juan Island
San Juan
Ensenada de
Boca Vieja
San Antonio
Canal
Bahia de
San Juan
Santurce
Laguna
La Torrrcilla
Laguna
San Jose
Water depth
(- m) & land
elev. (+ m)
50
40
30
20
10
0
-10
-20
-30
-40
-50

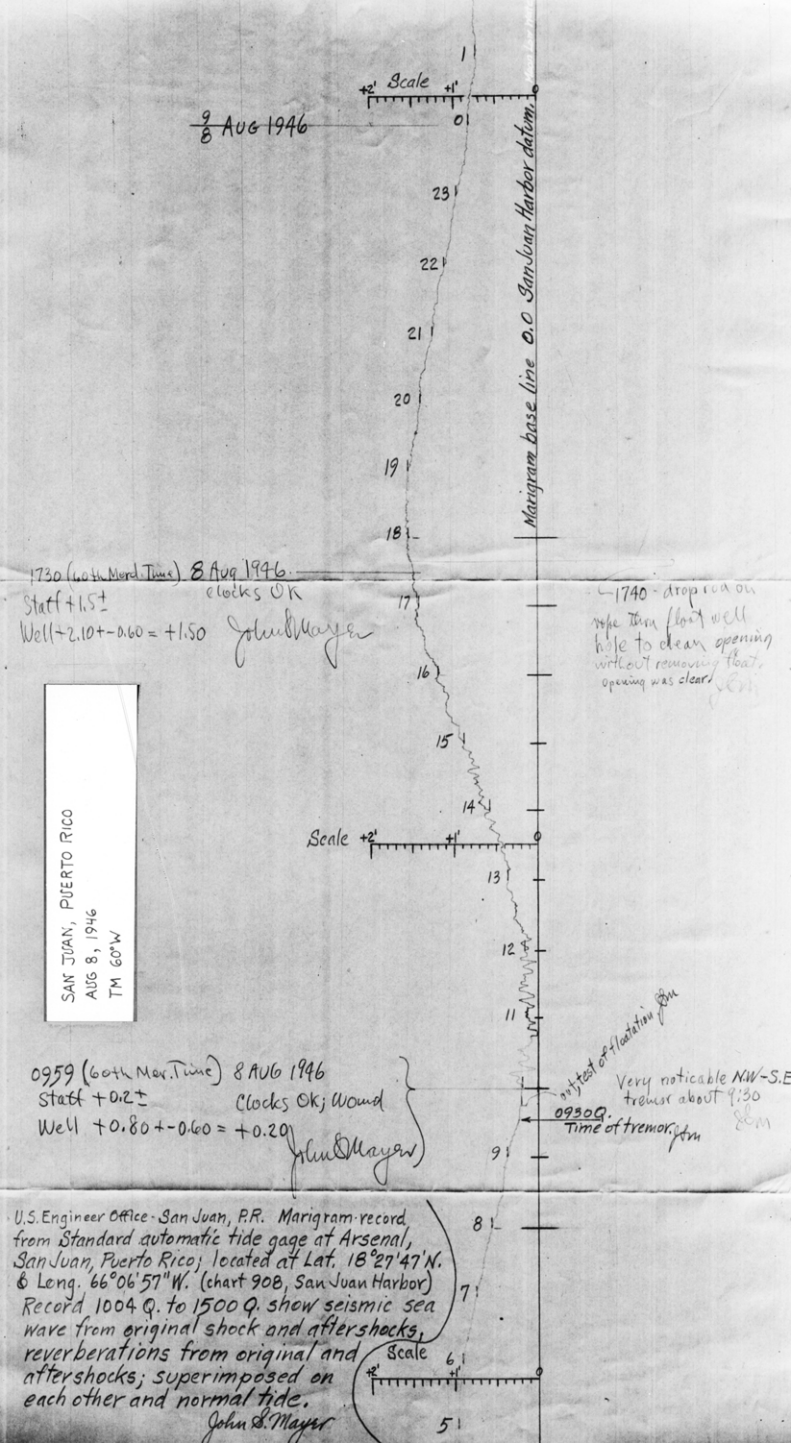
Scale +2' +1'
9/8 AUG 1946
Marigram base line 0.0 San Juan Harbor datum
1730 (60th Mer. Time) 8 Aug 1946
Staff +1.5±
Well +2.10 +-0.60 = +1.50
clocks OK
John S. Mayer
1740 - dropped on rope thru float well hole to clean opening without removing float. opening was clear. JSM
SAN JUAN, PUERTO RICO
AUG 8, 1946
TM 60°W
Scale +2' +1'
0959 (60th Mer. Time) 8 AUG 1946
Staff +0.2±
Well +0.80 +-0.60 = +0.20
Clocks Ok; Wound
John S. Mayer
0930Q. Time of tremor, JSM
Very noticable NW-S.E tremor about 9:30 JSM
U.S. Engineer Office - San Juan, P.R. Marigram record from Standard automatic tide gage at Arsenal, San Juan, Puerto Rico; located at Lat. 18°27'47"N. & Long. 66°06'57"W. (chart 908, San Juan Harbor)
Record 1004 Q. to 1500 Q. show seismic sea wave from original shock and aftershocks, reverberations from original and aftershocks; superimposed on each other and normal tide.
John S. Mayer
Scale +2' +1'

(a)

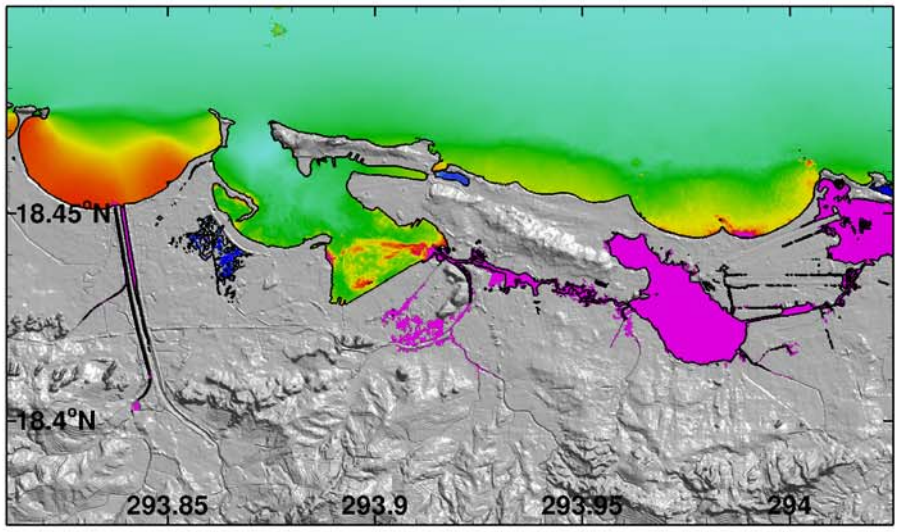
18.45°N
18.4°N
293.85
293.9
293.95
294

(b)

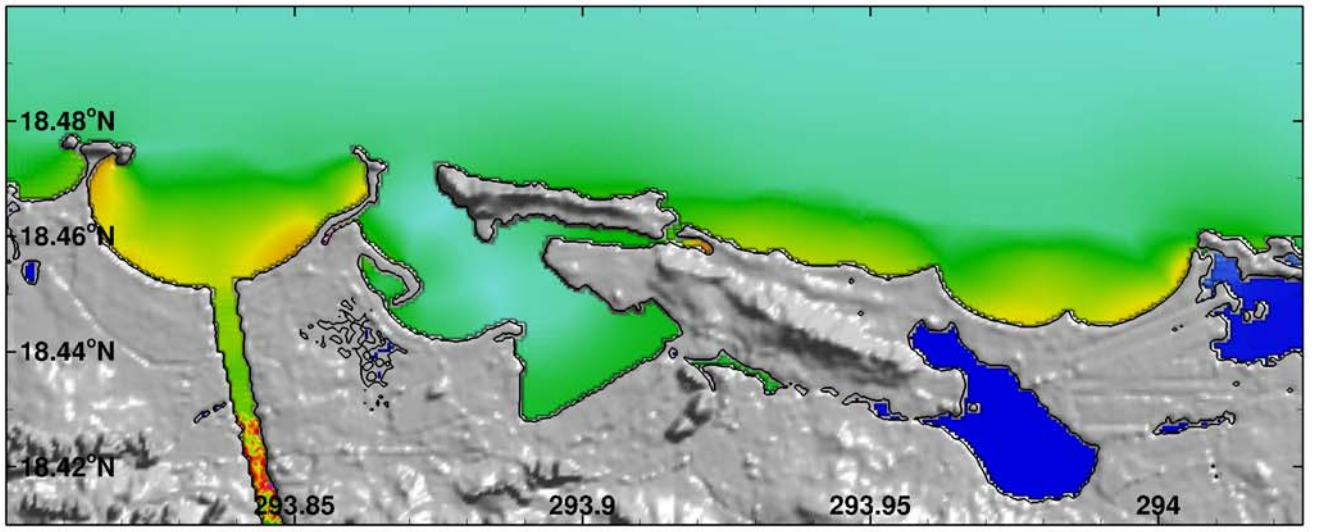
18.48°N
18.46°N
18.44°N
18.42°N
293.85
293.9
293.95
294

(c)

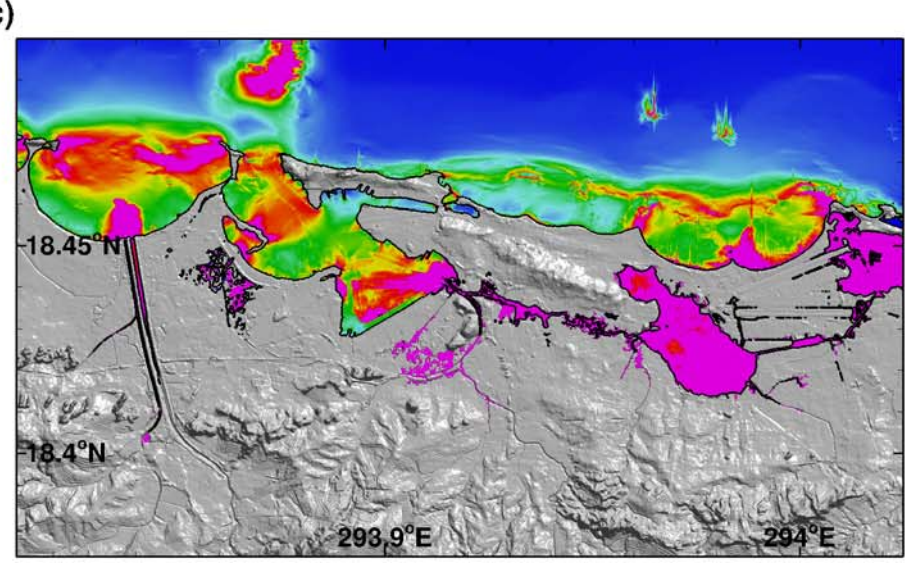
18.45°N
18.4°N
293.9°E
294°E

(d)

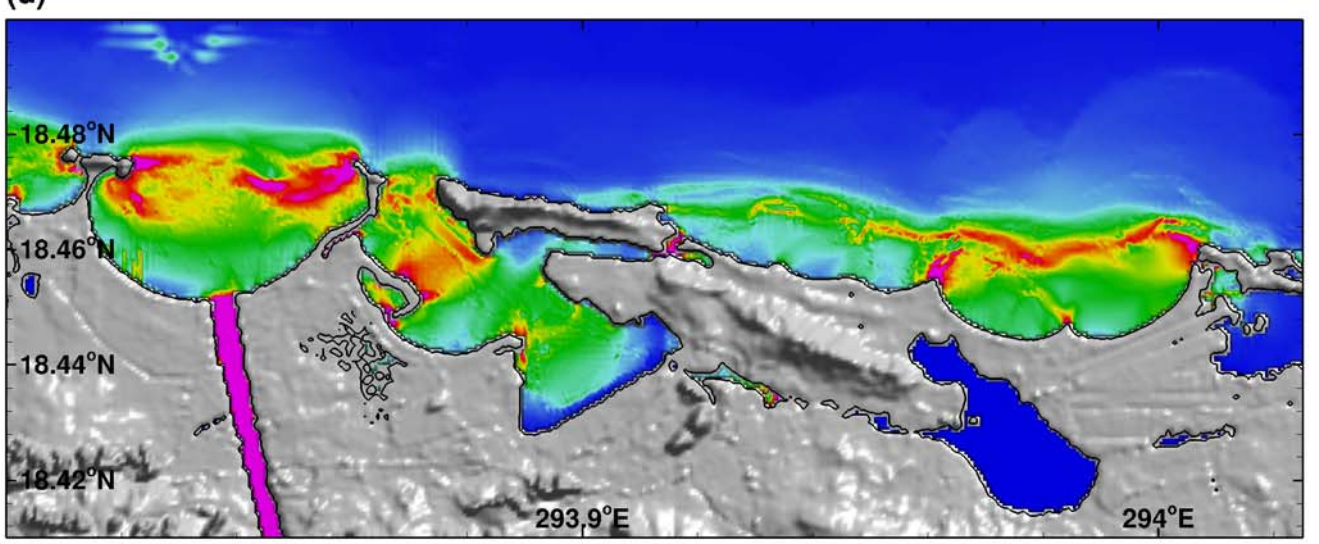
18.48°N
18.46°N
18.44°N
18.42°N
293.9°E
294°E

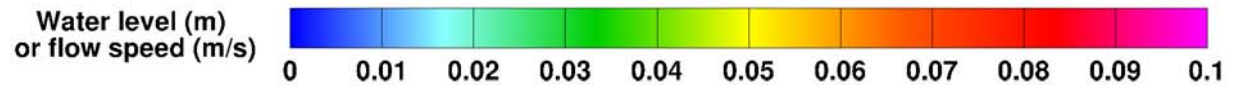
Water level (m)
or flow speed (m/s)
0
0.01
0.02
0.03
0.04
0.05
0.06
0.07
0.08
0.09
0.1

(e)

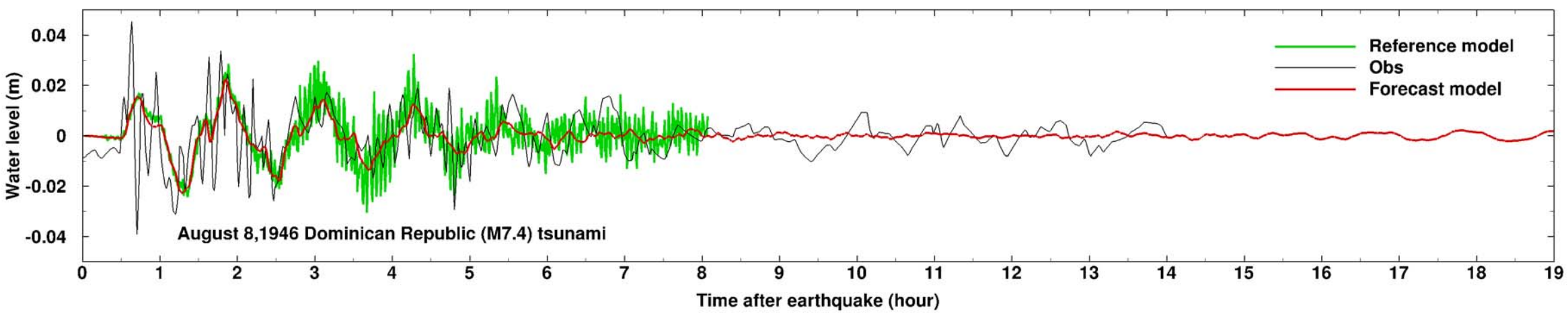
Water level (m)
0.04
0.02
0
-0.02
-0.04
0
1
2
3
4
5
6
7
8
9
10
11
12
13
14
15
16
17
18
19
Time after earthquake (hour)
Reference model
Obs
Forecast model
August 8,1946 Dominican Republic (M7.4) tsunami

(f)

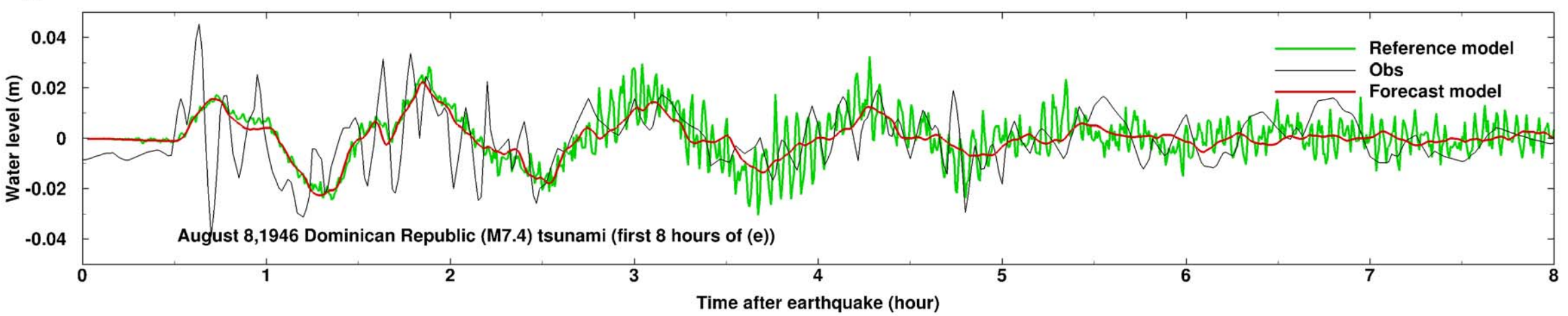
Water level (m)
0.04
0.02
0
-0.02
-0.04
0
1
2
3
4
5
6
7
8
Time after earthquake (hour)
Reference model
Obs
Forecast model
August 8,1946 Dominican Republic (M7.4) tsunami (first 8 hours of (e))

(a)

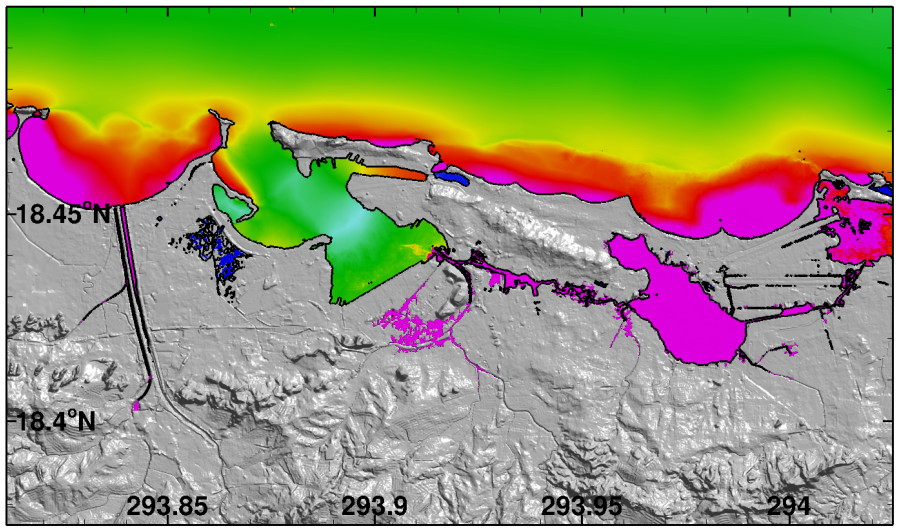

(b)

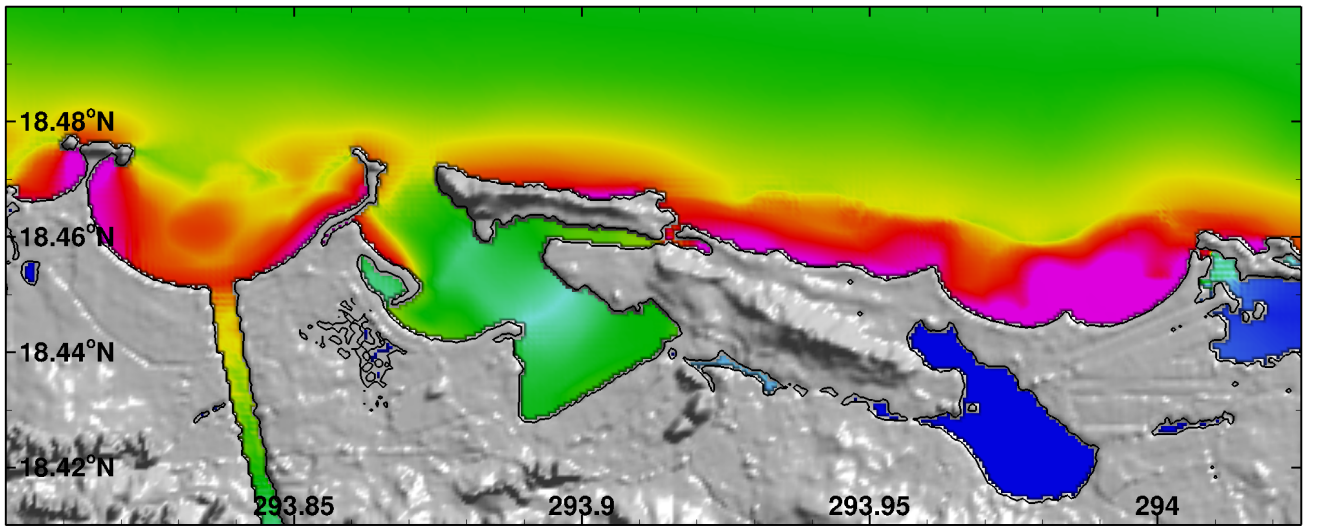

(c)

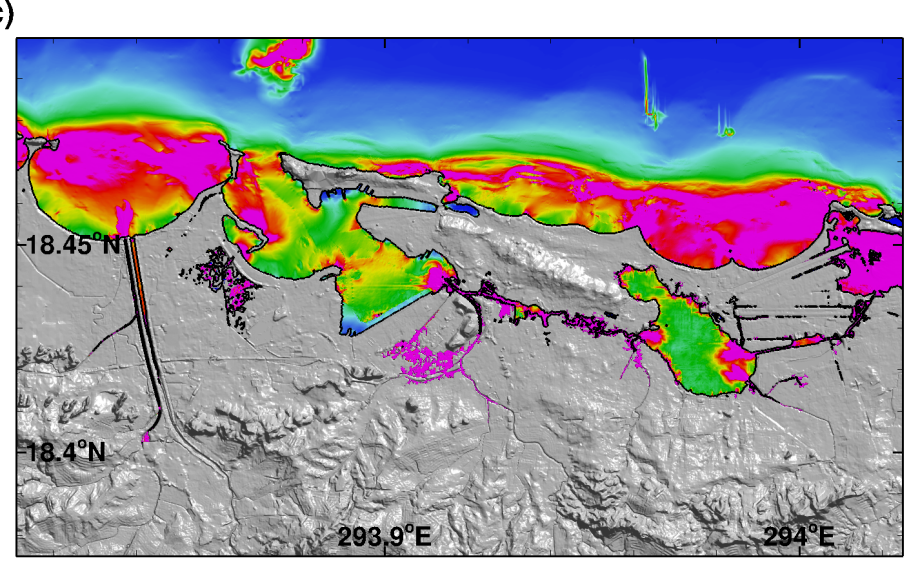

(d)

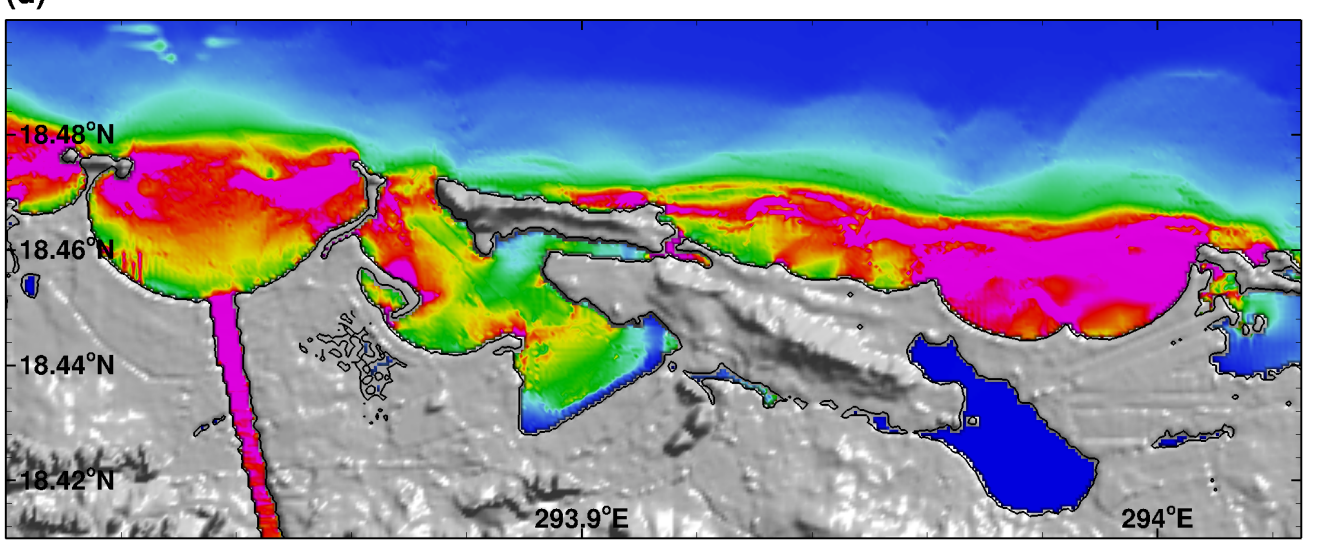

Water level (m)
or flow speed (m/s)

0 0.02 0.04 0.06 0.08 0.1 0.12 0.14 0.16 0.18 0.2 0.22 0.24 0.26 0.28 0.3

(e)

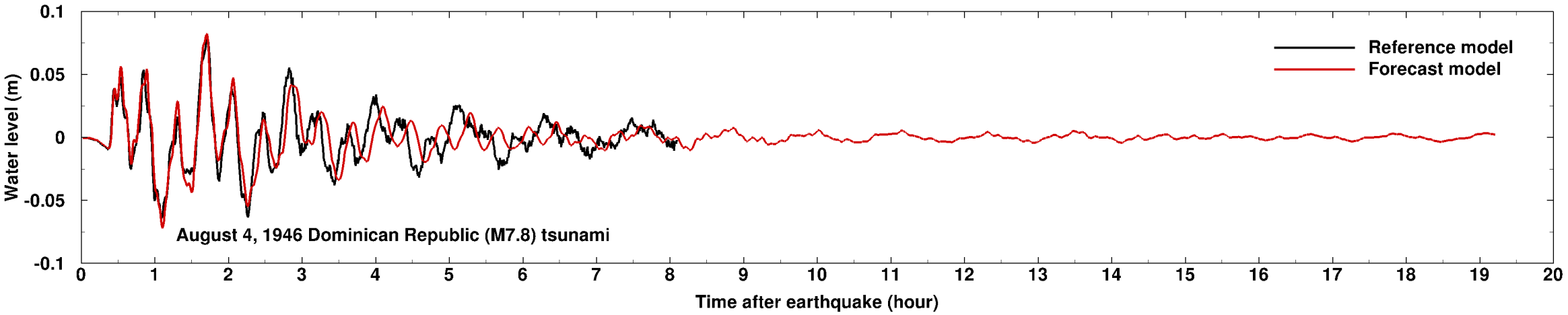

(f)

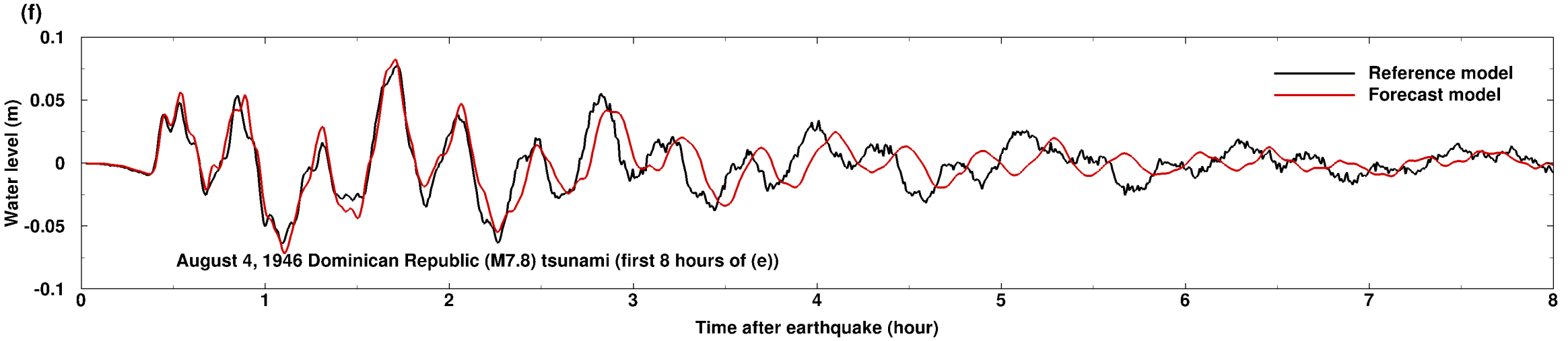

(a)

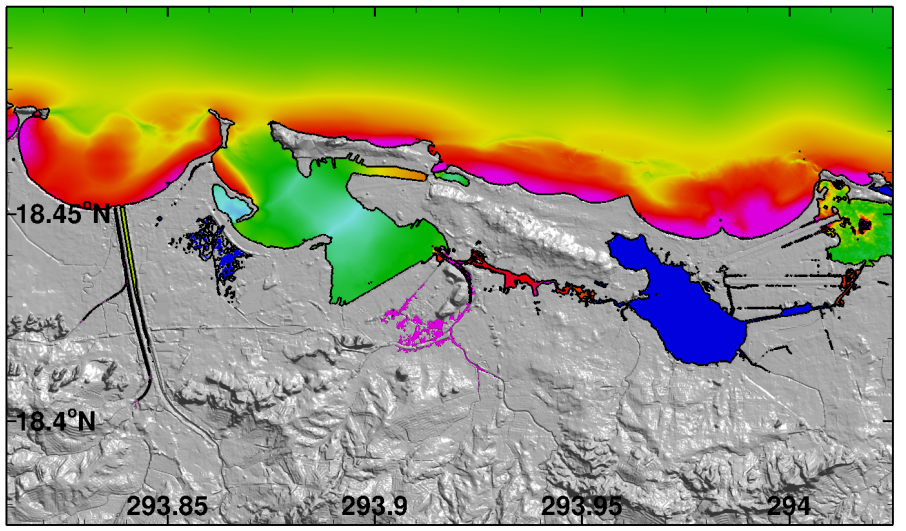

(b)

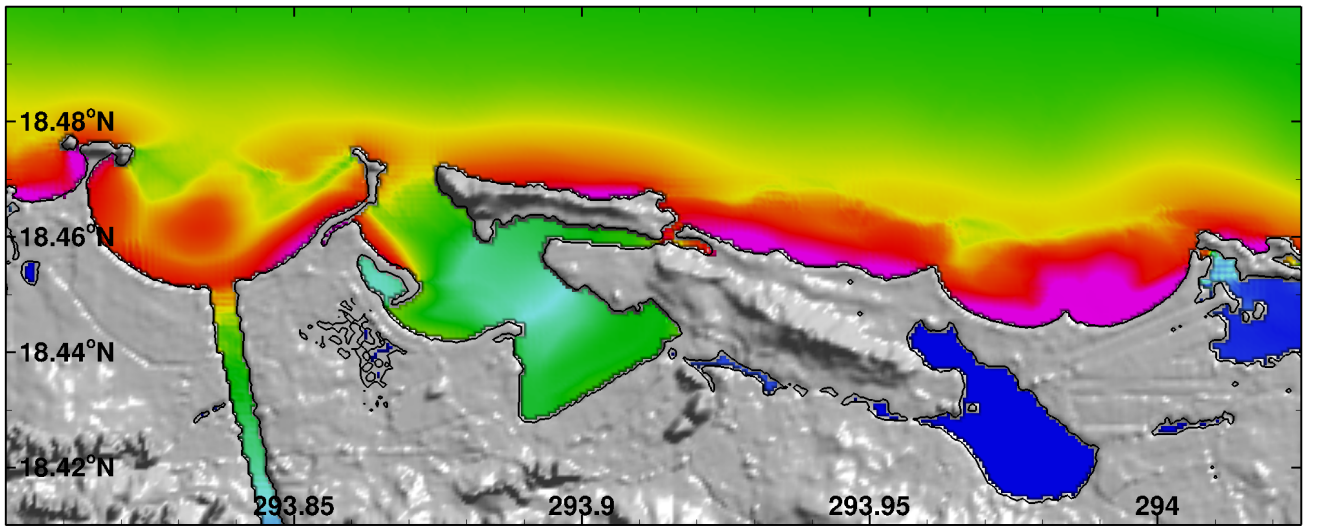

(c)

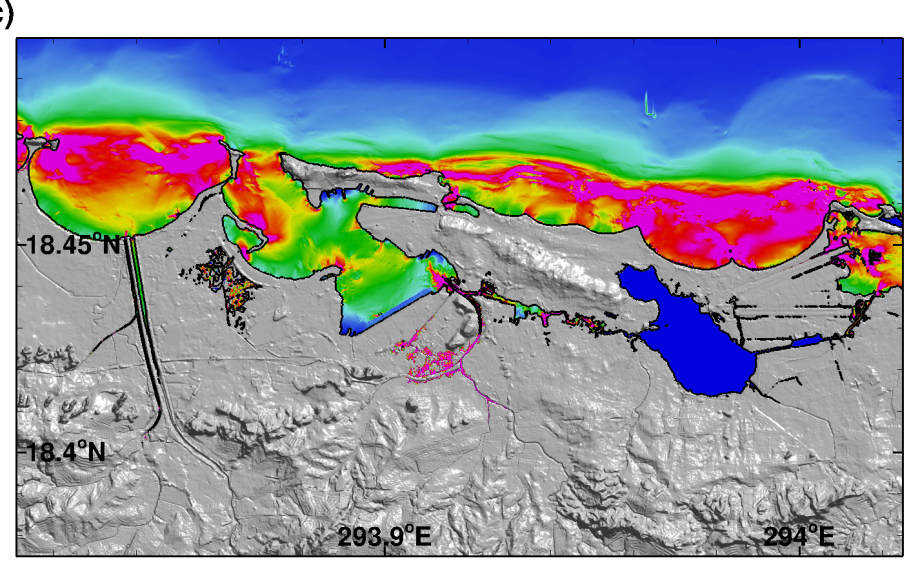

(d)

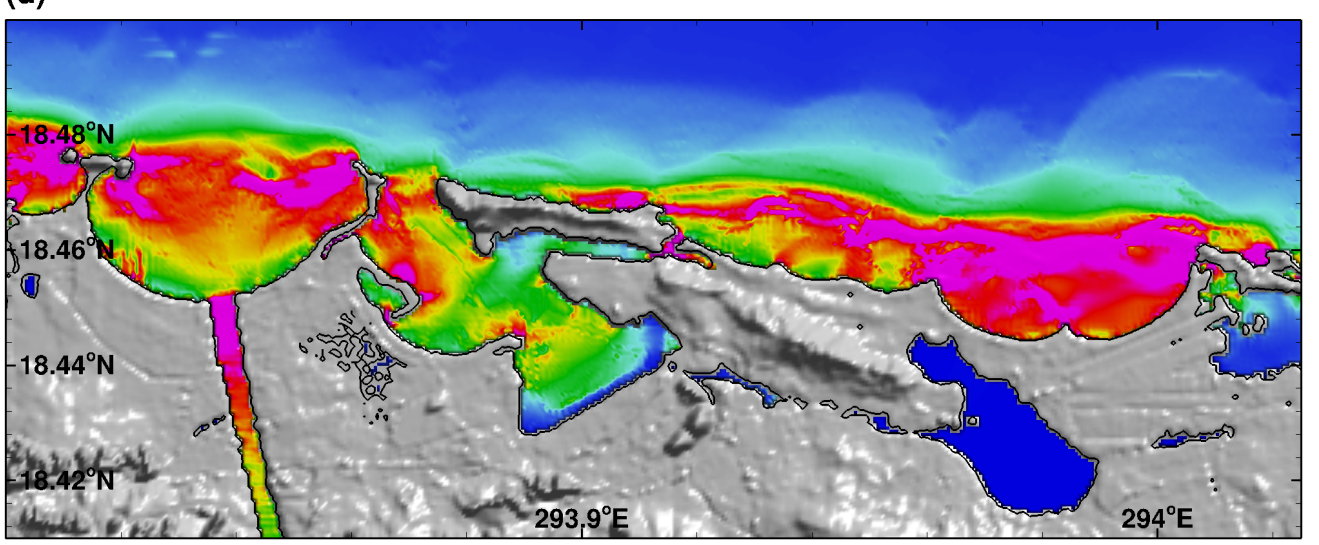

Water level (m)
or flow speed (m/s)

0 0.05 0.1 0.15 0.2 0.25 0.3 0.35 0.4 0.45 0.5 0.55 0.6 0.65 0.7 0.75 0.8

(e)

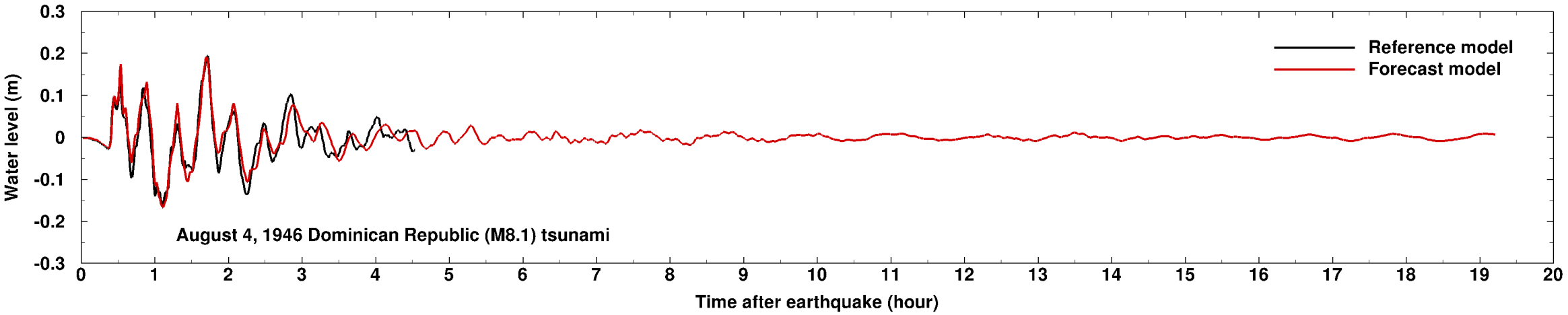

(f)

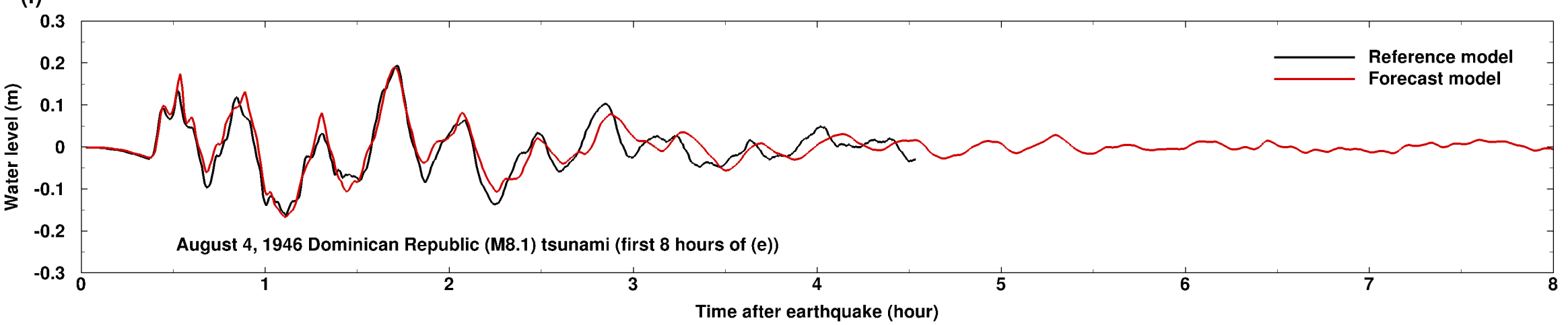

60
40
20
0
-20
-40
-60
-100
-80
-60
-40
-20
0
η_{max} (m)
1.0
0.9
0.8
0.7
0.6
0.5
0.4
0.3
0.2
0.1
0.0

(a)

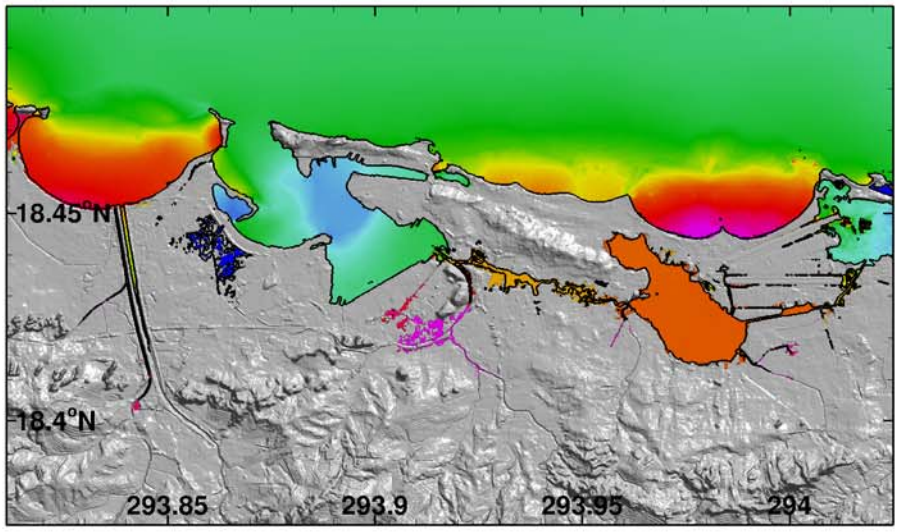
18.45°N
18.4°N
293.85
293.9
293.95
294

(b)

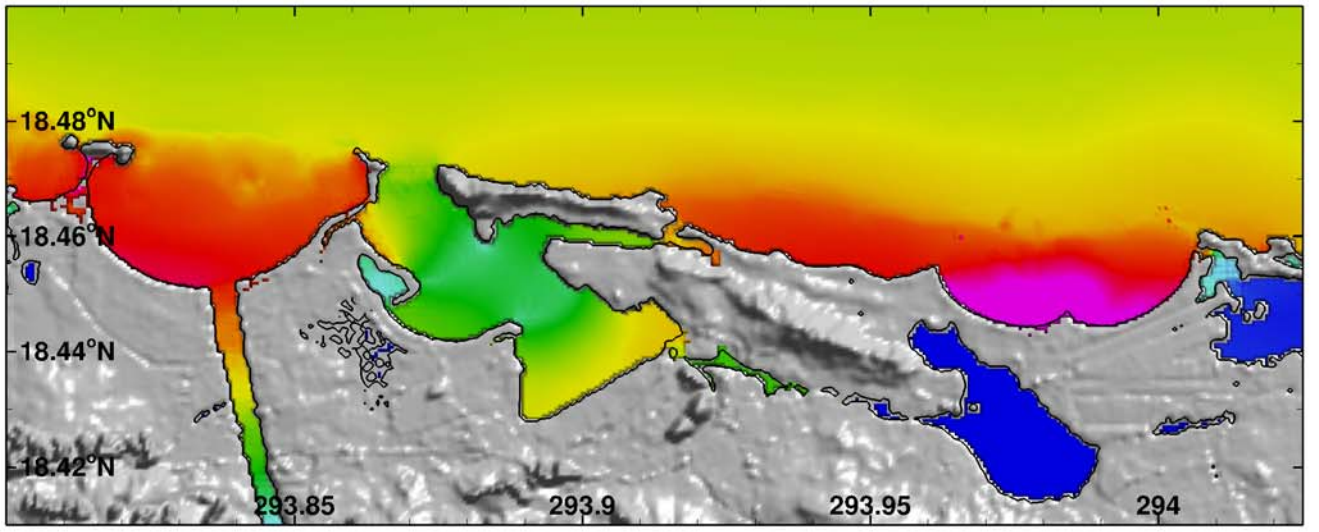
18.48°N
18.46°N
18.44°N
18.42°N
293.85
293.9
293.95
294

(c)

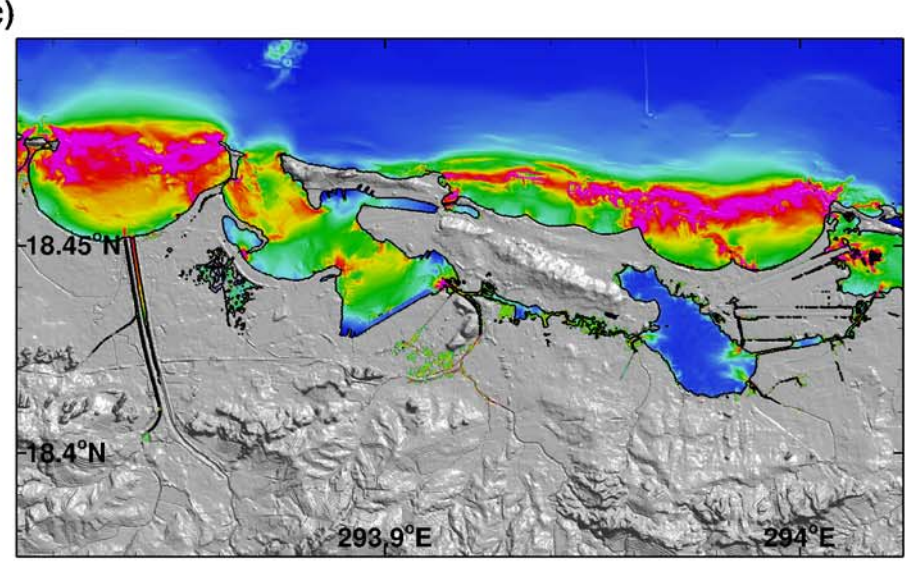
18.45°N
18.4°N
293.9°E
294°E

(d)

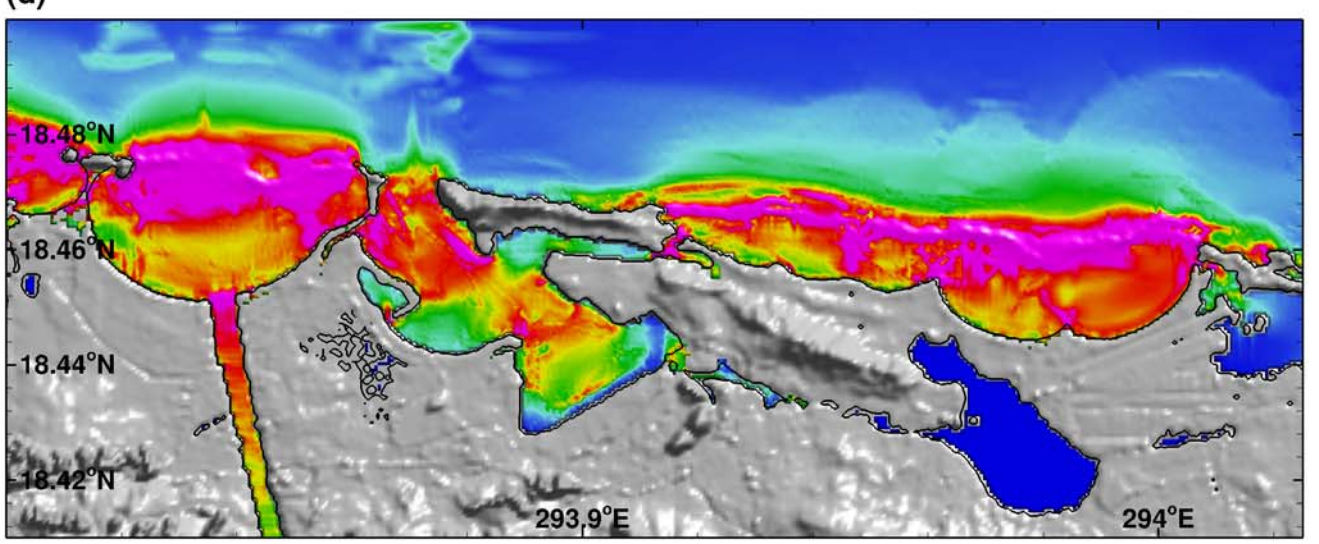
18.48°N
18.46°N
18.44°N
18.42°N
293.9°E
294°E

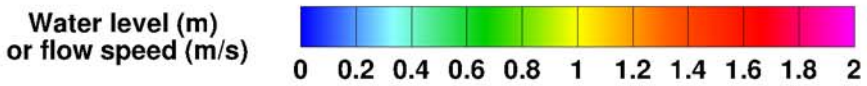
Water level (m)
or flow speed (m/s)
0 0.2 0.4 0.6 0.8 1 1.2 1.4 1.6 1.8 2

(e)

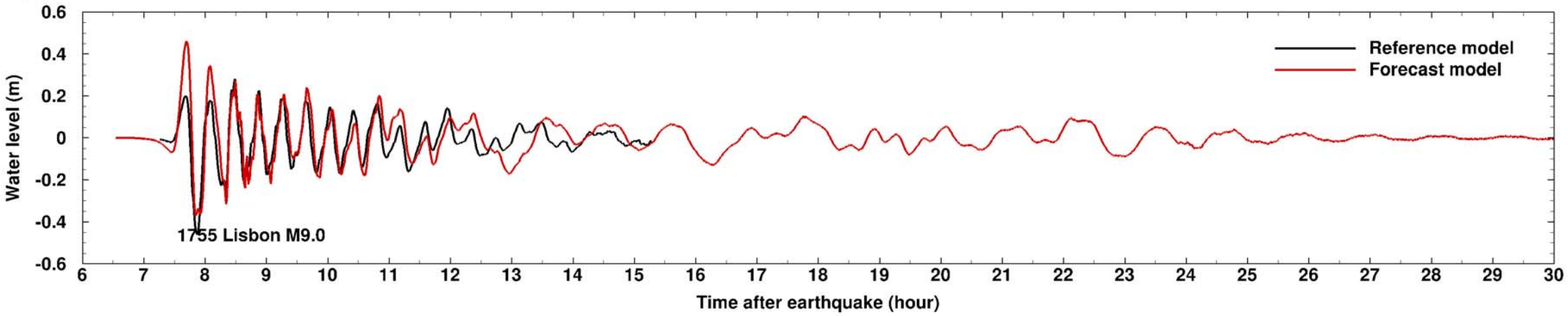
Water level (m)
0.6
0.4
0.2
0
-0.2
-0.4
-0.6
6 7 8 9 10 11 12 13 14 15 16 17 18 19 20 21 22 23 24 25 26 27 28 29 30
Time after earthquake (hour)
Reference model
Forecast model
1755 Lisbon M9.0

(f)

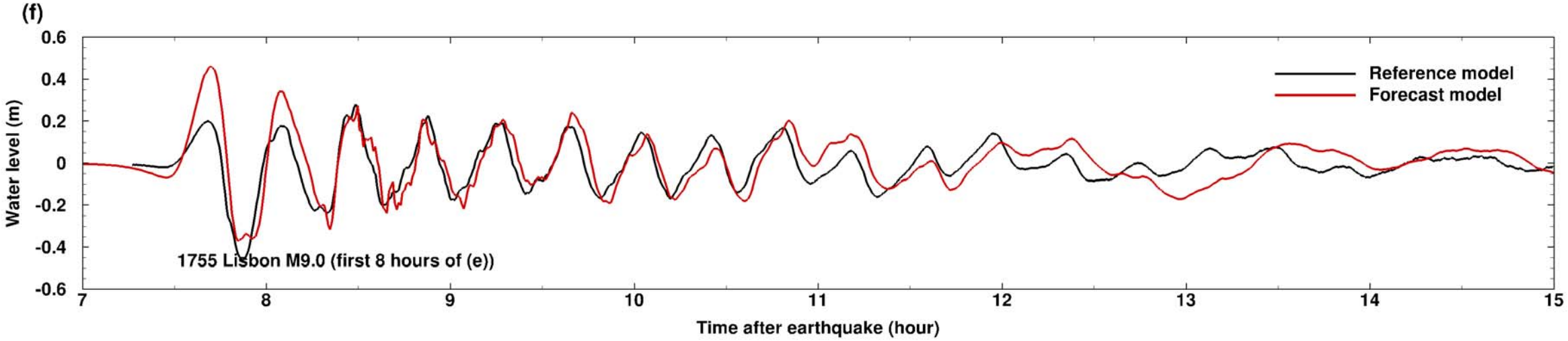
Water level (m)
0.6
0.4
0.2
0
-0.2
-0.4
-0.6
7 8 9 10 11 12 13 14 15
Time after earthquake (hour)
Reference model
Forecast model
1755 Lisbon M9.0 (first 8 hours of (e))

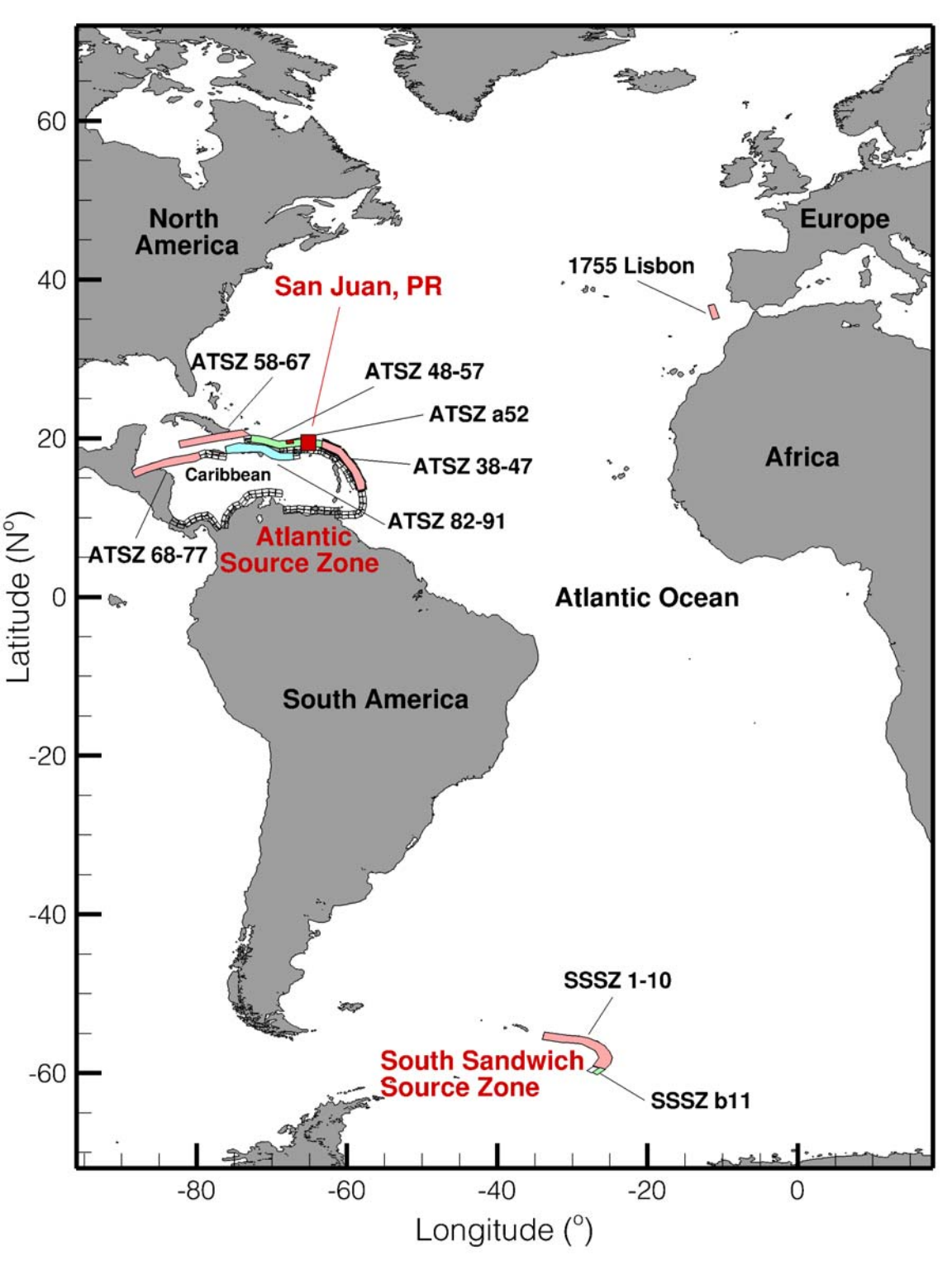
North America
Europe
Africa
South America
Atlantic Ocean
San Juan, PR
1755 Lisbon
ATSZ 58-67
ATSZ 48-57
ATSZ a52
ATSZ 38-47
ATSZ 82-91
ATSZ 68-77
Caribbean
Atlantic Source Zone
SSSZ 1-10
South Sandwich Source Zone
SSSZ b11
60
40
20
0
-20
-40
-60
-80
-60
-40
-20
0
Latitude (N°)
Longitude (°)

(a)

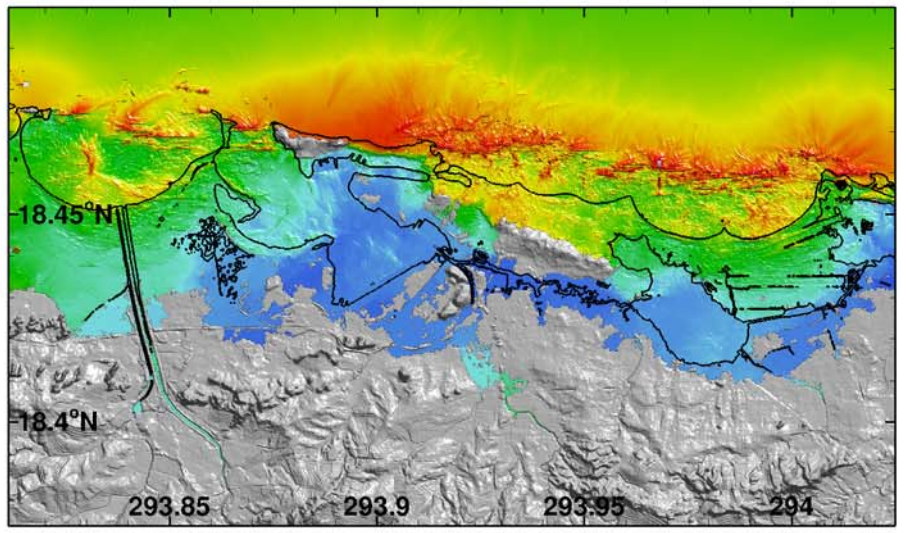
18.45°N
18.4°N
293.85
293.9
293.95
294

(b)

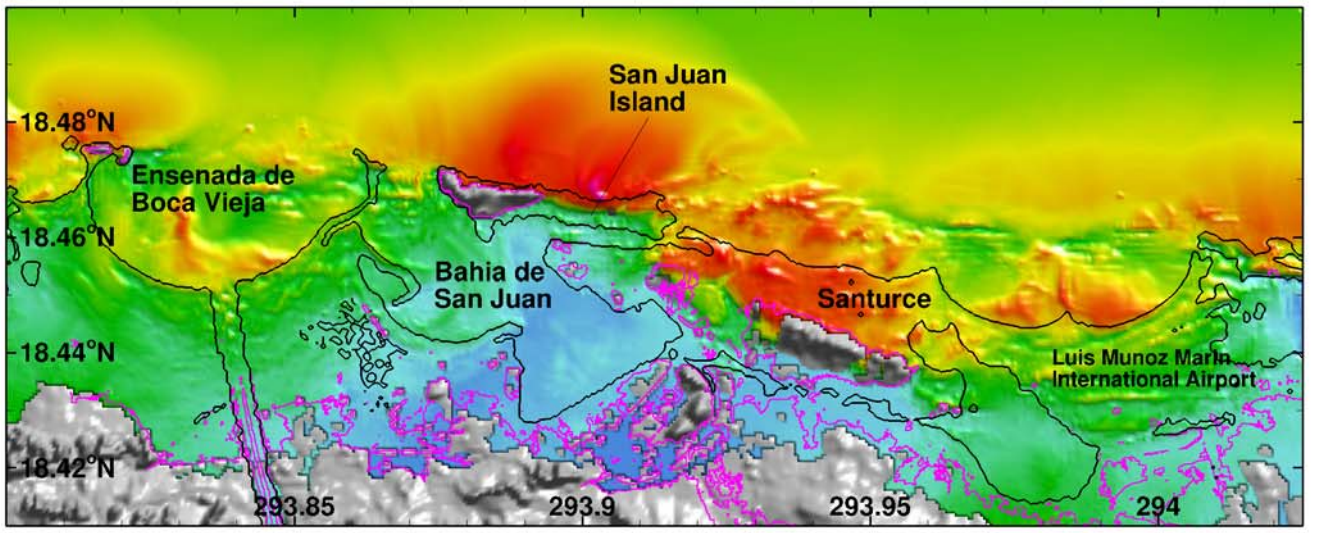
San Juan
Island
18.48°N
Ensenada de
Boca Vieja
18.46°N
Bahia de
San Juan
Santurce
18.44°N
Luis Munoz Marin
International Airport
18.42°N
293.85
293.9
293.95
294

(c)

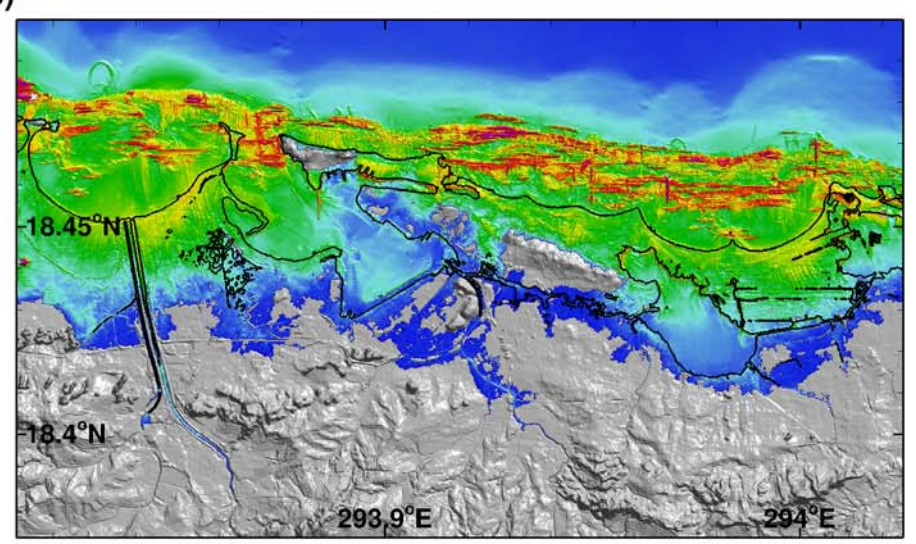
18.45°N
18.4°N
293.9°E
294°E

(d)

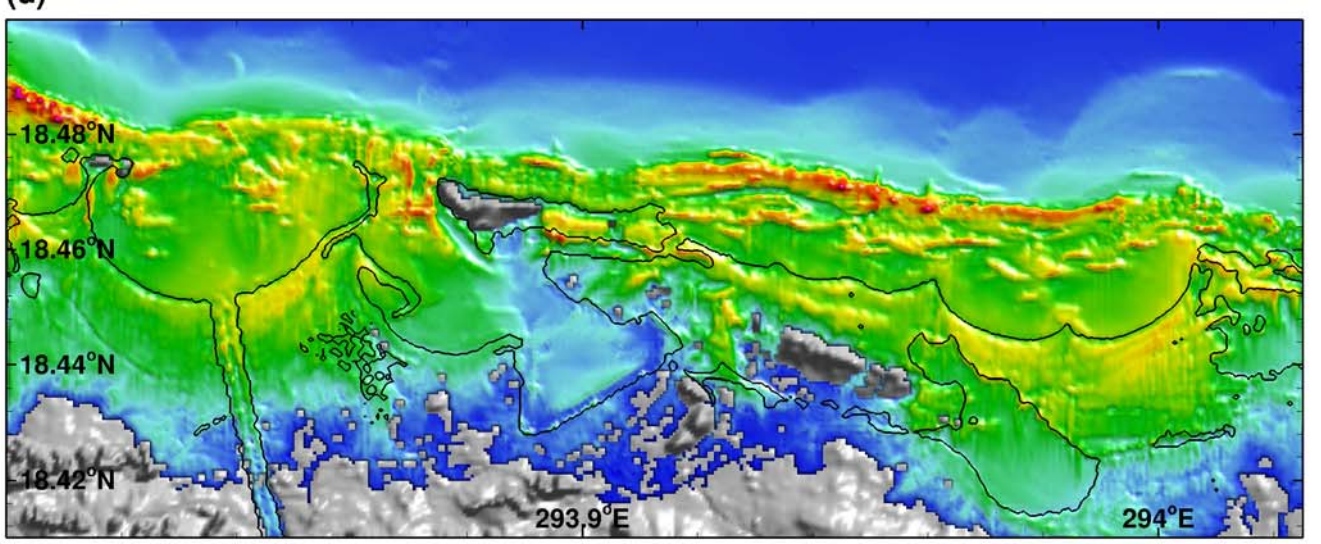
18.48°N
18.46°N
18.44°N
18.42°N
293.9°E
294°E


Water level (m)
or flow speed (m/s)
0 2 4 6 8 10 12 14 16 18 20 22 24 26 28 30

(e)

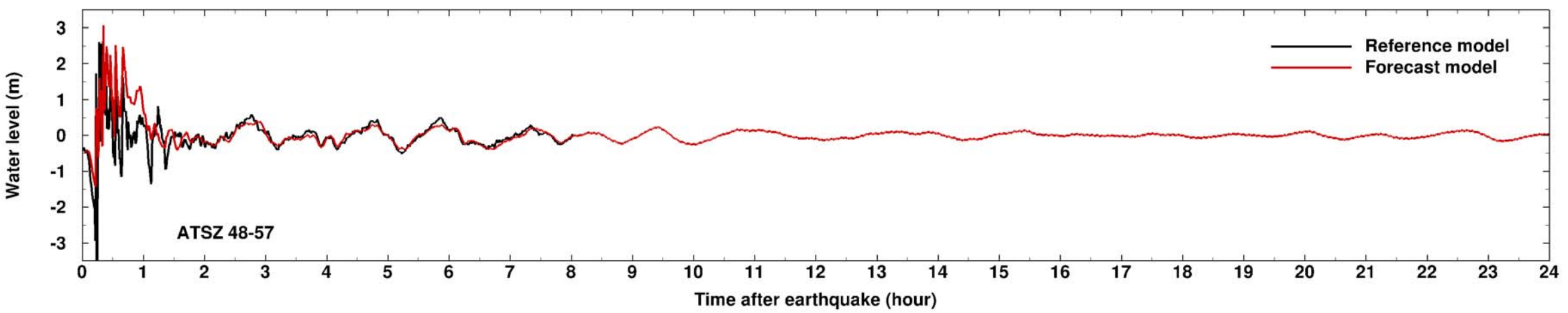
Water level (m)
Reference model
Forecast model
ATSZ 48-57
Time after earthquake (hour)

(f)

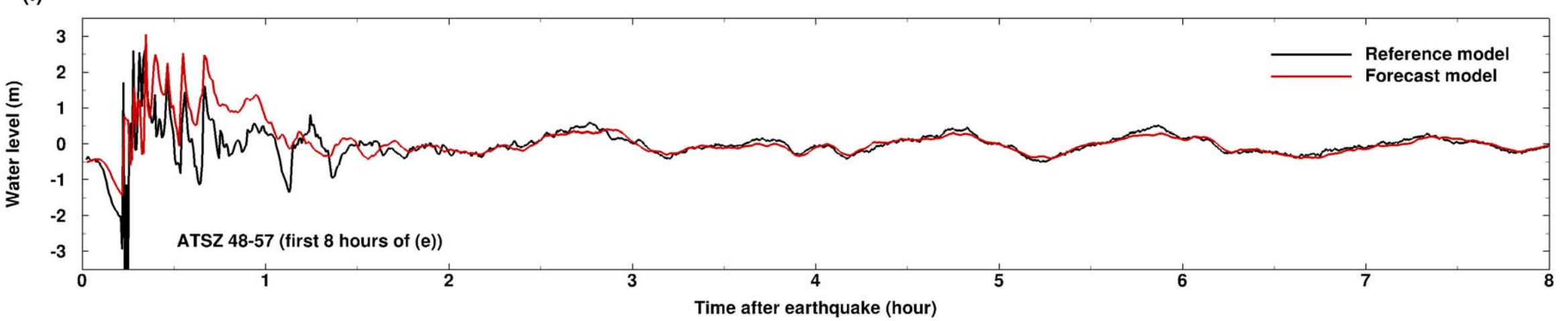
Water level (m)
Reference model
Forecast model
ATSZ 48-57 (first 8 hours of (e))
Time after earthquake (hour)

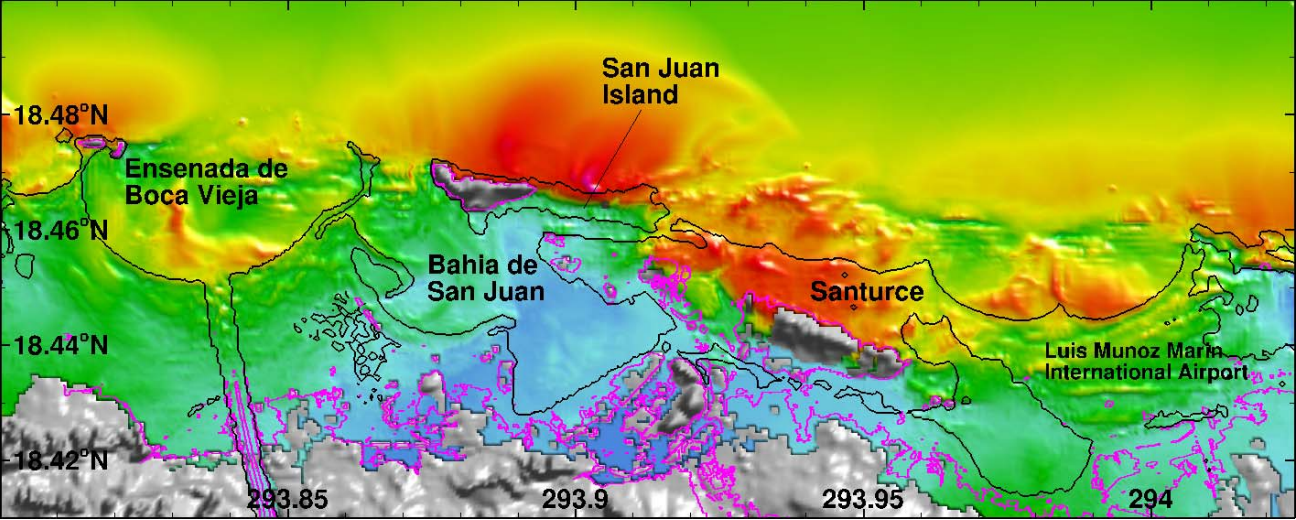
San Juan
Island
18.48°N
Ensenada de
Boca Vieja
18.46°N
Bahia de
San Juan
Santurce
18.44°N
Luis Munoz Marin
International Airport
18.42°N
293.85
293.9
293.95
294

(a)

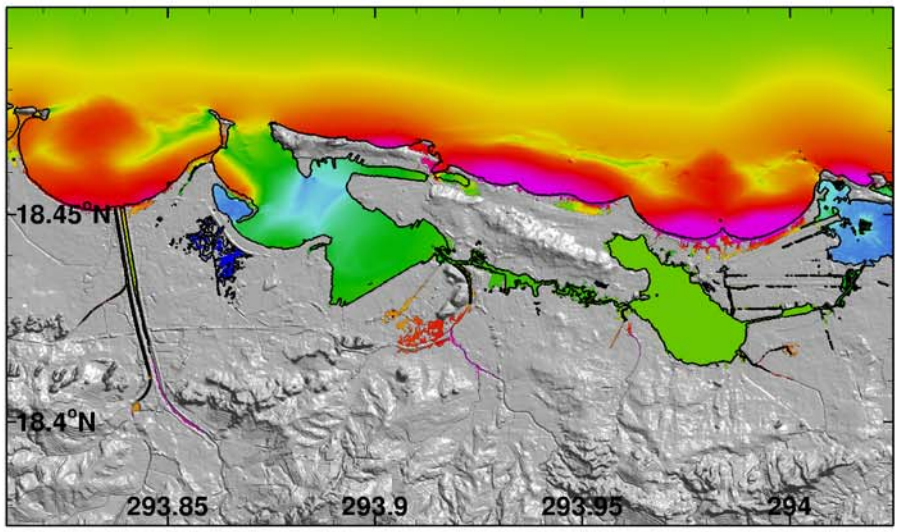
18.45°N
18.4°N
293.85
293.9
293.95
294

(b)

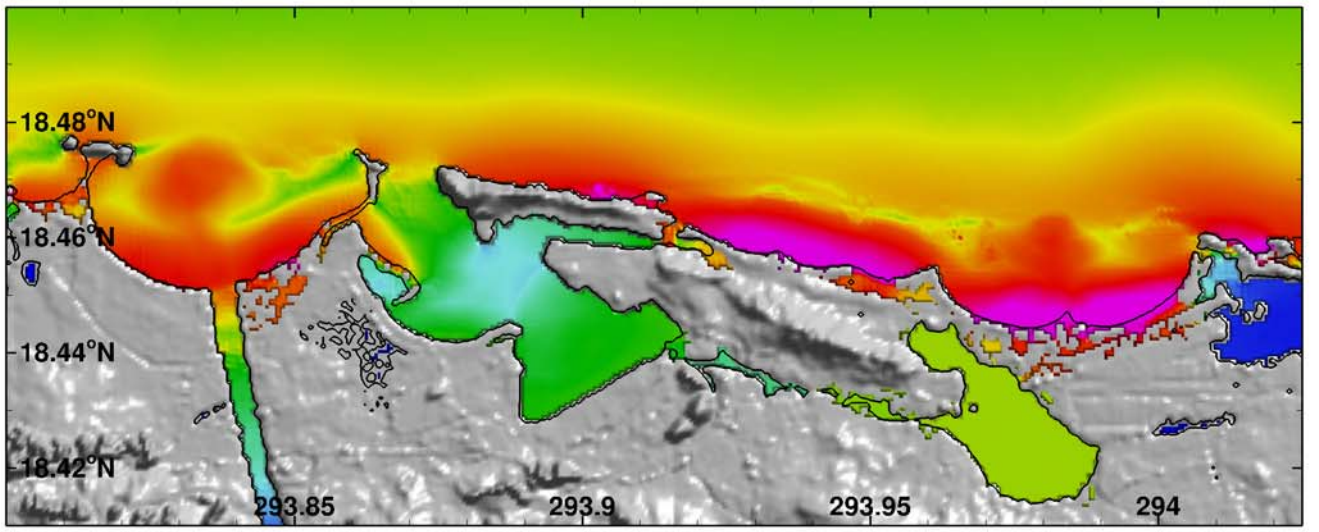
18.48°N
18.46°N
18.44°N
18.42°N
293.85
293.9
293.95
294

(c)

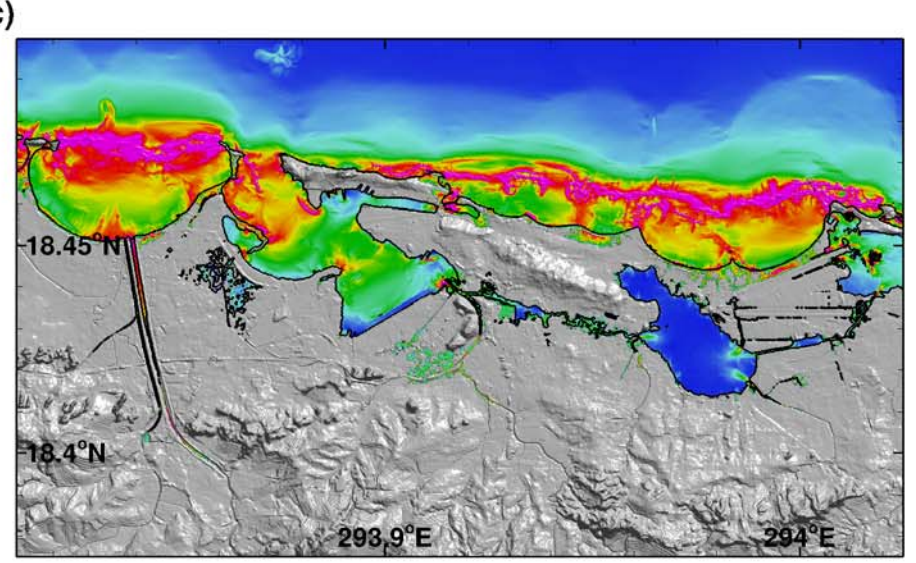
18.45°N
18.4°N
293.9°E
294°E

(d)

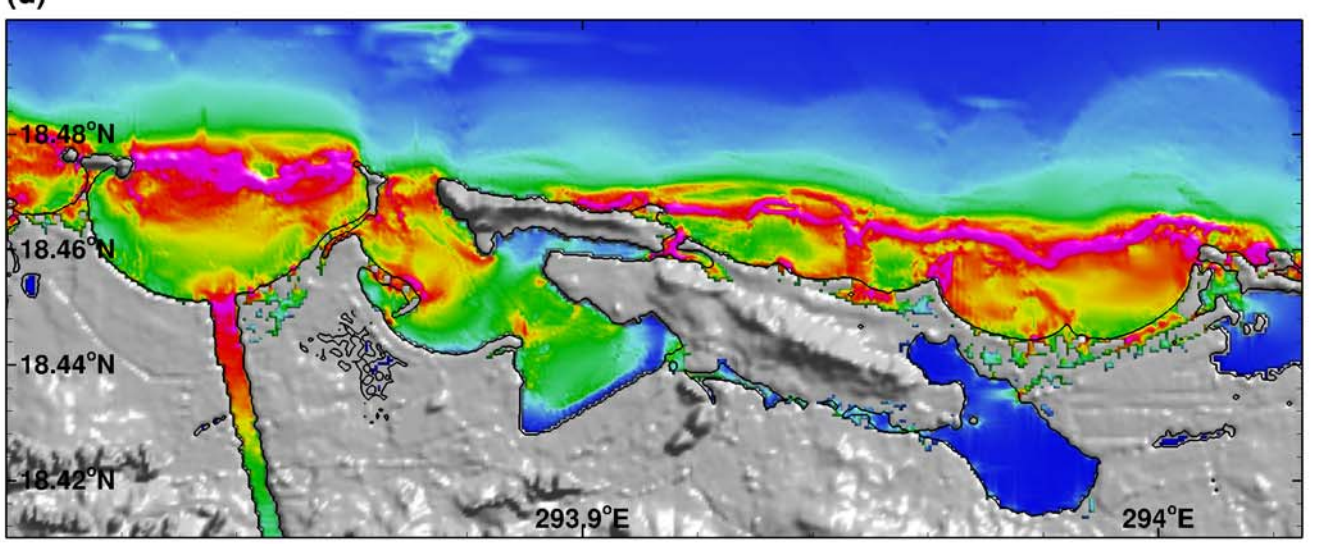
18.48°N
18.46°N
18.44°N
18.42°N
293.9°E
294°E


Water level (m)
or flow speed (m/s)
0 0.2 0.4 0.6 0.8 1 1.2 1.4 1.6 1.8 2 2.2 2.4 2.6 2.8 3

(e)

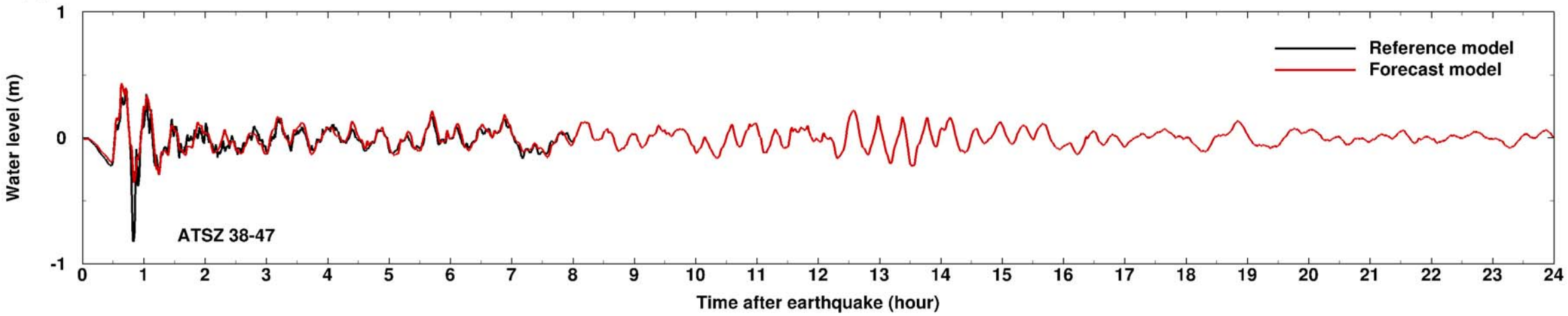
Water level (m)
Time after earthquake (hour)
Reference model
Forecast model
ATSZ 38-47

(f)

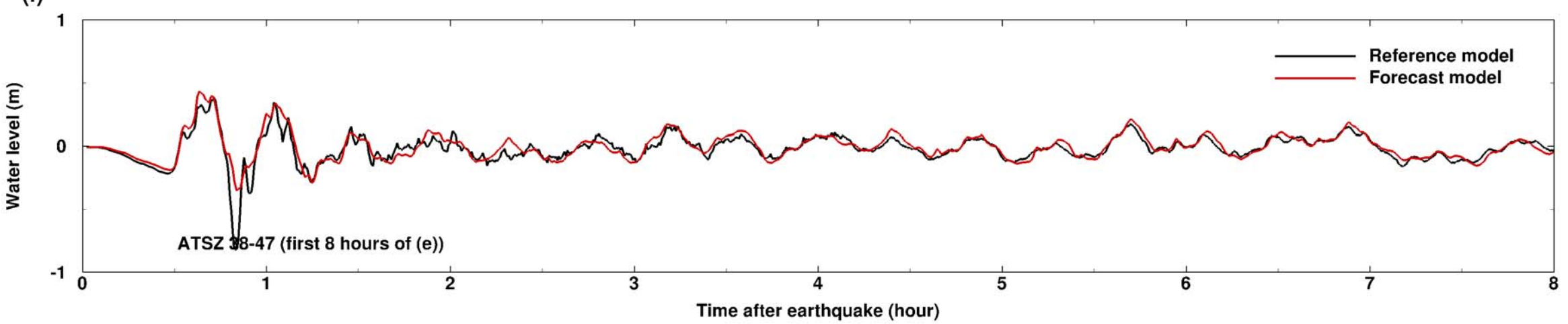
Water level (m)
Time after earthquake (hour)
Reference model
Forecast model
ATSZ 38-47 (first 8 hours of (e))

(a)

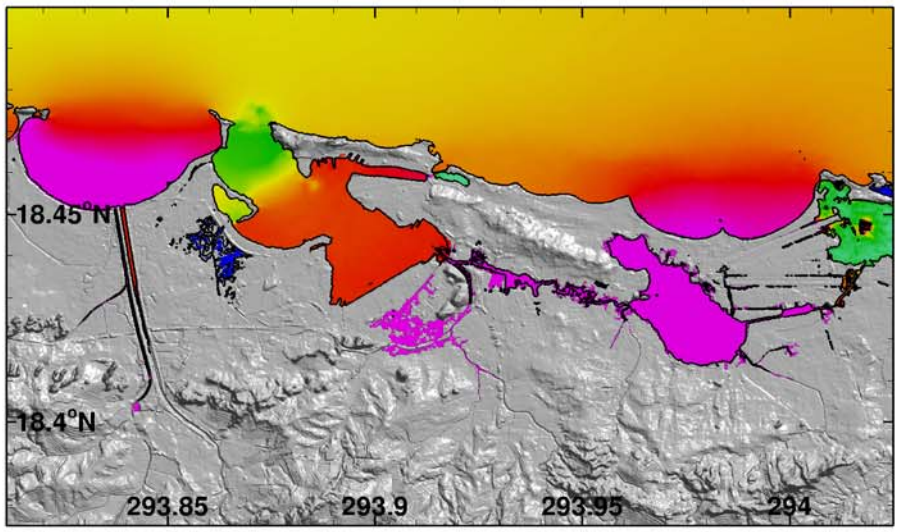
18.45°N
18.4°N
293.85
293.9
293.95
294

(b)

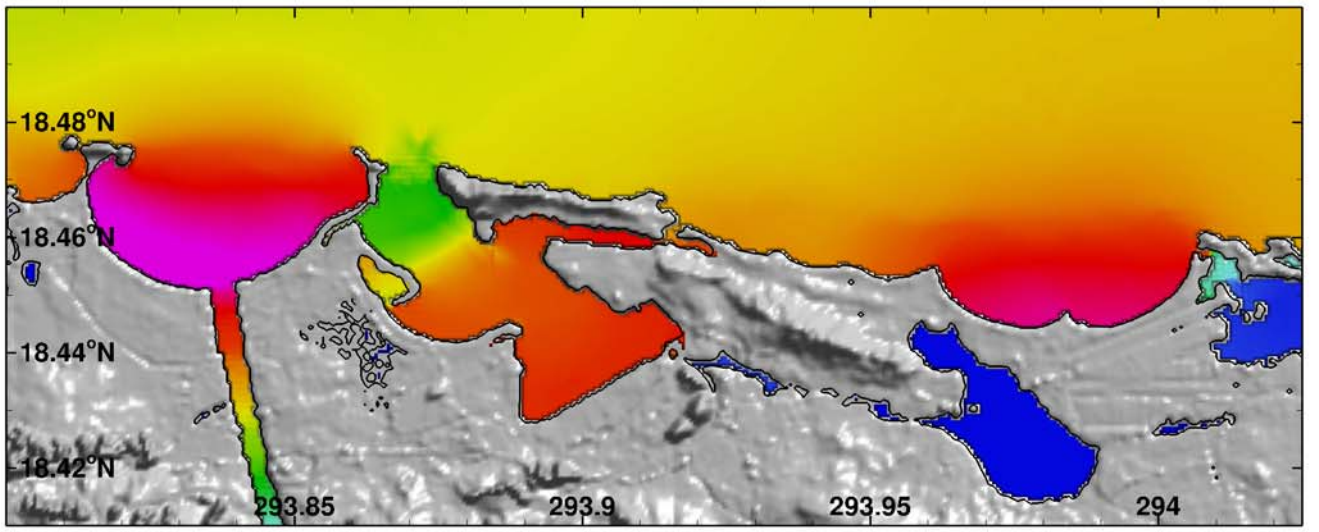
18.48°N
18.46°N
18.44°N
18.42°N
293.85
293.9
293.95
294

(c)

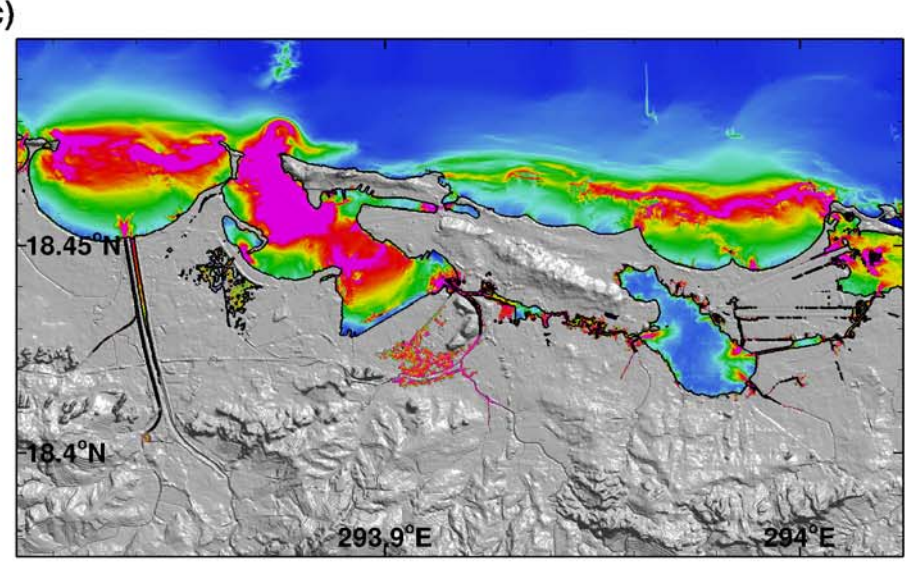
18.45°N
18.4°N
293.9°E
294°E

(d)

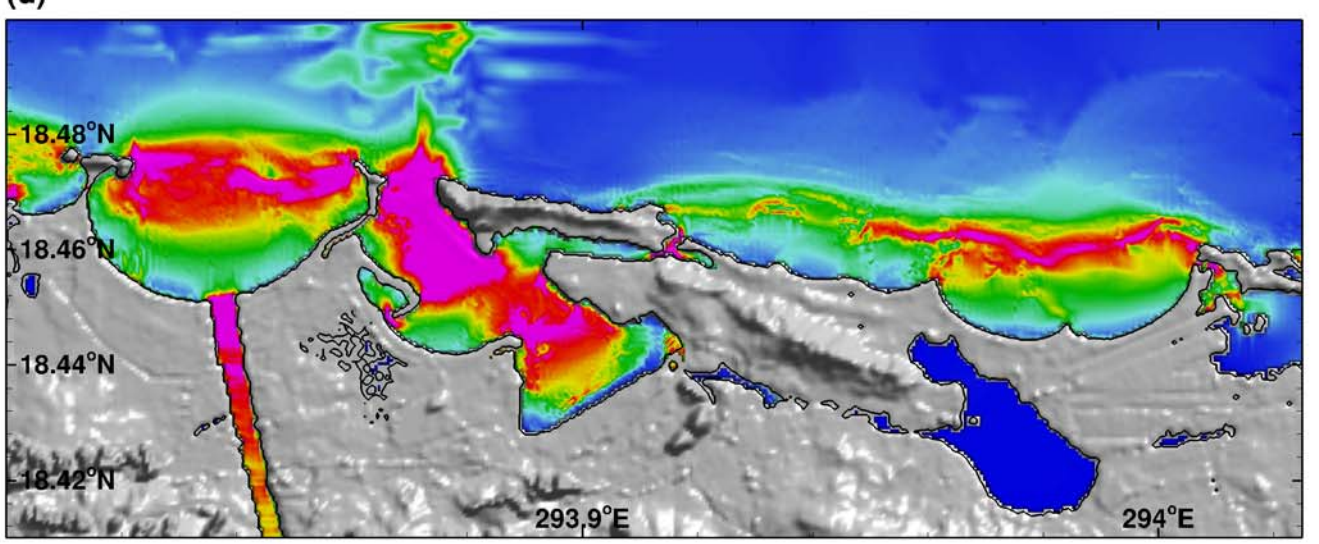
18.48°N
18.46°N
18.44°N
18.42°N
293.9°E
294°E

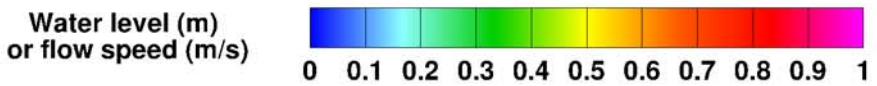
Water level (m)
or flow speed (m/s)
0 0.1 0.2 0.3 0.4 0.5 0.6 0.7 0.8 0.9 1

(e)

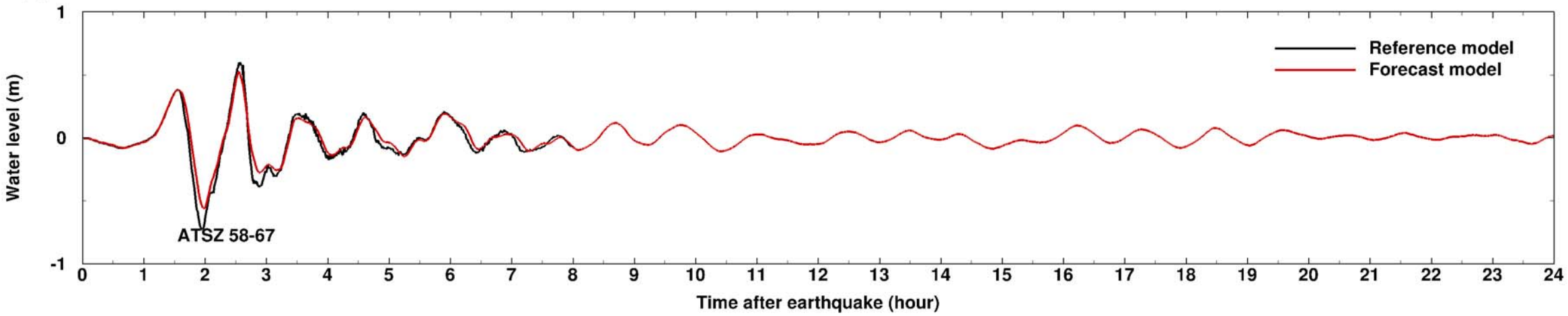
Water level (m)
1
0
-1
0 1 2 3 4 5 6 7 8 9 10 11 12 13 14 15 16 17 18 19 20 21 22 23 24
Time after earthquake (hour)
Reference model
Forecast model
ATSZ 58-67

(f)

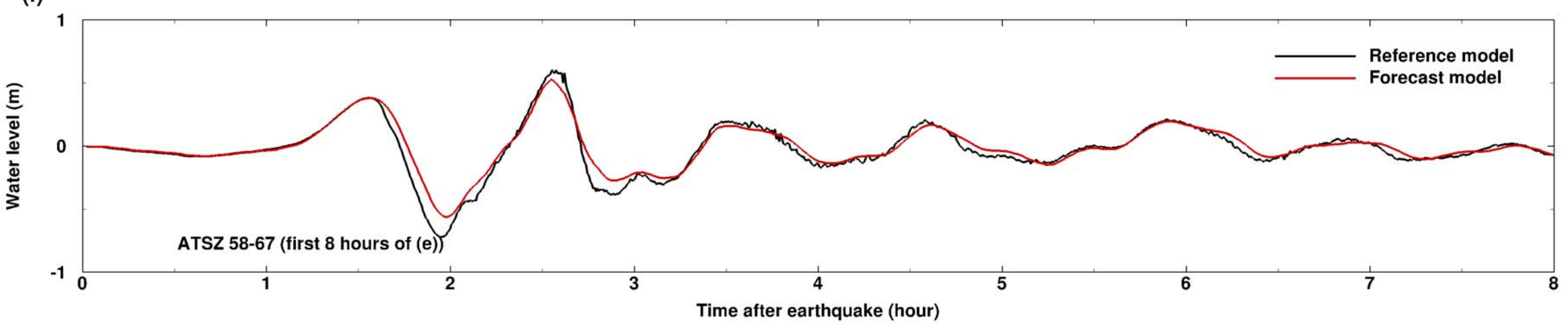
Water level (m)
1
0
-1
0 1 2 3 4 5 6 7 8
Time after earthquake (hour)
Reference model
Forecast model
ATSZ 58-67 (first 8 hours of (e))

(a)

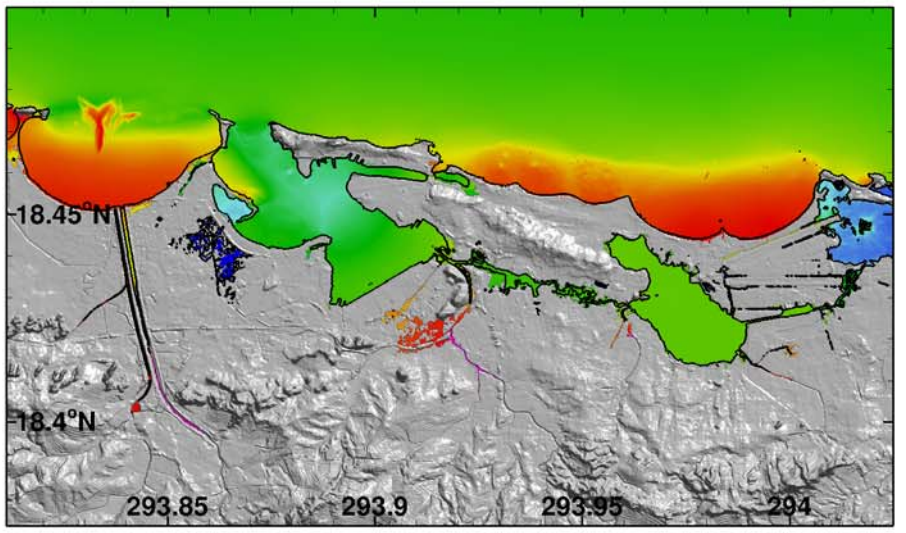
18.45°N
18.4°N
293.85
293.9
293.95
294

(b)

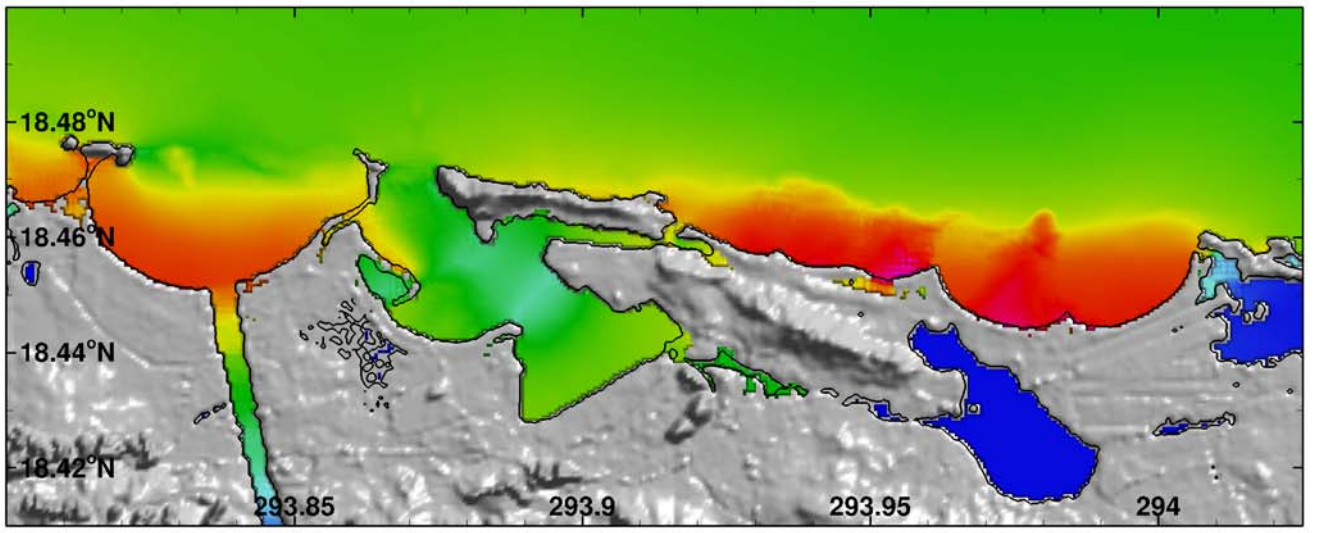
18.48°N
18.46°N
18.44°N
18.42°N
293.85
293.9
293.95
294

(c)

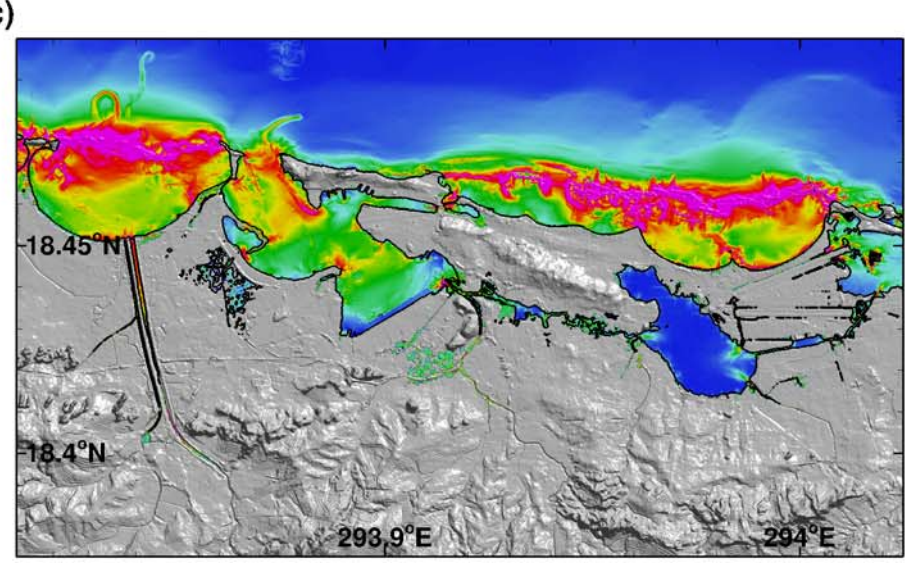
18.45°N
18.4°N
293.9°E
294°E

(d)

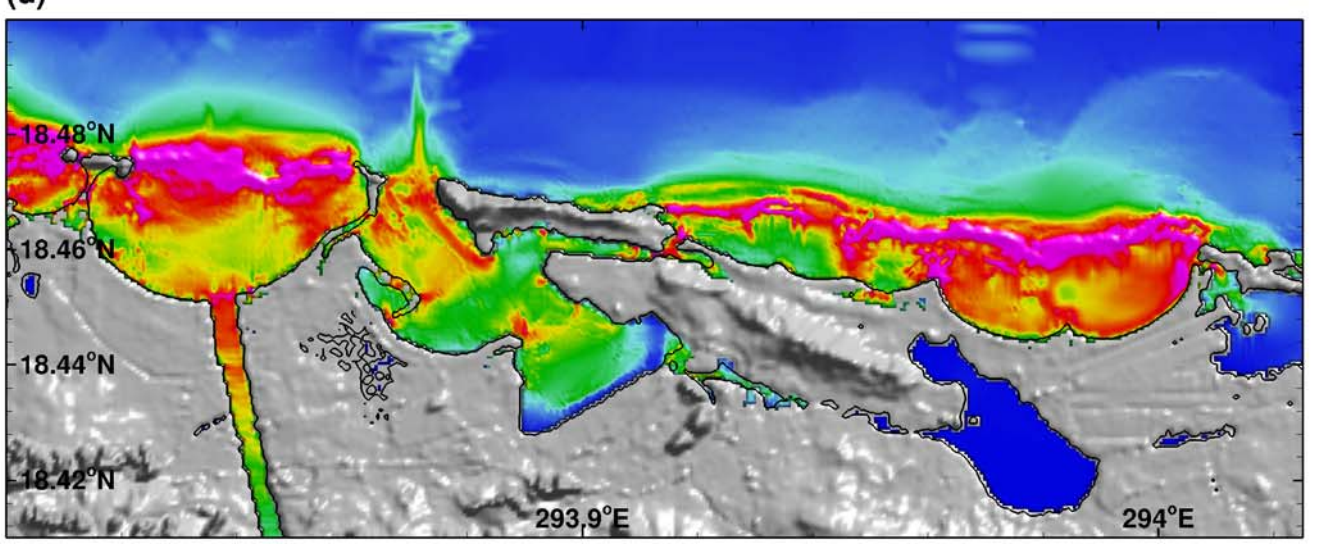
18.48°N
18.46°N
18.44°N
18.42°N
293.9°E
294°E


Water level (m)
or flow speed (m/s)
0 0.2 0.4 0.6 0.8 1 1.2 1.4 1.6 1.8 2 2.2 2.4 2.6 2.8 3

(e)

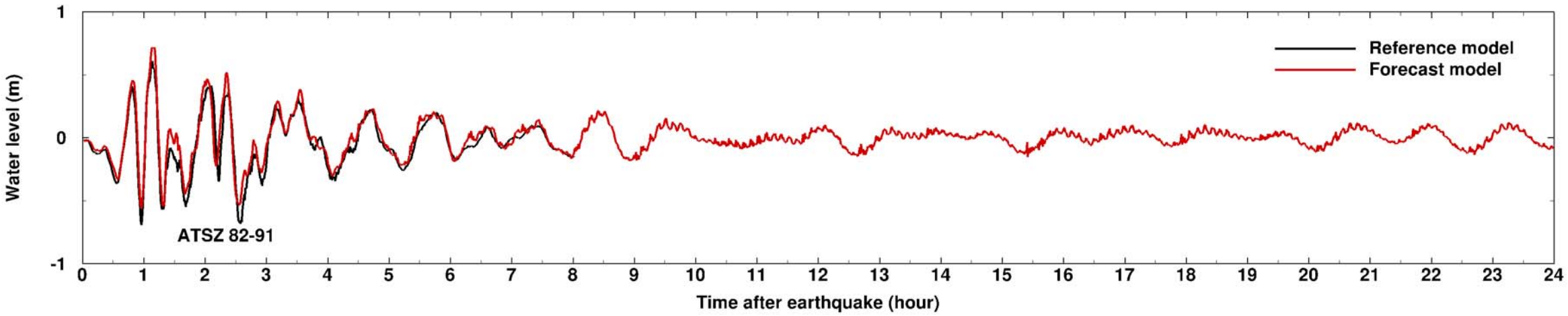
Water level (m)
Time after earthquake (hour)
Reference model
Forecast model
ATSZ 82-91

(f)

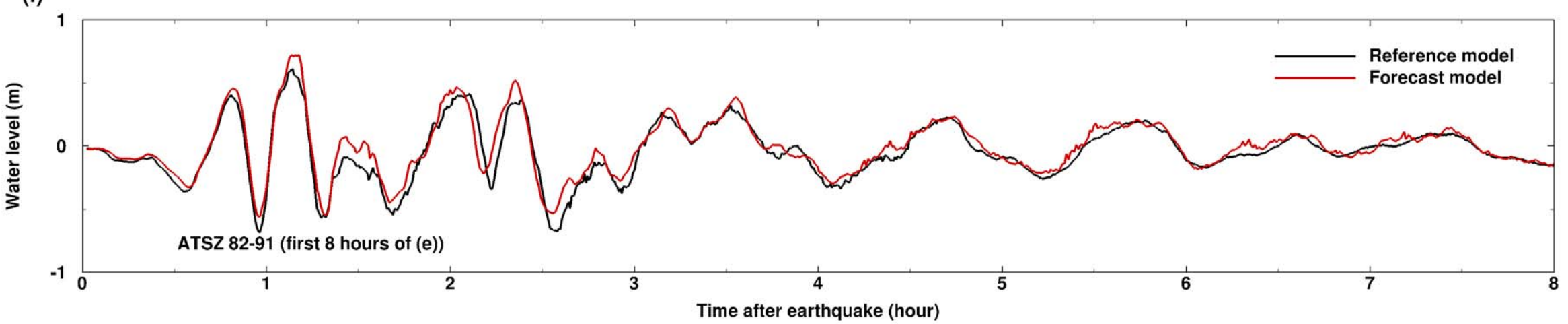
Water level (m)
Time after earthquake (hour)
Reference model
Forecast model
ATSZ 82-91 (first 8 hours of (e))

(a)

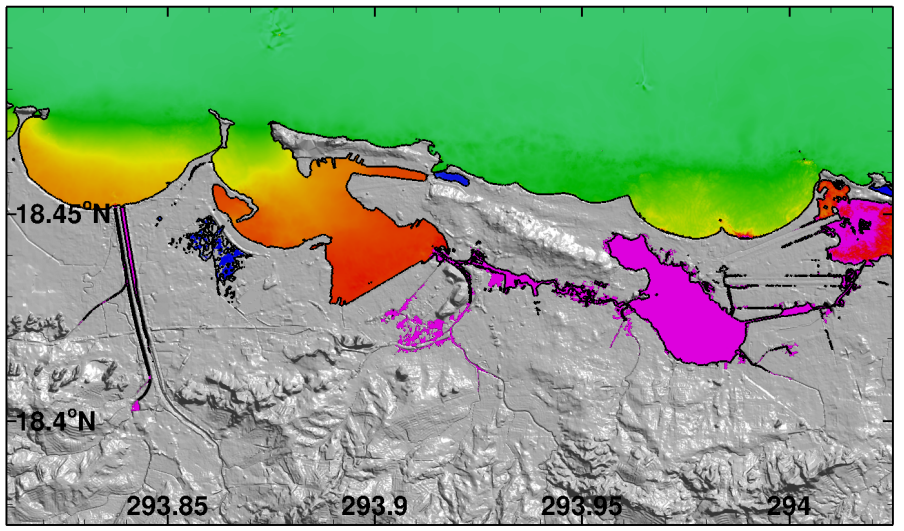
18.45°N
18.4°N
293.85
293.9
293.95
294

(b)

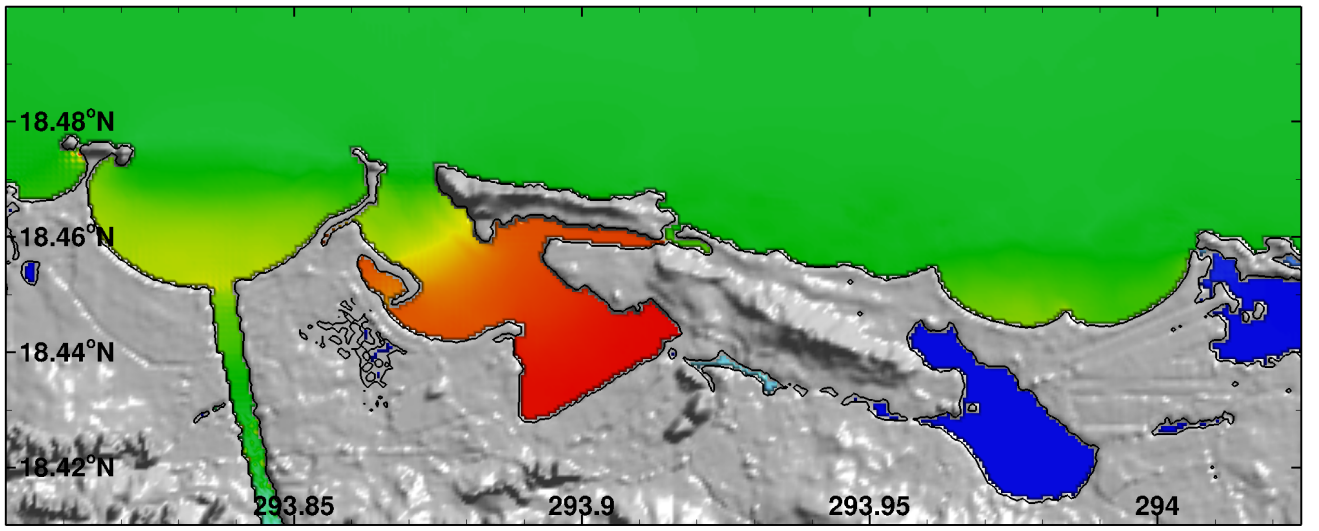
18.48°N
18.46°N
18.44°N
18.42°N
293.85
293.9
293.95
294

(c)

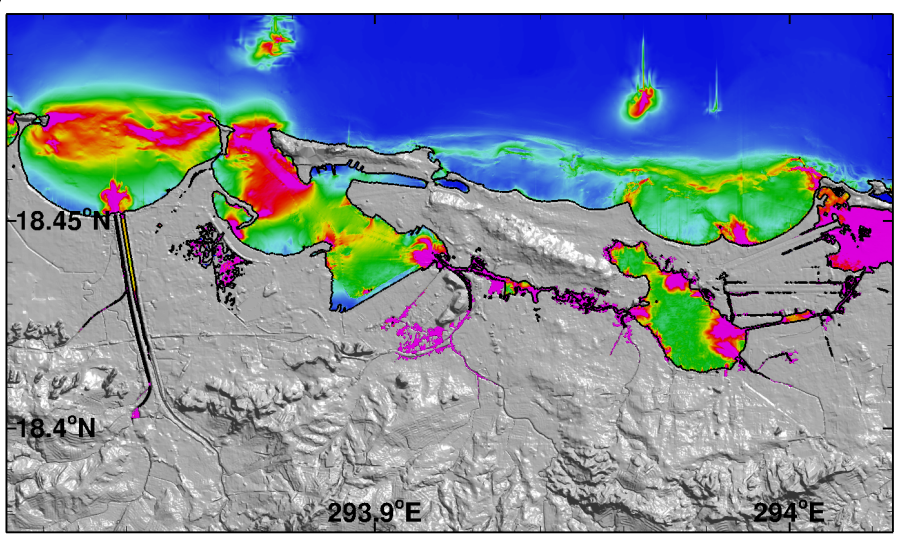
18.45°N
18.4°N
293.9°E
294°E

(d)

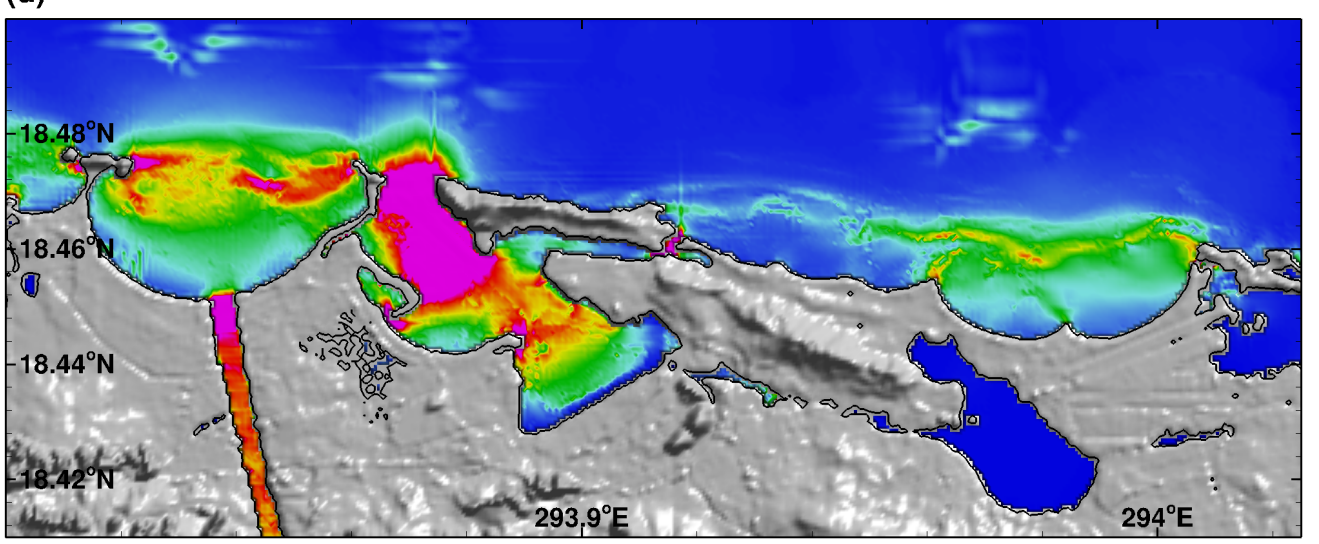
18.48°N
18.46°N
18.44°N
18.42°N
293.9°E
294°E

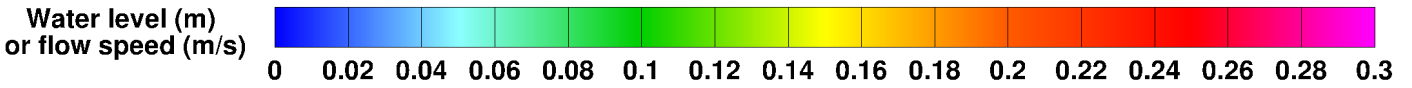
Water level (m)
or flow speed (m/s)
0 0.02 0.04 0.06 0.08 0.1 0.12 0.14 0.16 0.18 0.2 0.22 0.24 0.26 0.28 0.3

(e)

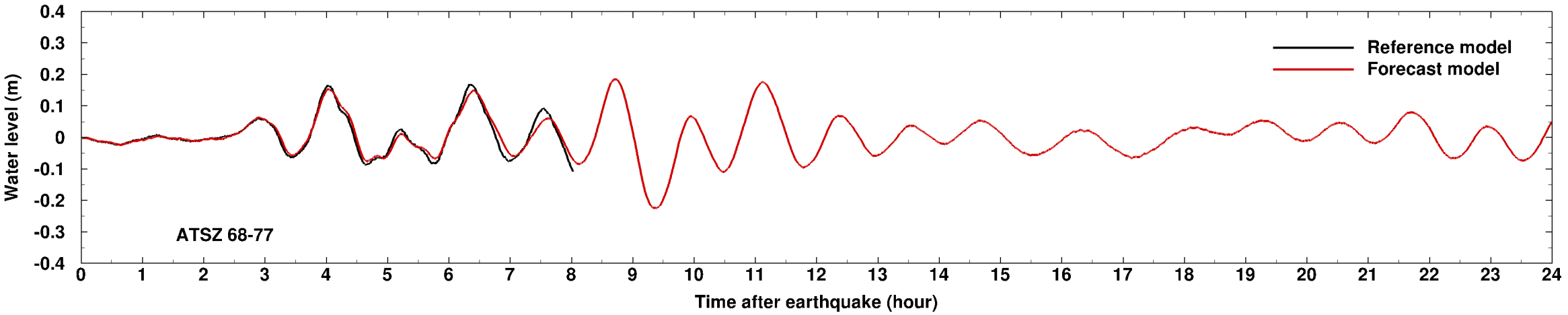
Water level (m)
Time after earthquake (hour)
Reference model
Forecast model
ATSZ 68-77

(f)

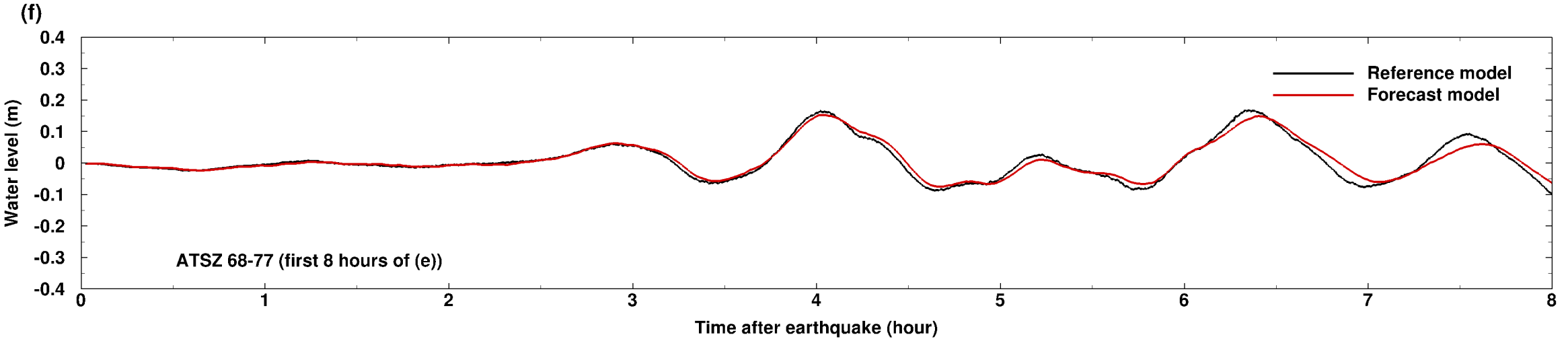
Water level (m)
Time after earthquake (hour)
Reference model
Forecast model
ATSZ 68-77 (first 8 hours of (e))

(a)

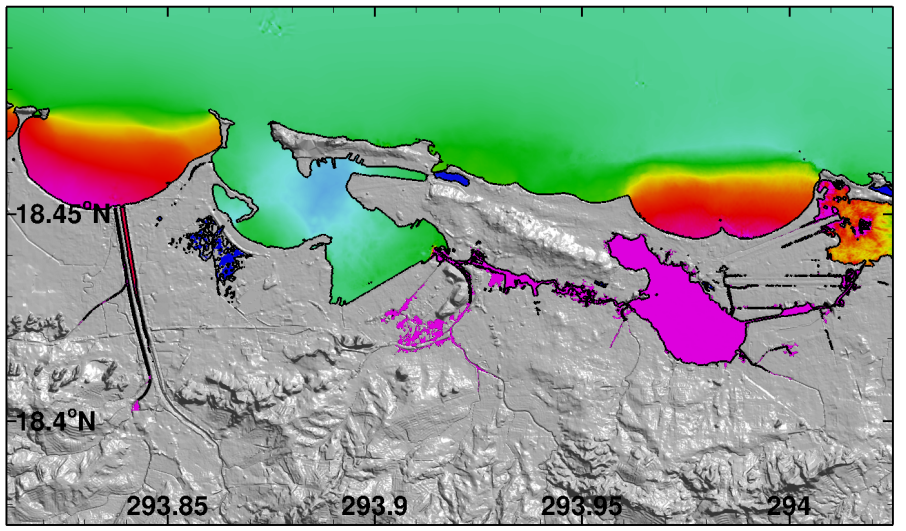

(b)

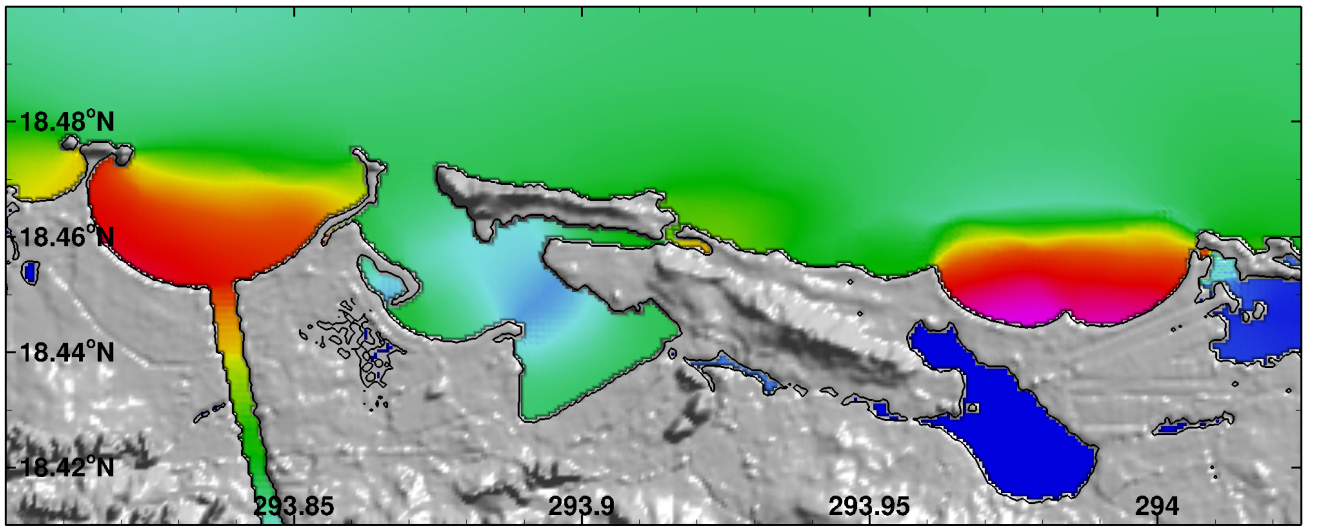

(c)

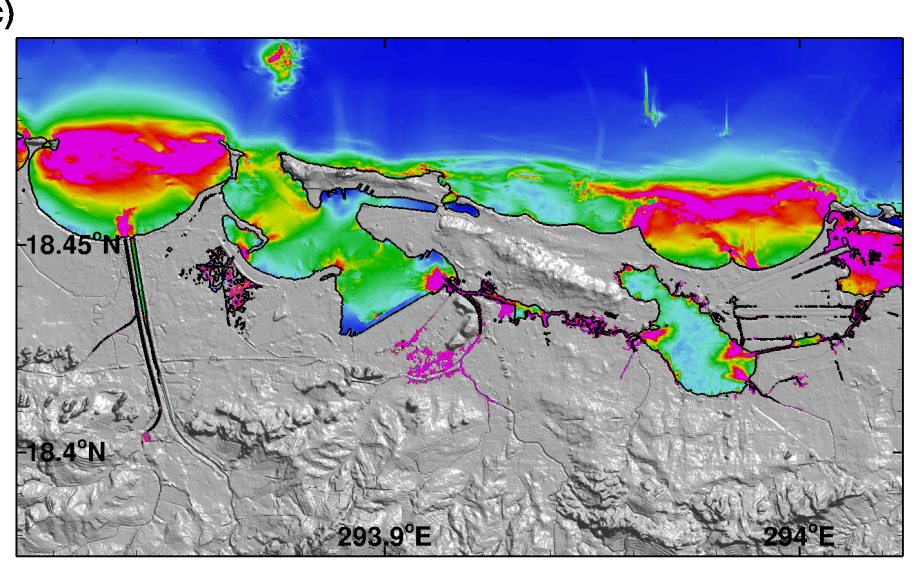

(d)

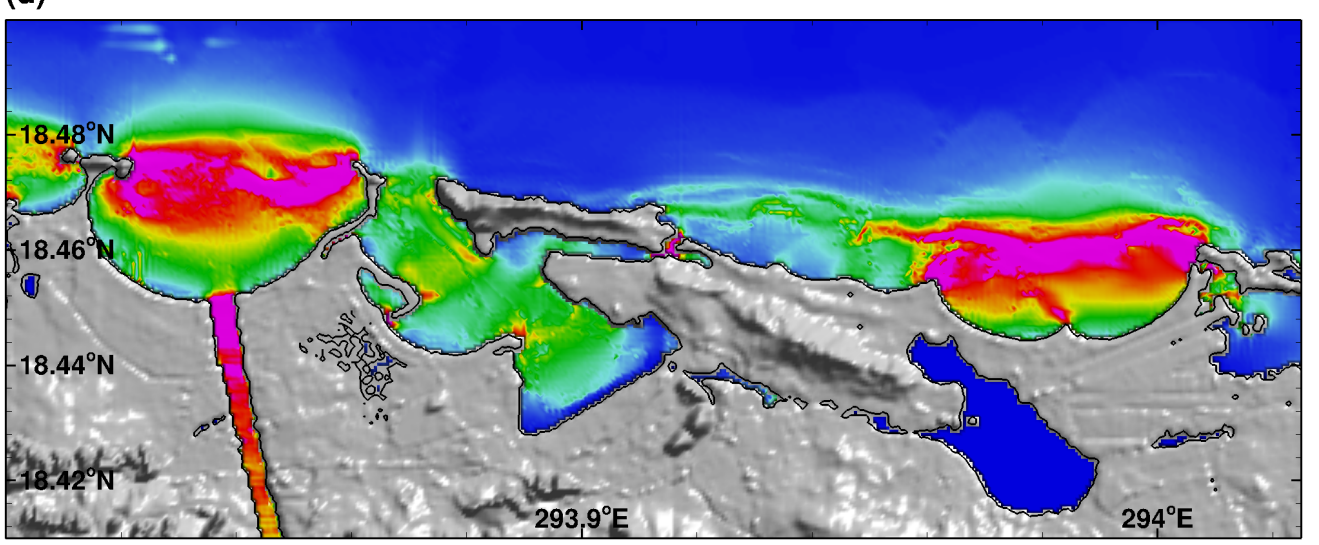

Water level (m)
or flow speed (m/s)

0 0.05 0.1 0.15 0.2 0.25 0.3 0.35 0.4 0.45 0.5

(e)

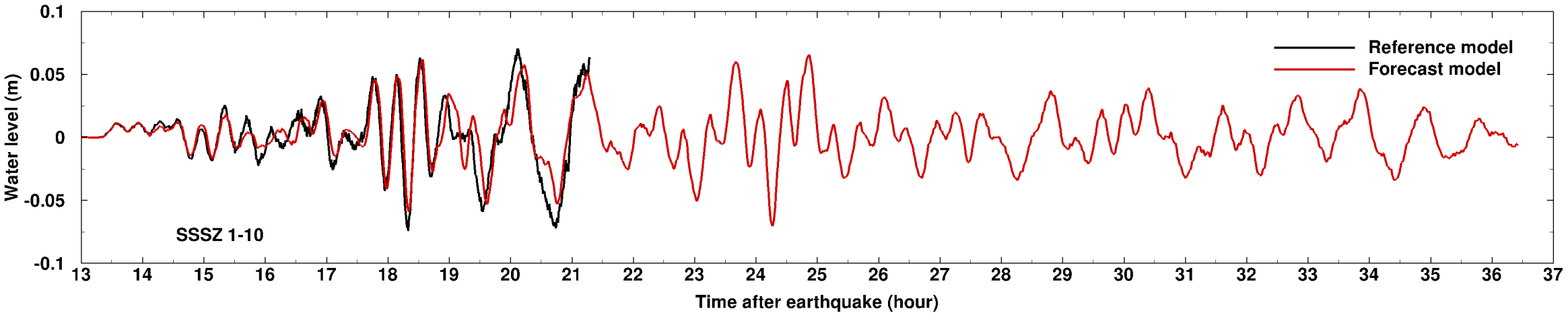

(f)

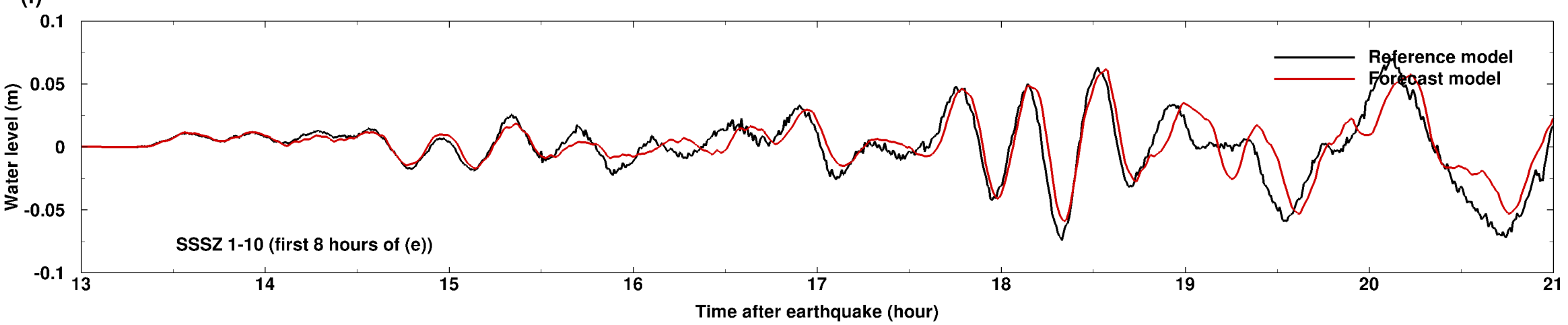

(a)

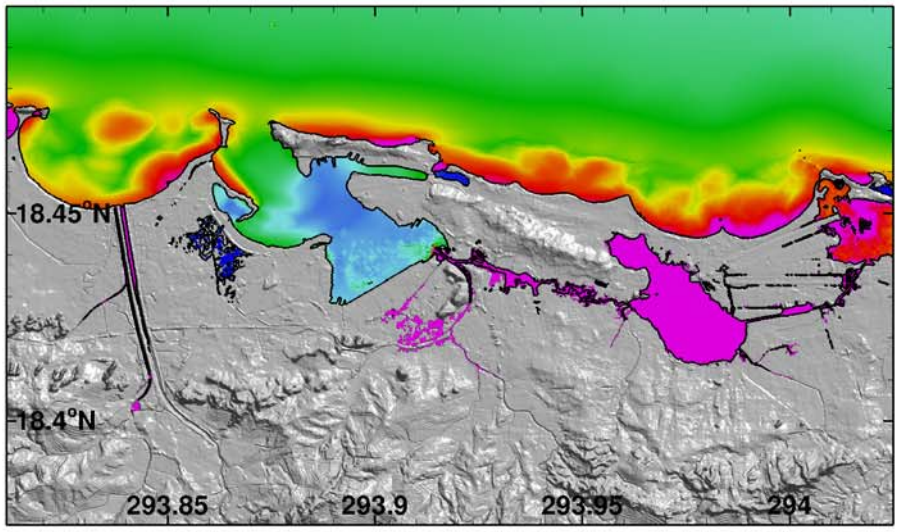
18.45°N
18.4°N
293.85
293.9
293.95
294

(b)

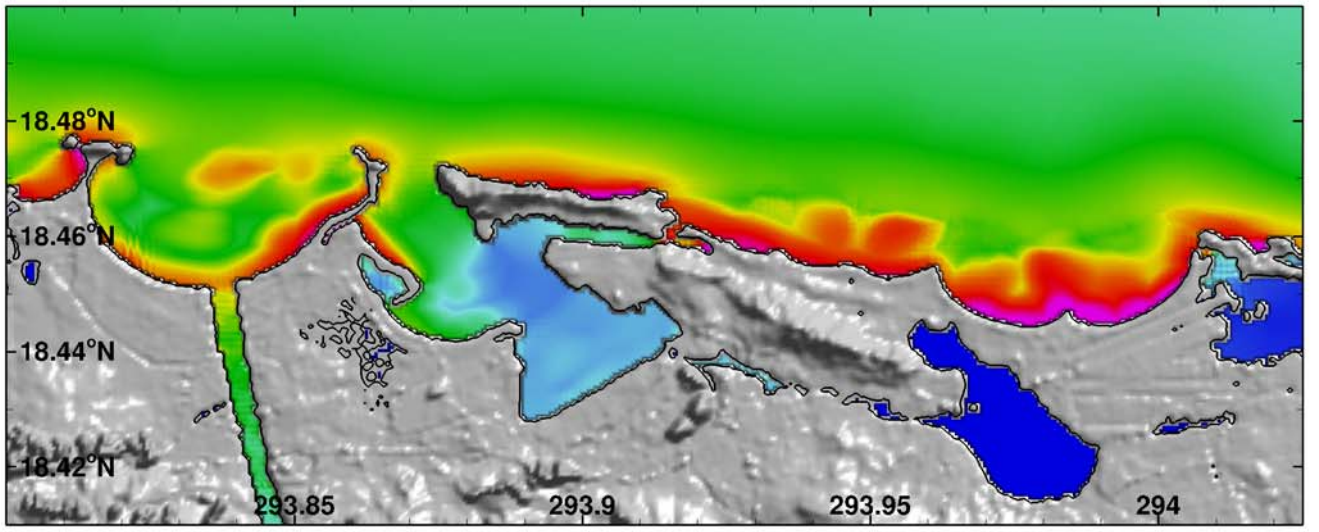
18.48°N
18.46°N
18.44°N
18.42°N
293.85
293.9
293.95
294

(c)

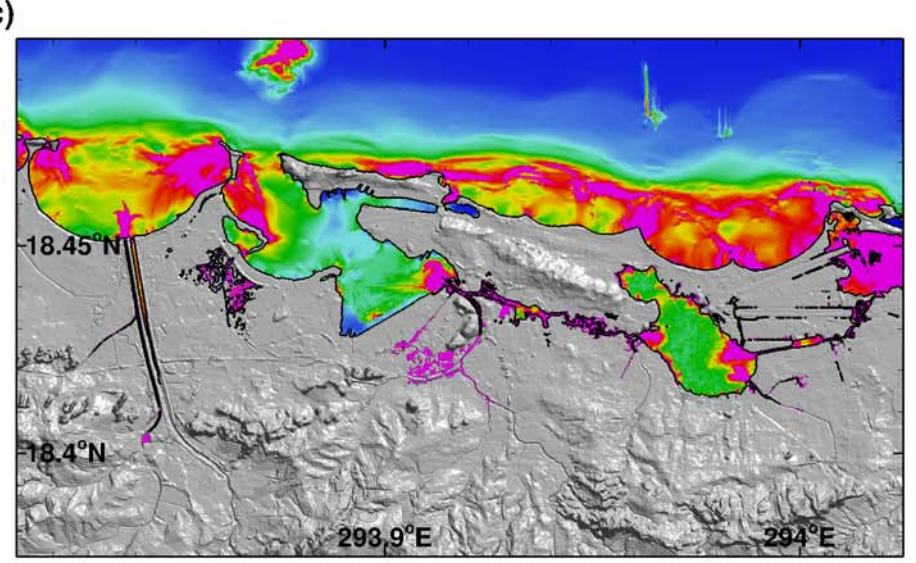
18.45°N
18.4°N
293.9°E
294°E

(d)

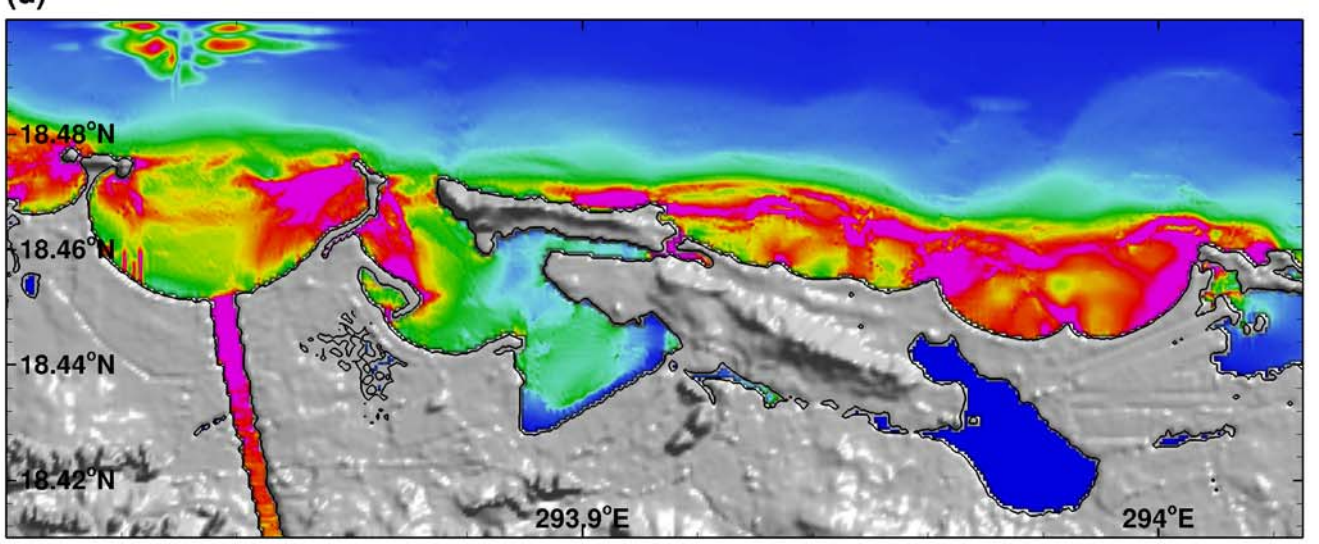
18.48°N
18.46°N
18.44°N
18.42°N
293.9°E
294°E

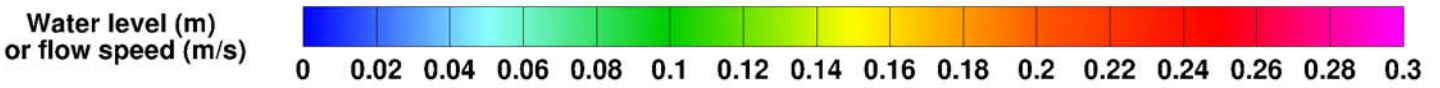
Water level (m)
or flow speed (m/s)
0
0.02
0.04
0.06
0.08
0.1
0.12
0.14
0.16
0.18
0.2
0.22
0.24
0.26
0.28
0.3

(e)

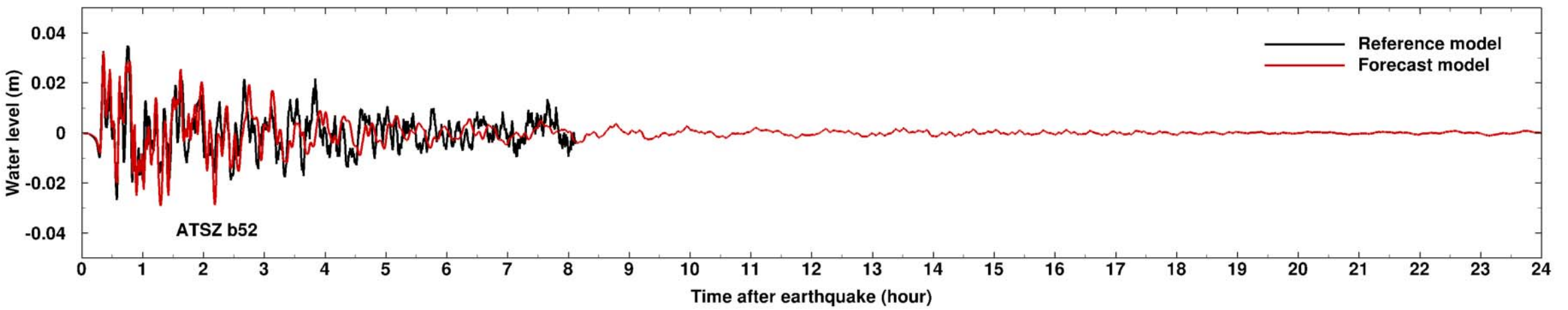
Water level (m)
0.04
0.02
0
-0.02
-0.04
Reference model
Forecast model
ATSZ b52
0
1
2
3
4
5
6
7
8
9
10
11
12
13
14
15
16
17
18
19
20
21
22
23
24
Time after earthquake (hour)

(f)

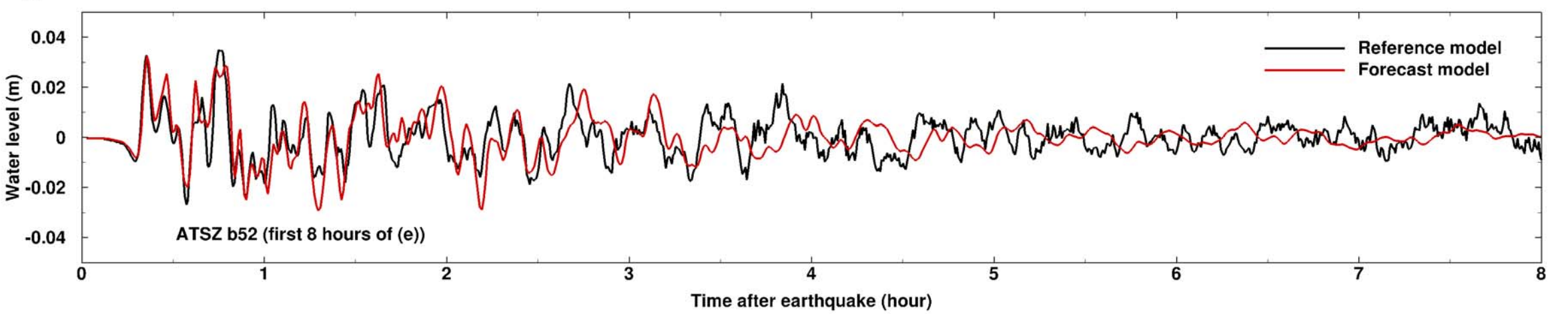
Water level (m)
0.04
0.02
0
-0.02
-0.04
Reference model
Forecast model
ATSZ b52 (first 8 hours of (e))
0
1
2
3
4
5
6
7
8
Time after earthquake (hour)

(a)

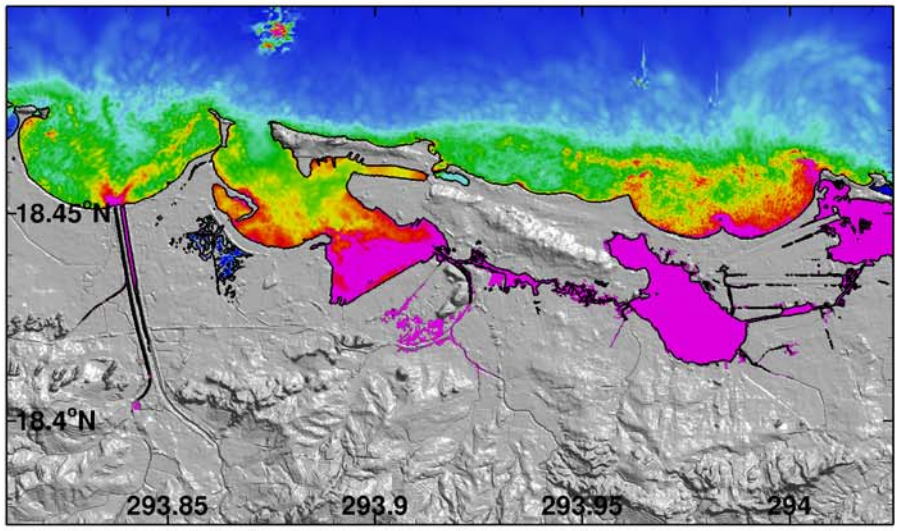

(b)

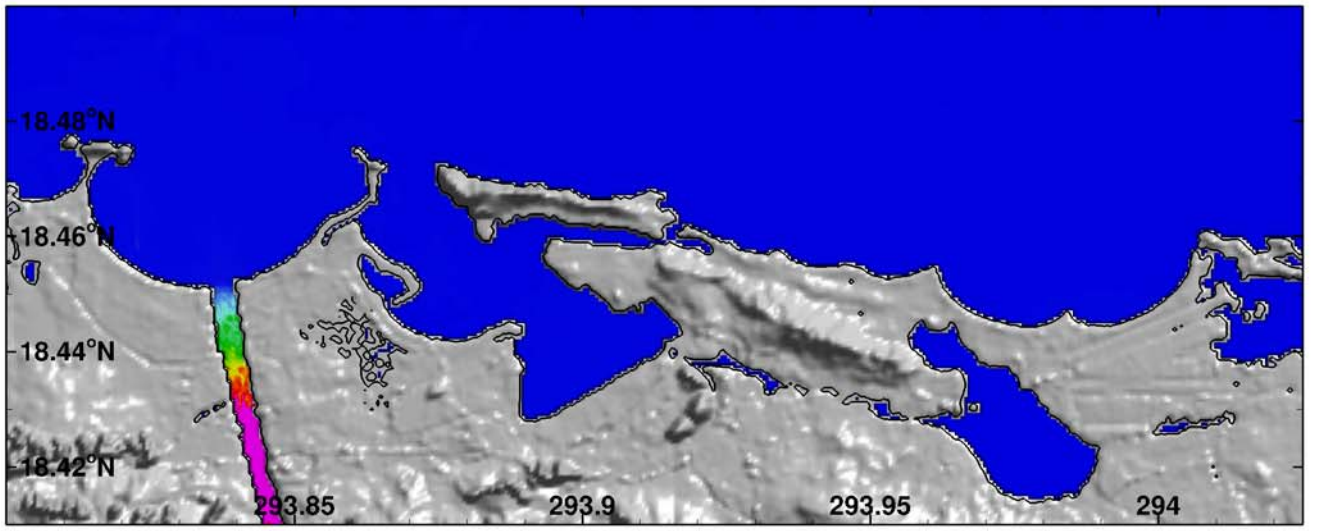

(c)

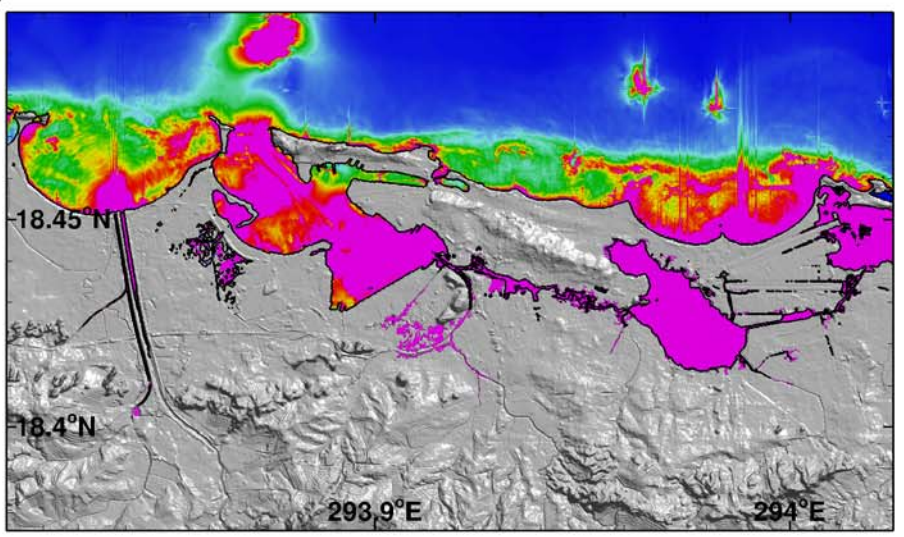

(d)

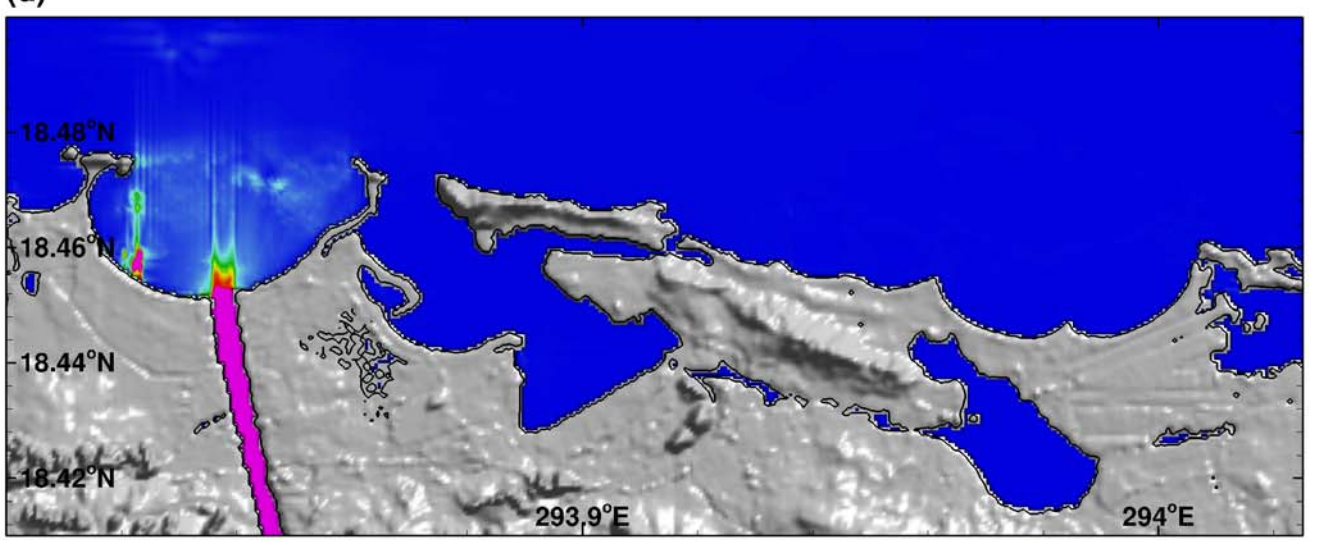

Water level (m)
or flow speed (m/s)

(e)

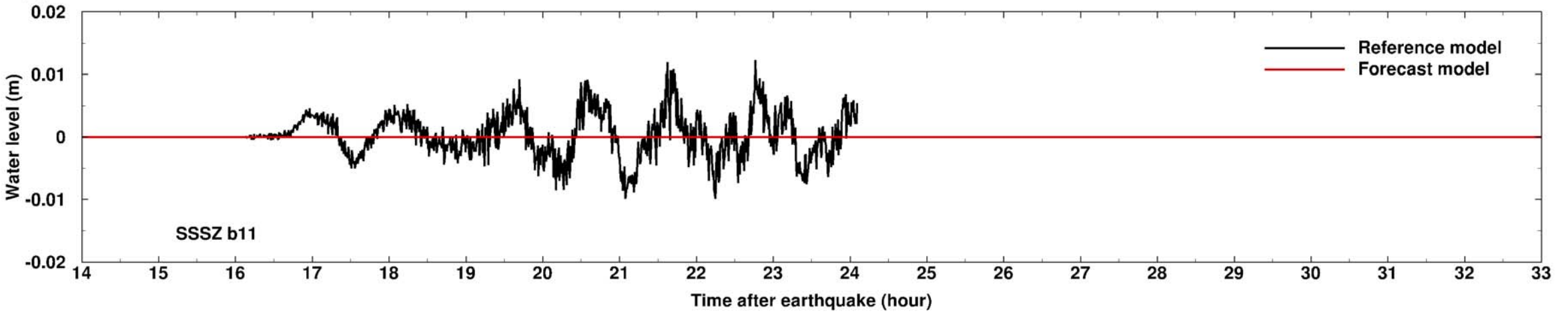

(f)

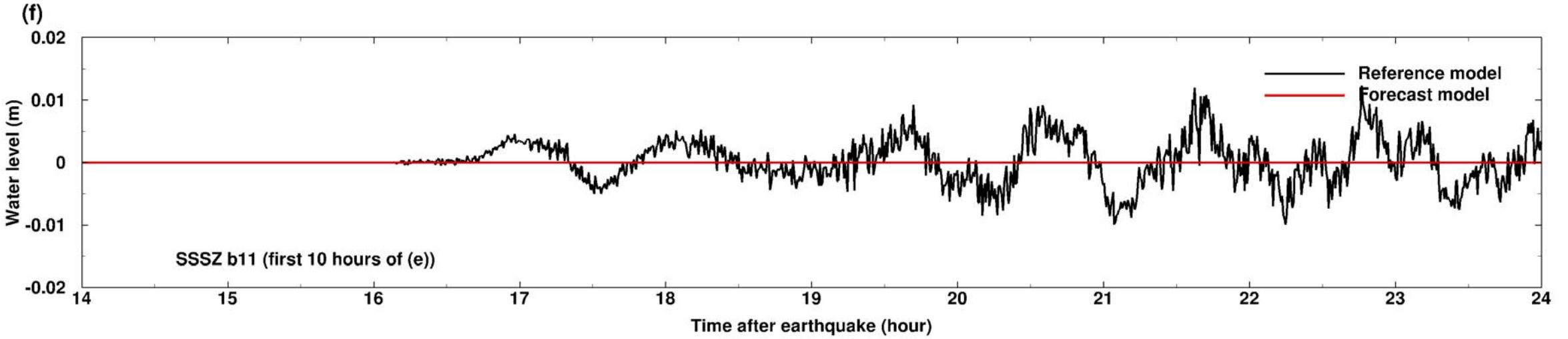

Maximum Tsunami Water Level

Maximum Tsunami Flow Speed

(a)

n^2 = 0.0001

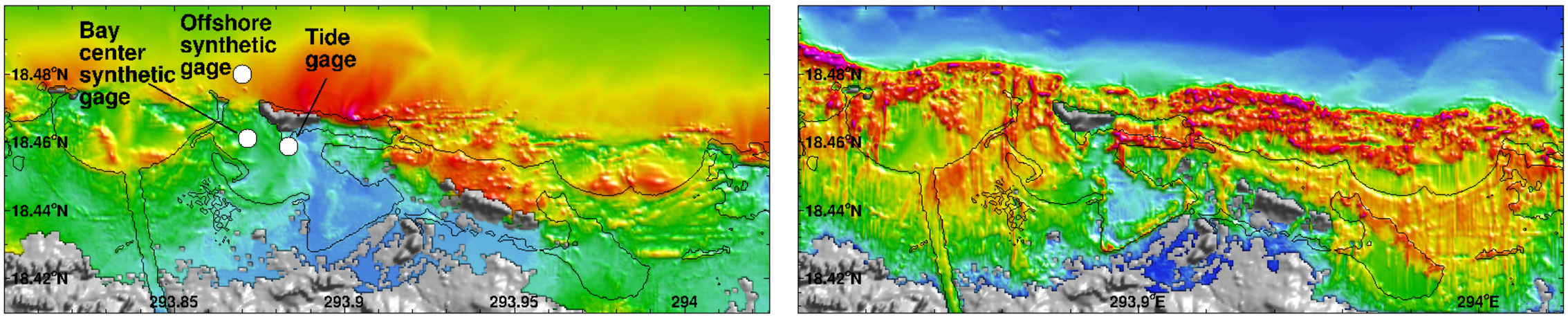

(b)

n^2 = 0.0004

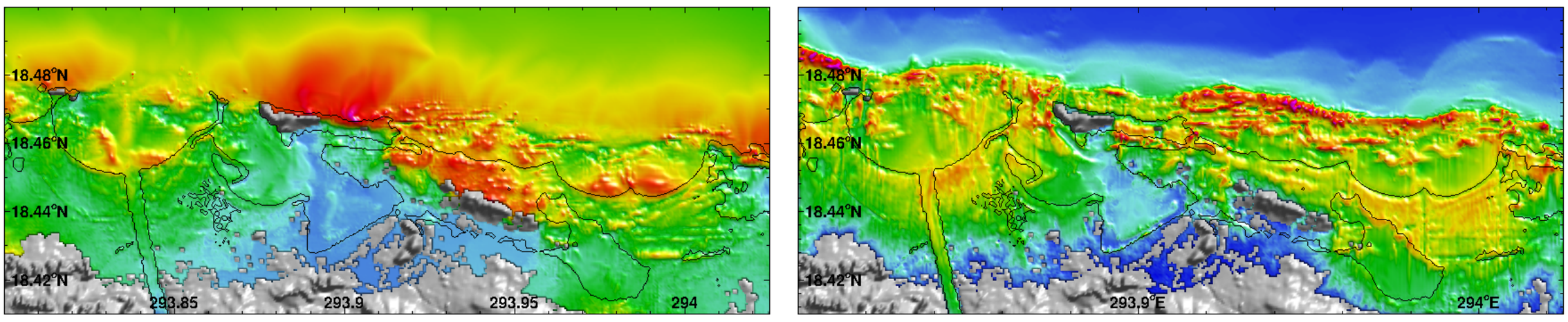

(c)

n^2 = 0.0009

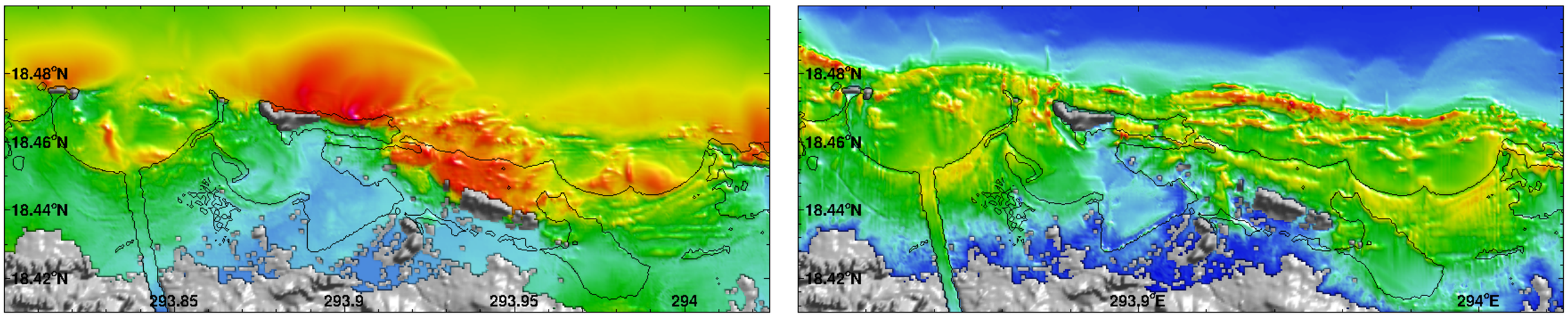

(d)

n^2 = 0.0016

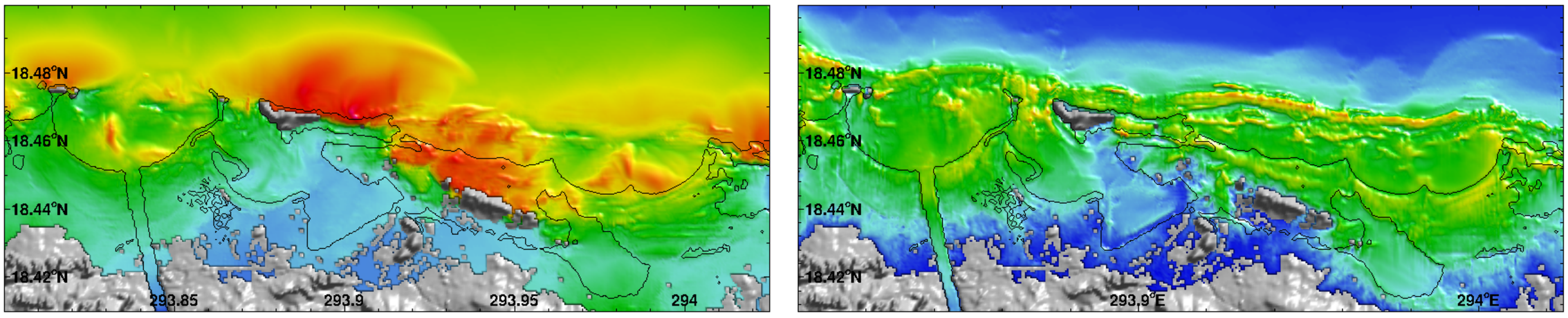

Water level (m) or flow speed (m/s)

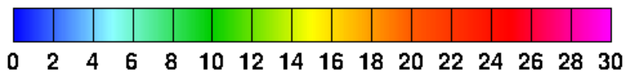

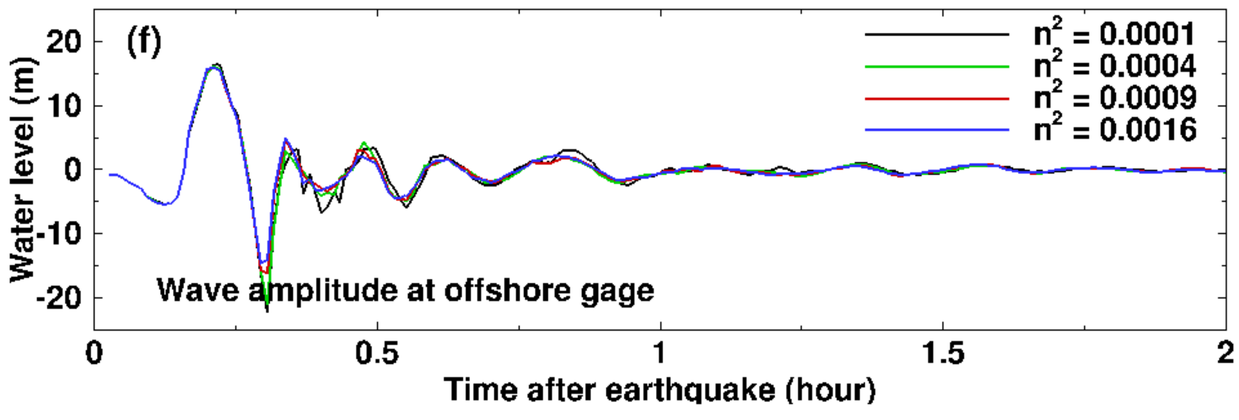

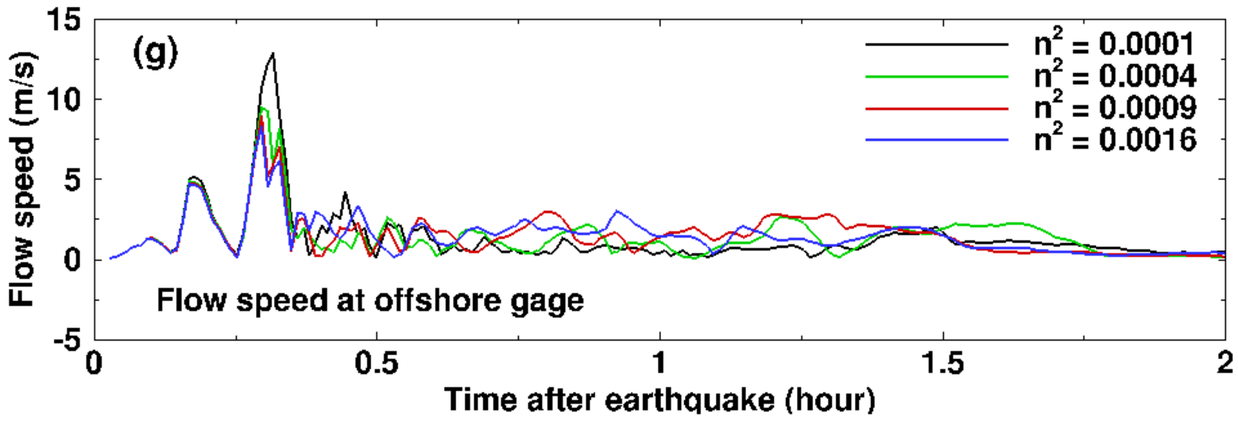

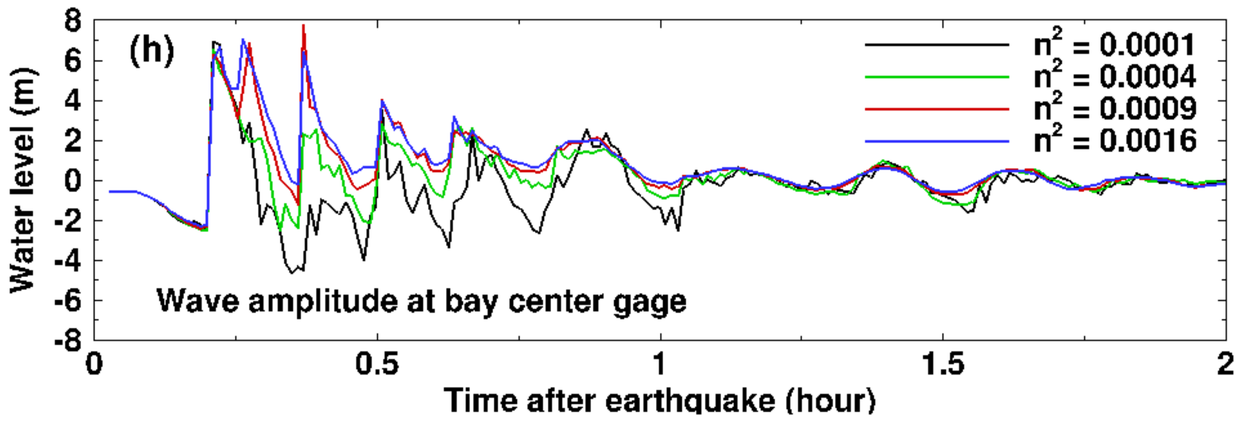

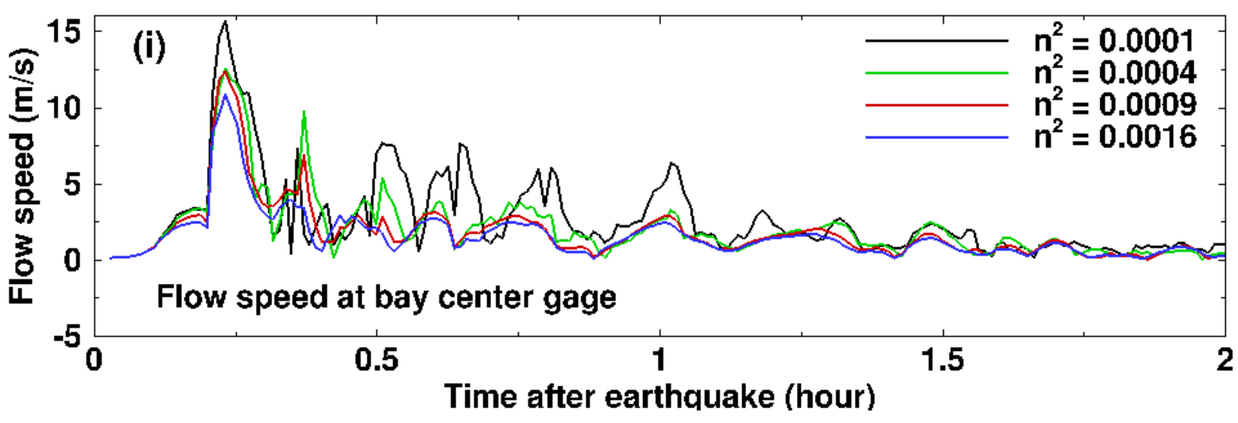

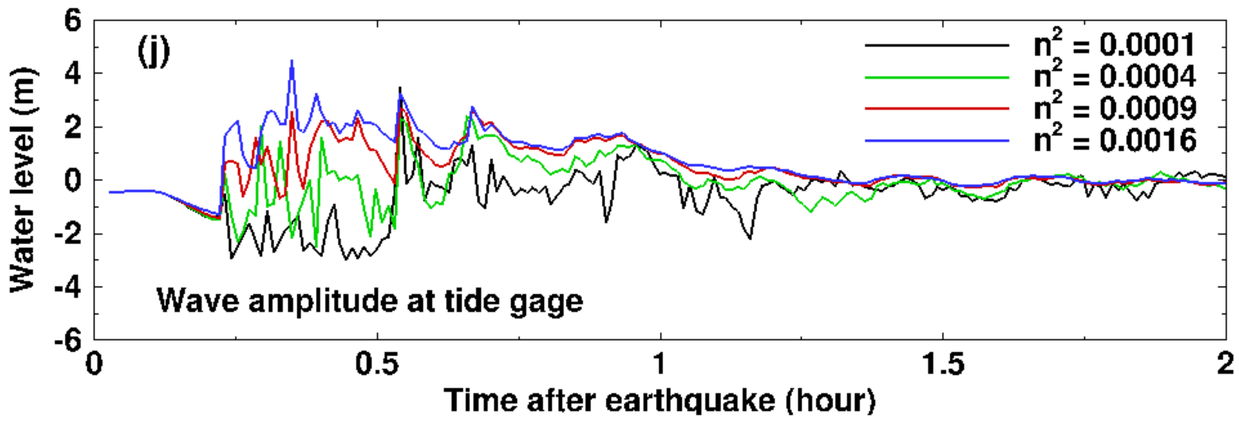

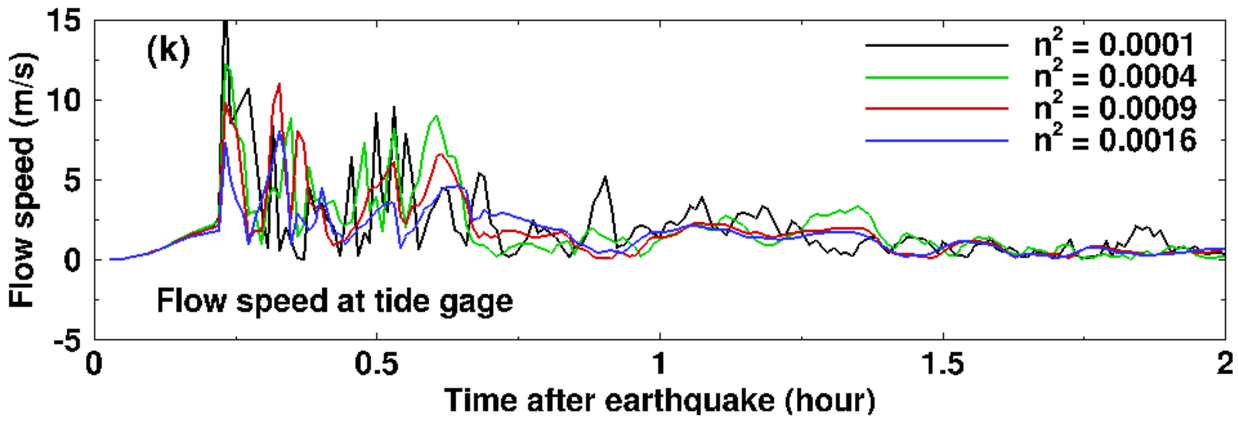

Tables

Table 1. Historical tsunami events that have affected Puerto Rico (data source: NGDC)

Event	Date, Time (UTC), Epicenter	Magnitude	Maximum reported water level (cm) at San Juan
1755 Lisbon	01 Nov. 10:16:00, 36.0ºN 11.0ºW	8.5 – 9.0	-
1867 Virgin Islands	18 November 18.1ºN 65.1ºW	7.5	0.9 – 1.5
1868 Virgin Islands	17 March 17:11:37 18.1ºN 65.1ºW	?	-
1918 Mona Passage	11 Oct. 11:14:14 18.5ºN 67.5ºW	7.3	110
1946 Dominican Republic	4 August 17:51:06 19.3ºN 68.9ºW	7.8	66
1946 Dominican Republic	8 August 13:28:00 19.71ºN 69.51ºW	7.4	60 (include both tides and tsunami)
1989 Mona Passage	1 Nov. 10:25:52 18.986ºN 68.833ºW	4.4	-
1991 Costa Rica	22 April 21:56:51.8 9.685ºN 83.073ºW	7.6	-
2004 Sumatra	26 Dec 00:58:53.4 3.295ºN 5.982ºE	9.0 - 9.3	2

Table 2: MOST setup parameters for reference and forecast models for San Juan, Puerto Rico.

		Reference Model				Forecast Model			
Grid	Region	Coverage Lat. [ºN] Lon. [ºW]	Cell Size [“]	nx x ny	Time Step [sec]	Coverage Lat. [ºX] Lon. [ºX]	Cell Size [“]	nx x ny	Time Step [sec]
A	Caribbean Sea	16.05 – 18.95 69.9 – 60.504014	20”	1614 × 523	2.3	16.5 – 18.95 69.0 – 61.008115	47.24”	610 × 197	4.8
B	Puerto Rico	17.8-18.6 67.4 – 65.2	6”	1321 × 481	0.8	17.8-18.6 67.35 – 65.55	12”	541 × 241	1.6
C	San Juan	18.375-18.5 66.188889 – 65.975	1/3”	2311 × 1351	0.14	18.4 -18.5 66.2 – 65.975	2”	406 × 181	0.8
Minimum offshore depth [m]				1.0				1.0	
Water depth for dry land [m]				0.1				0.1	
Friction coefficient [n^2]				0.0009				0.0009	
CPU time for 4-hr simulation				~ 490 min				~ 13 min	

Forecast model computations were performed on a single Intel Xeon processor at 3.6 GHz, Dell PowerEdge 1850. Reference model computations were performed using parallel version of MOST model with 12 processors on a Intel Xeon 24-core Dell workstation.

Table 3. Synthetic tsunami events – Atlantic

Sce. No	Scenario Name	Source Zone	Tsunami Source	α (m)
		Mega-tsunami scenario		
1	ATSZ 38-47	Atlantic	A38-A47, A38-A47	25
2	ATSZ 48-57	Atlantic	A48-A57, B48-B57	25
3	ATSZ 58-67	Atlantic	A58-A67, B58-B67	25
4	ATSZ 68-77	Atlantic	A68-A77, B68-B77	25
5	ATSZ 82-91	Atlantic	A82-A91, B82-B91	25
6	SSSZ 1-10	South Sandwich	A1-A10, B1-B10	25
		Mw 7.5 Scenario		
7	ATSZ B52	Atlantic	B52	1
		Micro-tsunami Scenario		
8	SSSZ B11	South Sandwich	B11	0.01

Appendix A.

Development of the San Juan, Puerto Rico, tsunami forecast model occurred prior to parameters changes that were made to reflect modification to the MOST model code. As a result, the input file for running both the optimized tsunami forecast model and the high-resolution reference inundation model in MOST have been updated accordingly. Appendix A1 and A2 provide the updated files for San Juan, Puerto Rico.

Forecast model 1 .in file:

```
0.0001   Minimum amplitude of input offshore wave (m)
1.0  Input minimum depth for offshore (m)
0.1  Input "dry land" depth for inundation (m)
0.0009   Input friction coefficient (n**2)
1    let a and b run up
300.0    blowup limit
0.8  input time step (sec)
108000   input amount of steps
6    Compute "A" arrays every n-th time step, n=
2    Compute "B" arrays every n-th time step, n=
48   Input number of steps between snapshots
0    ...Starting from
1    ...saving grid every n-th node, n=
```

Reference model (MOST V4) .in file for A grid:

```
0.0001 Minimum amplitude of input offshore wave (m)
1.0  Input minimum depth for offshore (m)
0.1   Input "dry land" depth for inundation (m)
0.0009 Input friction coefficient (n**2)
2     Number of grids
2      Interpolation domain for outer domain
2     Inner domain
gridA.nc
gridB.nc
1     Runup flag
2.3   input time step (sec)
18800 input amount of steps
1     Continue after input stops
13   Input number of steps between snapshots
1     ...saving grid every n-th node, n=
1     1=initial deformation
```

Reference model (MOST V4) .in file for B grid:

```
0.0001 Minimum amplitude of input offshore wave (m)
1.0  Input minimum depth for offshore (m)
```

```
0.1   Input "dry land" depth for inundation (m)
0.0009 Input friction coefficient (n**2)
2     Number of grids
2      Interpolation domain for outer domain
2     Inner domain
gridB.nc
gridC.nc
1     Runup flag
0.8   input time step (sec)
54000 input amount of steps
1     Continue after input stops
37   Input number of steps between snapshots
1     ...saving grid every n-th node, n=
1     1=initial deformation
```

Reference model (MOST V4) .in file for C grid:

```
0.0001 Minimum amplitude of input offshore wave (m)
-300  Input minimum depth for offshore (m)
0.1   Input "dry land" depth for inundation (m)
0.0009 Input friction coefficient (n**2)
1     Number of grids
2      Interpolation domain for outer domain
2     Inner domain
gridC.nc
2     Runup flag
0.14   input time step (sec)
206000 input amount of steps
1     Continue after input stops
200   Input number of steps between snapshots
1     ...saving grid every n-th node, n=
1     1=initial deformation
```

Appendix B

Propagation Database: Atlantic Ocean Unit Sources

NOAA Propagation Database presented in this section is the representation of the database as of March, 2013. This database may have been updated since March, 2013.

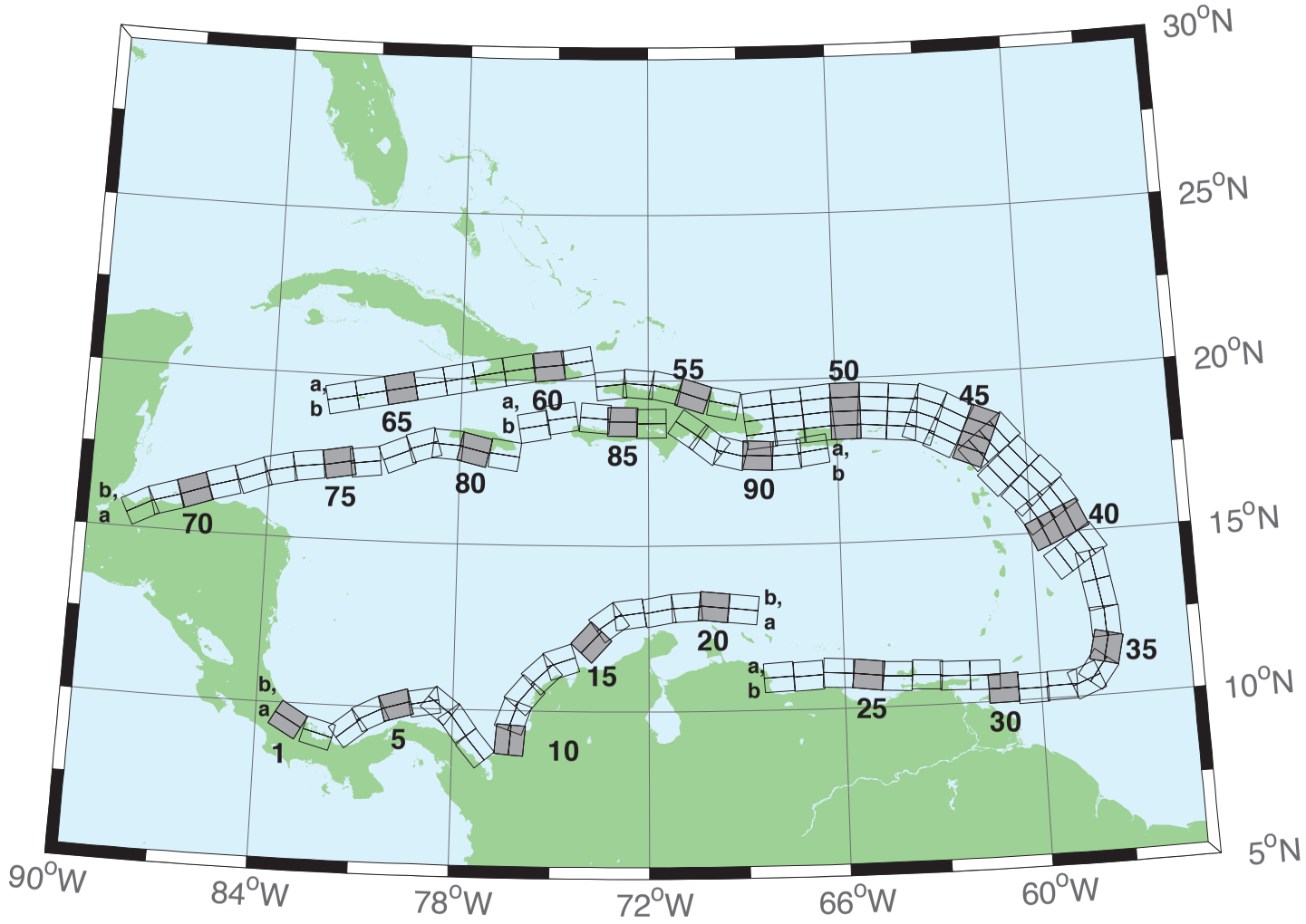

Figure B.1: Atlantic Source Zone unit sources.

Table B.1: Earthquake parameters for Atlantic Source Zone unit sources.

Segment	Description	Longitude(°E)	Latitude(°N)	Strike(°)	Dip(°)	Depth (km)
atsz–1a	Atlantic Source Zone	-83.2020	9.1449	120	27.5	28.09
atsz–1b	Atlantic Source Zone	-83.0000	9.4899	120	27.5	5
atsz–2a	Atlantic Source Zone	-82.1932	8.7408	105.1	27.5	28.09
atsz–2b	Atlantic Source Zone	-82.0880	9.1254	105.1	27.5	5
atsz–3a	Atlantic Source Zone	-80.9172	9.0103	51.31	30	30
atsz–3b	Atlantic Source Zone	-81.1636	9.3139	51.31	30	5
atsz–4a	Atlantic Source Zone	-80.3265	9.4308	63.49	30	30
atsz–4b	Atlantic Source Zone	-80.5027	9.7789	63.49	30	5
atsz–5a	Atlantic Source Zone	-79.6247	9.6961	74.44	30	30
atsz–5b	Atlantic Source Zone	-79.7307	10.0708	74.44	30	5
atsz–6a	Atlantic Source Zone	-78.8069	9.8083	79.71	30	30
atsz–6b	Atlantic Source Zone	-78.8775	10.1910	79.71	30	5
atsz–7a	Atlantic Source Zone	-78.6237	9.7963	127.2	30	30
atsz–7b	Atlantic Source Zone	-78.3845	10.1059	127.2	30	5
atsz–8a	Atlantic Source Zone	-78.1693	9.3544	143.8	30	30
atsz–8b	Atlantic Source Zone	-77.8511	9.5844	143.8	30	5
atsz–9a	Atlantic Source Zone	-77.5913	8.5989	139.9	30	30
atsz–9b	Atlantic Source Zone	-77.2900	8.8493	139.9	30	5
atsz–10a	Atlantic Source Zone	-75.8109	9.0881	4.67	17	19.62
atsz–10b	Atlantic Source Zone	-76.2445	9.1231	4.67	17	5
atsz–11a	Atlantic Source Zone	-75.7406	9.6929	19.67	17	19.62
atsz–11b	Atlantic Source Zone	-76.1511	9.8375	19.67	17	5
atsz–12a	Atlantic Source Zone	-75.4763	10.2042	40.4	17	19.62
atsz–12b	Atlantic Source Zone	-75.8089	10.4826	40.4	17	5
atsz–13a	Atlantic Source Zone	-74.9914	10.7914	47.17	17	19.62
atsz–13b	Atlantic Source Zone	-75.2890	11.1064	47.17	17	5
atsz–14a	Atlantic Source Zone	-74.5666	11.0708	71.68	17	19.62
atsz–14b	Atlantic Source Zone	-74.7043	11.4786	71.68	17	5
atsz–15a	Atlantic Source Zone	-73.4576	11.8012	42.69	17	19.62
atsz–15b	Atlantic Source Zone	-73.7805	12.0924	42.69	17	5
atsz–16a	Atlantic Source Zone	-72.9788	12.3365	54.75	17	19.62
atsz–16b	Atlantic Source Zone	-73.2329	12.6873	54.75	17	5
atsz–17a	Atlantic Source Zone	-72.5454	12.5061	81.96	17	19.62
atsz–17b	Atlantic Source Zone	-72.6071	12.9314	81.96	17	5
atsz–18a	Atlantic Source Zone	-71.6045	12.6174	79.63	17	19.62
atsz–18b	Atlantic Source Zone	-71.6839	13.0399	79.63	17	5
atsz–19a	Atlantic Source Zone	-70.7970	12.7078	86.32	17	19.62
atsz–19b	Atlantic Source Zone	-70.8253	13.1364	86.32	17	5
atsz–20a	Atlantic Source Zone	-70.0246	12.7185	95.94	17	19.62
atsz–20b	Atlantic Source Zone	-69.9789	13.1457	95.94	17	5
atsz–21a	Atlantic Source Zone	-69.1244	12.6320	95.94	17	19.62
atsz–21b	Atlantic Source Zone	-69.0788	13.0592	95.94	17	5
atsz–22a	Atlantic Source Zone	-68.0338	11.4286	266.9	15	17.94
atsz–22b	Atlantic Source Zone	-68.0102	10.9954	266.9	15	5
atsz–23a	Atlantic Source Zone	-67.1246	11.4487	266.9	15	17.94
atsz–23b	Atlantic Source Zone	-67.1010	11.0155	266.9	15	5
atsz–24a	Atlantic Source Zone	-66.1656	11.5055	273.3	15	17.94
atsz–24b	Atlantic Source Zone	-66.1911	11.0724	273.3	15	5
atsz–25a	Atlantic Source Zone	-65.2126	11.4246	276.4	15	17.94
atsz–25b	Atlantic Source Zone	-65.2616	10.9934	276.4	15	5
atsz–26a	Atlantic Source Zone	-64.3641	11.3516	272.9	15	17.94
atsz–26b	Atlantic Source Zone	-64.3862	10.9183	272.9	15	5
atsz–27a	Atlantic Source Zone	-63.4472	11.3516	272.9	15	17.94

Continued on next page

Table B.1 – continued from previous page

Segment	Description	Longitude(°E)	Latitude(°N)	Strike(°)	Dip(°)	Depth (km)
atsz–27b	Atlantic Source Zone	-63.4698	10.9183	272.9	15	5
atsz–28a	Atlantic Source Zone	-62.6104	11.2831	271.1	15	17.94
atsz–28b	Atlantic Source Zone	-62.6189	10.8493	271.1	15	5
atsz–29a	Atlantic Source Zone	-61.6826	11.2518	271.6	15	17.94
atsz–29b	Atlantic Source Zone	-61.6947	10.8181	271.6	15	5
atsz–30a	Atlantic Source Zone	-61.1569	10.8303	269	15	17.94
atsz–30b	Atlantic Source Zone	-61.1493	10.3965	269	15	5
atsz–31a	Atlantic Source Zone	-60.2529	10.7739	269	15	17.94
atsz–31b	Atlantic Source Zone	-60.2453	10.3401	269	15	5
atsz–32a	Atlantic Source Zone	-59.3510	10.8123	269	15	17.94
atsz–32b	Atlantic Source Zone	-59.3734	10.3785	269	15	5
atsz–33a	Atlantic Source Zone	-58.7592	10.8785	248.6	15	17.94
atsz–33b	Atlantic Source Zone	-58.5984	10.4745	248.6	15	5
atsz–34a	Atlantic Source Zone	-58.5699	11.0330	217.2	15	17.94
atsz–34b	Atlantic Source Zone	-58.2179	10.7710	217.2	15	5
atsz–35a	Atlantic Source Zone	-58.3549	11.5300	193.7	15	17.94
atsz–35b	Atlantic Source Zone	-57.9248	11.4274	193.7	15	5
atsz–36a	Atlantic Source Zone	-58.3432	12.1858	177.7	15	17.94
atsz–36b	Atlantic Source Zone	-57.8997	12.2036	177.7	15	5
atsz–37a	Atlantic Source Zone	-58.4490	12.9725	170.7	15	17.94
atsz–37b	Atlantic Source Zone	-58.0095	13.0424	170.7	15	5
atsz–38a	Atlantic Source Zone	-58.6079	13.8503	170.2	15	17.94
atsz–38b	Atlantic Source Zone	-58.1674	13.9240	170.2	15	5
atsz–39a	Atlantic Source Zone	-58.6667	14.3915	146.8	15	17.94
atsz–39b	Atlantic Source Zone	-58.2913	14.6287	146.8	15	5
atsz–39y	Atlantic Source Zone	-59.4168	13.9171	146.8	15	43.82
atsz–39z	Atlantic Source Zone	-59.0415	14.1543	146.8	15	30.88
atsz–40a	Atlantic Source Zone	-59.1899	15.2143	156.2	15	17.94
atsz–40b	Atlantic Source Zone	-58.7781	15.3892	156.2	15	5
atsz–40y	Atlantic Source Zone	-60.0131	14.8646	156.2	15	43.82
atsz–40z	Atlantic Source Zone	-59.6012	15.0395	156.2	15	30.88
atsz–41a	Atlantic Source Zone	-59.4723	15.7987	146.3	15	17.94
atsz–41b	Atlantic Source Zone	-59.0966	16.0392	146.3	15	5
atsz–41y	Atlantic Source Zone	-60.2229	15.3177	146.3	15	43.82
atsz–41z	Atlantic Source Zone	-59.8473	15.5582	146.3	15	30.88
atsz–42a	Atlantic Source Zone	-59.9029	16.4535	137	15	17.94
atsz–42b	Atlantic Source Zone	-59.5716	16.7494	137	15	5
atsz–42y	Atlantic Source Zone	-60.5645	15.8616	137	15	43.82
atsz–42z	Atlantic Source Zone	-60.2334	16.1575	137	15	30.88
atsz–43a	Atlantic Source Zone	-60.5996	17.0903	138.7	15	17.94
atsz–43b	Atlantic Source Zone	-60.2580	17.3766	138.7	15	5
atsz–43y	Atlantic Source Zone	-61.2818	16.5177	138.7	15	43.82
atsz–43z	Atlantic Source Zone	-60.9404	16.8040	138.7	15	30.88
atsz–44a	Atlantic Source Zone	-61.1559	17.8560	141.1	15	17.94
atsz–44b	Atlantic Source Zone	-60.8008	18.1286	141.1	15	5
atsz–44y	Atlantic Source Zone	-61.8651	17.3108	141.1	15	43.82
atsz–44z	Atlantic Source Zone	-61.5102	17.5834	141.1	15	30.88
atsz–45a	Atlantic Source Zone	-61.5491	18.0566	112.8	15	17.94
atsz–45b	Atlantic Source Zone	-61.3716	18.4564	112.8	15	5
atsz–45y	Atlantic Source Zone	-61.9037	17.2569	112.8	15	43.82
atsz–45z	Atlantic Source Zone	-61.7260	17.6567	112.8	15	30.88
atsz–46a	Atlantic Source Zone	-62.4217	18.4149	117.9	15	17.94
atsz–46b	Atlantic Source Zone	-62.2075	18.7985	117.9	15	5
atsz–46y	Atlantic Source Zone	-62.8493	17.6477	117.9	15	43.82
atsz–46z	Atlantic Source Zone	-62.6352	18.0313	117.9	15	30.88

Continued on next page

Table B.1 – continued from previous page

Segment	Description	Longitude(°E)	Latitude(°N)	Strike(°)	Dip(°)	Depth (km)
atsz–47a	Atlantic Source Zone	-63.1649	18.7844	110.5	20	22.1
atsz–47b	Atlantic Source Zone	-63.0087	19.1798	110.5	20	5
atsz–47y	Atlantic Source Zone	-63.4770	17.9936	110.5	20	56.3
atsz–47z	Atlantic Source Zone	-63.3205	18.3890	110.5	20	39.2
atsz–48a	Atlantic Source Zone	-63.8800	18.8870	95.37	20	22.1
atsz–48b	Atlantic Source Zone	-63.8382	19.3072	95.37	20	5
atsz–48y	Atlantic Source Zone	-63.9643	18.0465	95.37	20	56.3
atsz–48z	Atlantic Source Zone	-63.9216	18.4667	95.37	20	39.2
atsz–49a	Atlantic Source Zone	-64.8153	18.9650	94.34	20	22.1
atsz–49b	Atlantic Source Zone	-64.7814	19.3859	94.34	20	5
atsz–49y	Atlantic Source Zone	-64.8840	18.1233	94.34	20	56.3
atsz–49z	Atlantic Source Zone	-64.8492	18.5442	94.34	20	39.2
atsz–50a	Atlantic Source Zone	-65.6921	18.9848	89.59	20	22.1
atsz–50b	Atlantic Source Zone	-65.6953	19.4069	89.59	20	5
atsz–50y	Atlantic Source Zone	-65.6874	18.1407	89.59	20	56.3
atsz–50z	Atlantic Source Zone	-65.6887	18.5628	89.59	20	39.2
atsz–51a	Atlantic Source Zone	-66.5742	18.9484	84.98	20	22.1
atsz–51b	Atlantic Source Zone	-66.6133	19.3688	84.98	20	5
atsz–51y	Atlantic Source Zone	-66.4977	18.1076	84.98	20	56.3
atsz–51z	Atlantic Source Zone	-66.5353	18.5280	84.98	20	39.2
atsz–52a	Atlantic Source Zone	-67.5412	18.8738	85.87	20	22.1
atsz–52b	Atlantic Source Zone	-67.5734	19.2948	85.87	20	5
atsz–52y	Atlantic Source Zone	-67.4781	18.0319	85.87	20	56.3
atsz–52z	Atlantic Source Zone	-67.5090	18.4529	85.87	20	39.2
atsz–53a	Atlantic Source Zone	-68.4547	18.7853	83.64	20	22.1
atsz–53b	Atlantic Source Zone	-68.5042	19.2048	83.64	20	5
atsz–53y	Atlantic Source Zone	-68.3575	17.9463	83.64	20	56.3
atsz–53z	Atlantic Source Zone	-68.4055	18.3658	83.64	20	39.2
atsz–54a	Atlantic Source Zone	-69.6740	18.8841	101.5	20	22.1
atsz–54b	Atlantic Source Zone	-69.5846	19.2976	101.5	20	5
atsz–55a	Atlantic Source Zone	-70.7045	19.1376	108.2	20	22.1
atsz–55b	Atlantic Source Zone	-70.5647	19.5386	108.2	20	5
atsz–56a	Atlantic Source Zone	-71.5368	19.3853	102.6	20	22.1
atsz–56b	Atlantic Source Zone	-71.4386	19.7971	102.6	20	5
atsz–57a	Atlantic Source Zone	-72.3535	19.4838	94.2	20	22.1
atsz–57b	Atlantic Source Zone	-72.3206	19.9047	94.2	20	5
atsz–58a	Atlantic Source Zone	-73.1580	19.4498	84.34	20	22.1
atsz–58b	Atlantic Source Zone	-73.2022	19.8698	84.34	20	5
atsz–59a	Atlantic Source Zone	-74.3567	20.9620	259.7	20	22.1
atsz–59b	Atlantic Source Zone	-74.2764	20.5467	259.7	20	5
atsz–60a	Atlantic Source Zone	-75.2386	20.8622	264.2	15	17.94
atsz–60b	Atlantic Source Zone	-75.1917	20.4306	264.2	15	5
atsz–61a	Atlantic Source Zone	-76.2383	20.7425	260.7	15	17.94
atsz–61b	Atlantic Source Zone	-76.1635	20.3144	260.7	15	5
atsz–62a	Atlantic Source Zone	-77.2021	20.5910	259.9	15	17.94
atsz–62b	Atlantic Source Zone	-77.1214	20.1638	259.9	15	5
atsz–63a	Atlantic Source Zone	-78.1540	20.4189	259	15	17.94
atsz–63b	Atlantic Source Zone	-78.0661	19.9930	259	15	5
atsz–64a	Atlantic Source Zone	-79.0959	20.2498	259.2	15	17.94
atsz–64b	Atlantic Source Zone	-79.0098	19.8236	259.2	15	5
atsz–65a	Atlantic Source Zone	-80.0393	20.0773	258.9	15	17.94
atsz–65b	Atlantic Source Zone	-79.9502	19.6516	258.9	15	5
atsz–66a	Atlantic Source Zone	-80.9675	19.8993	258.6	15	17.94
atsz–66b	Atlantic Source Zone	-80.8766	19.4740	258.6	15	5
atsz–67a	Atlantic Source Zone	-81.9065	19.7214	258.5	15	17.94

Continued on next page

Table B.1 – continued from previous page

Segment	Description	Longitude(°E)	Latitude(°N)	Strike(°)	Dip(°)	Depth (km)
atsz–67b	Atlantic Source Zone	-81.8149	19.2962	258.5	15	5
atsz–68a	Atlantic Source Zone	-87.8003	15.2509	62.69	15	17.94
atsz–68b	Atlantic Source Zone	-88.0070	15.6364	62.69	15	5
atsz–69a	Atlantic Source Zone	-87.0824	15.5331	72.73	15	17.94
atsz–69b	Atlantic Source Zone	-87.2163	15.9474	72.73	15	5
atsz–70a	Atlantic Source Zone	-86.1622	15.8274	70.64	15	17.94
atsz–70b	Atlantic Source Zone	-86.3120	16.2367	70.64	15	5
atsz–71a	Atlantic Source Zone	-85.3117	16.1052	73.7	15	17.94
atsz–71b	Atlantic Source Zone	-85.4387	16.5216	73.7	15	5
atsz–72a	Atlantic Source Zone	-84.3470	16.3820	69.66	15	17.94
atsz–72b	Atlantic Source Zone	-84.5045	16.7888	69.66	15	5
atsz–73a	Atlantic Source Zone	-83.5657	16.6196	77.36	15	17.94
atsz–73b	Atlantic Source Zone	-83.6650	17.0429	77.36	15	5
atsz–74a	Atlantic Source Zone	-82.7104	16.7695	82.35	15	17.94
atsz–74b	Atlantic Source Zone	-82.7709	17.1995	82.35	15	5
atsz–75a	Atlantic Source Zone	-81.7297	16.9003	79.86	15	17.94
atsz–75b	Atlantic Source Zone	-81.8097	17.3274	79.86	15	5
atsz–76a	Atlantic Source Zone	-80.9196	16.9495	82.95	15	17.94
atsz–76b	Atlantic Source Zone	-80.9754	17.3801	82.95	15	5
atsz–77a	Atlantic Source Zone	-79.8086	17.2357	67.95	15	17.94
atsz–77b	Atlantic Source Zone	-79.9795	17.6378	67.95	15	5
atsz–78a	Atlantic Source Zone	-79.0245	17.5415	73.61	15	17.94
atsz–78b	Atlantic Source Zone	-79.1532	17.9577	73.61	15	5
atsz–79a	Atlantic Source Zone	-78.4122	17.5689	94.07	15	17.94
atsz–79b	Atlantic Source Zone	-78.3798	18.0017	94.07	15	5
atsz–80a	Atlantic Source Zone	-77.6403	17.4391	103.3	15	17.94
atsz–80b	Atlantic Source Zone	-77.5352	17.8613	103.3	15	5
atsz–81a	Atlantic Source Zone	-76.6376	17.2984	98.21	15	17.94
atsz–81b	Atlantic Source Zone	-76.5726	17.7278	98.21	15	5
atsz–82a	Atlantic Source Zone	-75.7299	19.0217	260.1	15	17.94
atsz–82b	Atlantic Source Zone	-75.6516	18.5942	260.1	15	5
atsz–83a	Atlantic Source Zone	-74.8351	19.2911	260.8	15	17.94
atsz–83b	Atlantic Source Zone	-74.7621	18.8628	260.8	15	5
atsz–84a	Atlantic Source Zone	-73.6639	19.2991	274.8	15	17.94
atsz–84b	Atlantic Source Zone	-73.7026	18.8668	274.8	15	5
atsz–85a	Atlantic Source Zone	-72.8198	19.2019	270.6	15	17.94
atsz–85b	Atlantic Source Zone	-72.8246	18.7681	270.6	15	5
atsz–86a	Atlantic Source Zone	-71.9143	19.1477	269.1	15	17.94
atsz–86b	Atlantic Source Zone	-71.9068	18.7139	269.1	15	5
atsz–87a	Atlantic Source Zone	-70.4738	18.8821	304.5	15	17.94
atsz–87b	Atlantic Source Zone	-70.7329	18.5245	304.5	15	5
atsz–88a	Atlantic Source Zone	-69.7710	18.3902	308.9	15	17.94
atsz–88b	Atlantic Source Zone	-70.0547	18.0504	308.4	15	5
atsz–89a	Atlantic Source Zone	-69.2635	18.2099	283.9	15	17.94
atsz–89b	Atlantic Source Zone	-69.3728	17.7887	283.9	15	5
atsz–90a	Atlantic Source Zone	-68.5059	18.1443	272.9	15	17.94
atsz–90b	Atlantic Source Zone	-68.5284	17.7110	272.9	15	5
atsz–91a	Atlantic Source Zone	-67.6428	18.1438	267.8	15	17.94
atsz–91b	Atlantic Source Zone	-67.6256	17.7103	267.8	15	5
atsz–92a	Atlantic Source Zone	-66.8261	18.2536	262	15	17.94
atsz–92b	Atlantic Source Zone	-66.7627	17.8240	262	15	5

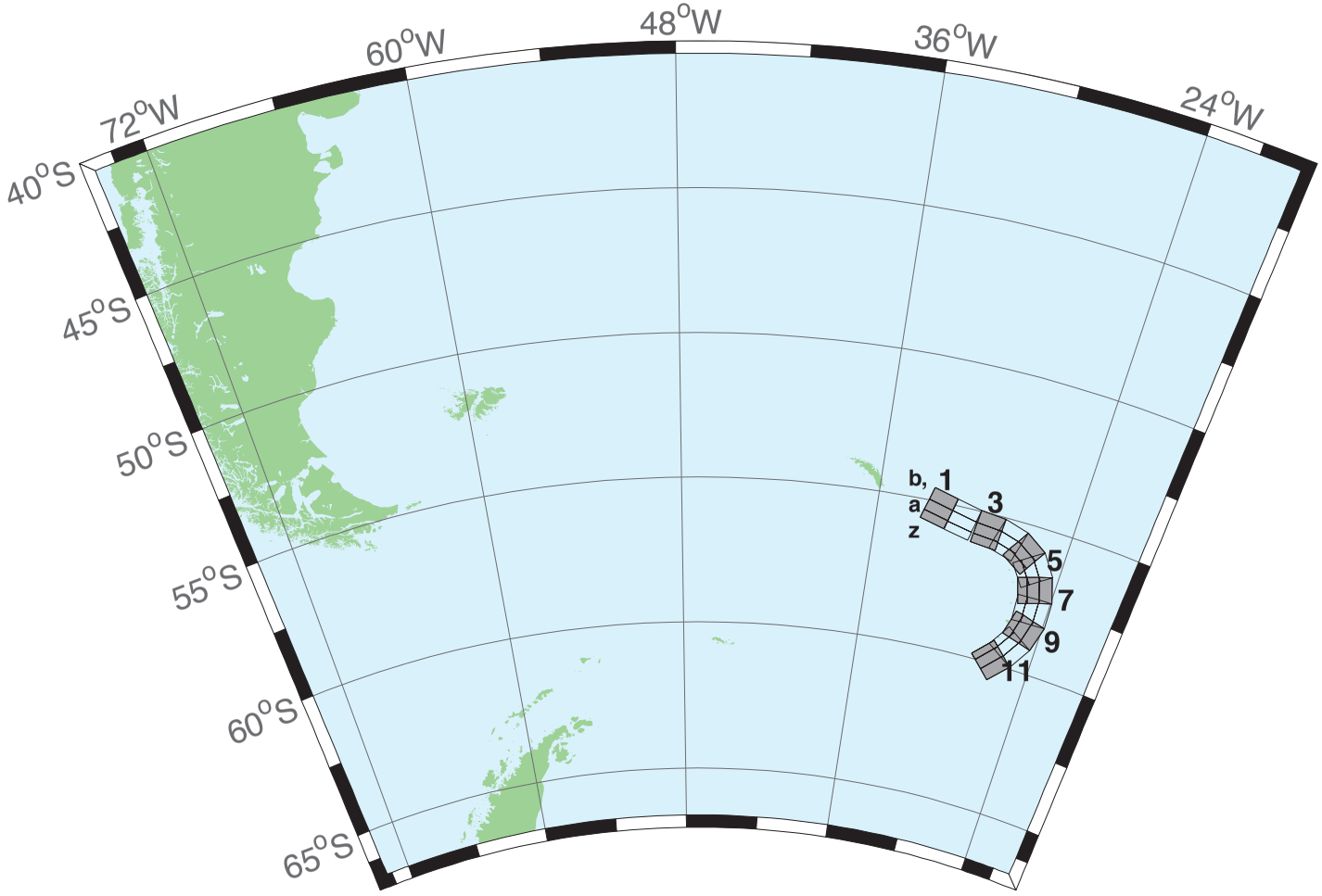

Figure B.2: South Sandwich Islands Subduction Zone.

Appendix C. SIFT Testing Results

Authors: Lindsey Wright, Yong Wei

1.0 PURPOSE

Forecast models are tested with synthetic tsunami events covering a range of tsunami source locations and magnitudes. Testing is also done with selected historical tsunami events when available.

The purpose of forecast model testing is three-fold. The first objective is to assure that the results obtained with the NOAA's tsunami forecast system software, which has been released to the Tsunami Warning Centers for operational use, are consistent with those obtained by the researcher during the development of the forecast model. The second objective is to test the forecast model for consistency, accuracy, time efficiency, and quality of results over a range of possible tsunami locations and magnitudes. The third objective is to identify bugs and issues in need of resolution by the researcher who developed the Forecast Model or by the forecast system software development team before the next version release to NOAA's two Tsunami Warning Centers.

Local hardware and software applications, and tools familiar to the researcher(s), are used to run the Method of Splitting Tsunamis (MOST) model during the forecast model development. The test results presented in this report lend confidence that the model performs as developed and produces the same results when initiated within the forecast system application in an operational setting as those produced by the researcher during the forecast model development. The test results assure those who rely on the San Juan tsunami forecast model that consistent results are produced irrespective of system.

2.0 TESTING PROCEDURE

The general procedure for forecast model testing is to run a set of synthetic tsunami scenarios and a selected set of historical tsunami events through the forecast system application and compare the results with those obtained by the researcher during the forecast model development and presented in the Tsunami Forecast Model Report. Specific steps taken to test the model include:

1. Identification of testing scenarios, including the standard set of synthetic events, appropriate historical events, and customized synthetic scenarios that may have been used by the researcher(s) in developing the forecast model.
2. Creation of new events to represent customized synthetic scenarios used by the researcher(s) in developing the forecast model, if any.
3. Submission of test model runs with the forecast system, and export of the results from A, B, and C grids, along with time series.
4. Recording applicable metadata, including the specific forecast system version used for testing.
5. Examination of forecast model results for instabilities in both time series and plot results.
6. Comparison of forecast model results obtained through the forecast system with those obtained during the forecast model development.
7. Summarization of results with specific mention of quality, consistency, and time efficiency.
8. Reporting of issues identified to modeler and forecast system software development team.
9. Retesting the forecast models in the forecast system when reported issues have been addressed or explained.

Synthetic model runs were tested on a DELL PowerEdge R510 computer equipped with two Xeon E5670 processors at 2.93 Ghz, each with 12 MBytes of cache and 32GB memory. The processors are hex core and support hyperthreading, resulting in the computer performing as a 24 processor core machine. Additionally, the testing computer supports 10 Gigabit Ethernet for fast network connections. This computer configuration is similar or the same as the configurations of the computers installed at the Tsunami Warning Centers so the compute times should only vary slightly.

3.0 Results

The San Juan forecast model was tested with SIFT version 3.2.

The San Juan, Puerto Rico forecast model was tested with three synthetic scenarios. Test results from the forecast system and comparisons with the results obtained during the forecast model development are shown numerically in Table 1 and graphically in Figures 1 to 3. The results show that the minimum and maximum amplitudes and time series obtained from the forecast system agree with those obtained during the forecast model development, and that the forecast model is stable and robust, with consistent and high quality results across geographically distributed tsunami sources. The model run time (wall clock time) was less than 42 minutes for 12 hours of simulation time, and 14.5 minutes for 4.0 hours. This run time is not within the 10 minute run time for 4 hours of simulation time and does not satisfy run time requirements.

A suite of three synthetic events was run on the San Juan forecast model. The modeled scenarios were stable for all cases run with no inconsistencies or ringing. The largest modeled height was 317 centimeters (cm) from the Atlantic (ATSZ 48-57) source zone. The smallest signal of 8 cm was recorded at the far field South Sandwich (SSSZ 1-10) source zone. Maximum and minimum values between the development cases and the forecast system output were mostly consistent in shape and amplitude for all cases run (Table 1). For synthetic scenario ATSZ 48-57, the small difference between the SIFT and development max is caused by different boundaries between SIFT and development to extract boundary conditions from the propagation database for forecast model input. As SIFT currently sets the simulation time to 10 hours for San Juan model, the SIFT Max for synthetic scenario SSSZ 1-10 is 7.8 cm. The max amplitude (8.3 cm) at the tide gage location for SSSZ 1-10 actually occurs at about 12th hour, so was not reported by SIFT. It is verified that the max in the first 10 hours of development run is 7.8 cm, consistent with SIFT Max. Because of this reason, SIFT simulation time for San Juan is reset to 14 hours. The San Juan reference point used for the forecast model development is the same as what is deployed in the forecast system, so the results can be considered valid for the three cases studied.

List of Figures

List of Tables

Source Zone	Tsunami Source	α [m]	SIFT Max (cm)	Development Max (cm)	SIFT Min (cm)	Development Min (cm)
Atlantic	A38-A47, B38-B47	25	43.5	43.5	-35.6	-35.6
Atlantic	A48-A57, B48-B57	25	316.7	305.9	-142.8	-142.8
South Sandwich	A1-A10, B1-B10	25	7.8	7.8 (10h run) 8.25 (24h run)	-8.1	-8.1

Table 1. Table of maximum and minimum amplitudes (cm) at the San Juan, Puerto Rico warning point for synthetic and historical events tested using SIFT 3.2 and obtained during development.

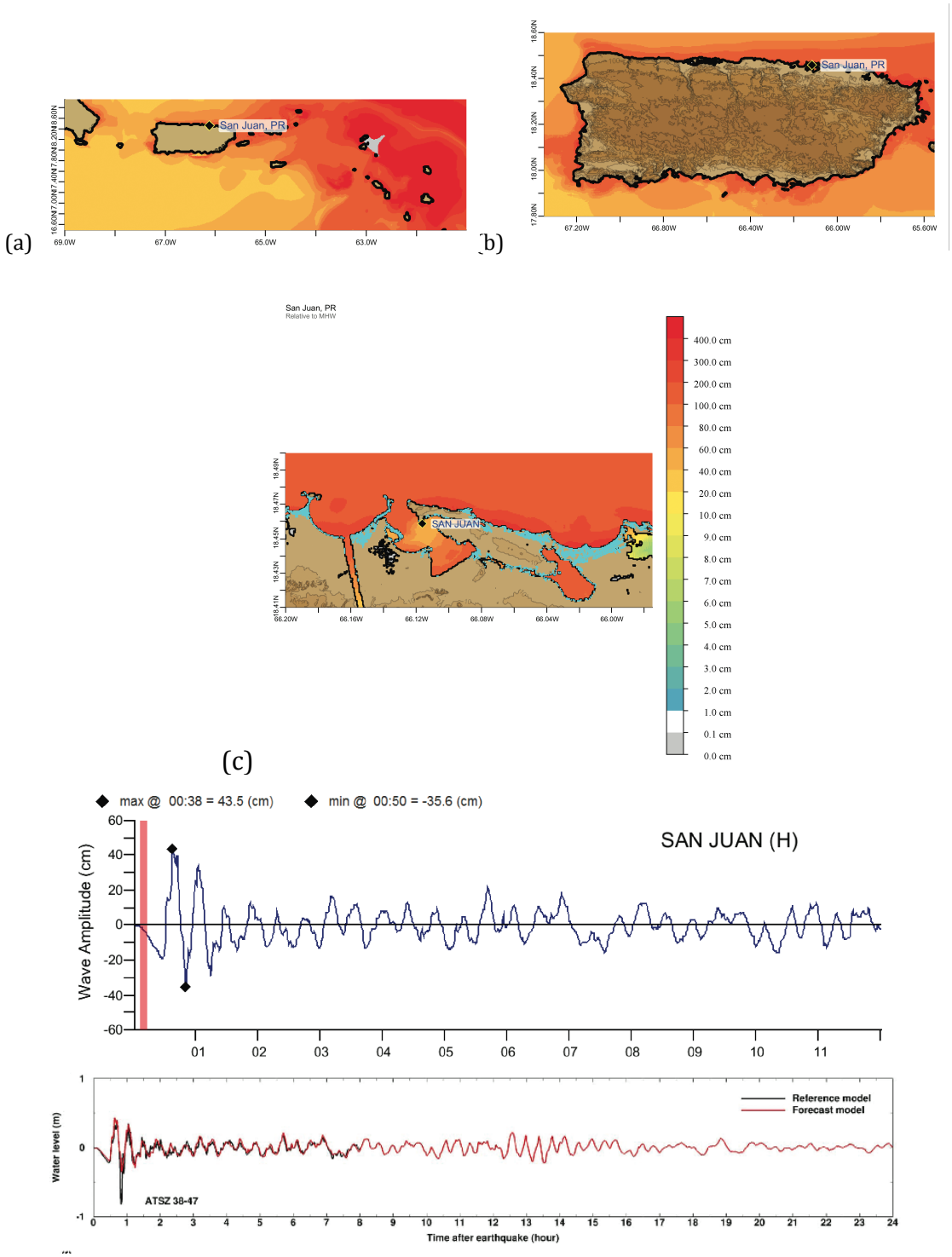

Figure 1: Response of the San Juan forecast model to synthetic scenario ATSZ 38-47 (alpha=25). Maximum computed wave amplitude for (a) A-grid, b) B-grid, and c) C-grid. (d) Time series of wave amplitude at the C-grid warning point obtained from SIFT (e) Time series obtained during model development and is shown for comparison with SIFT test results.

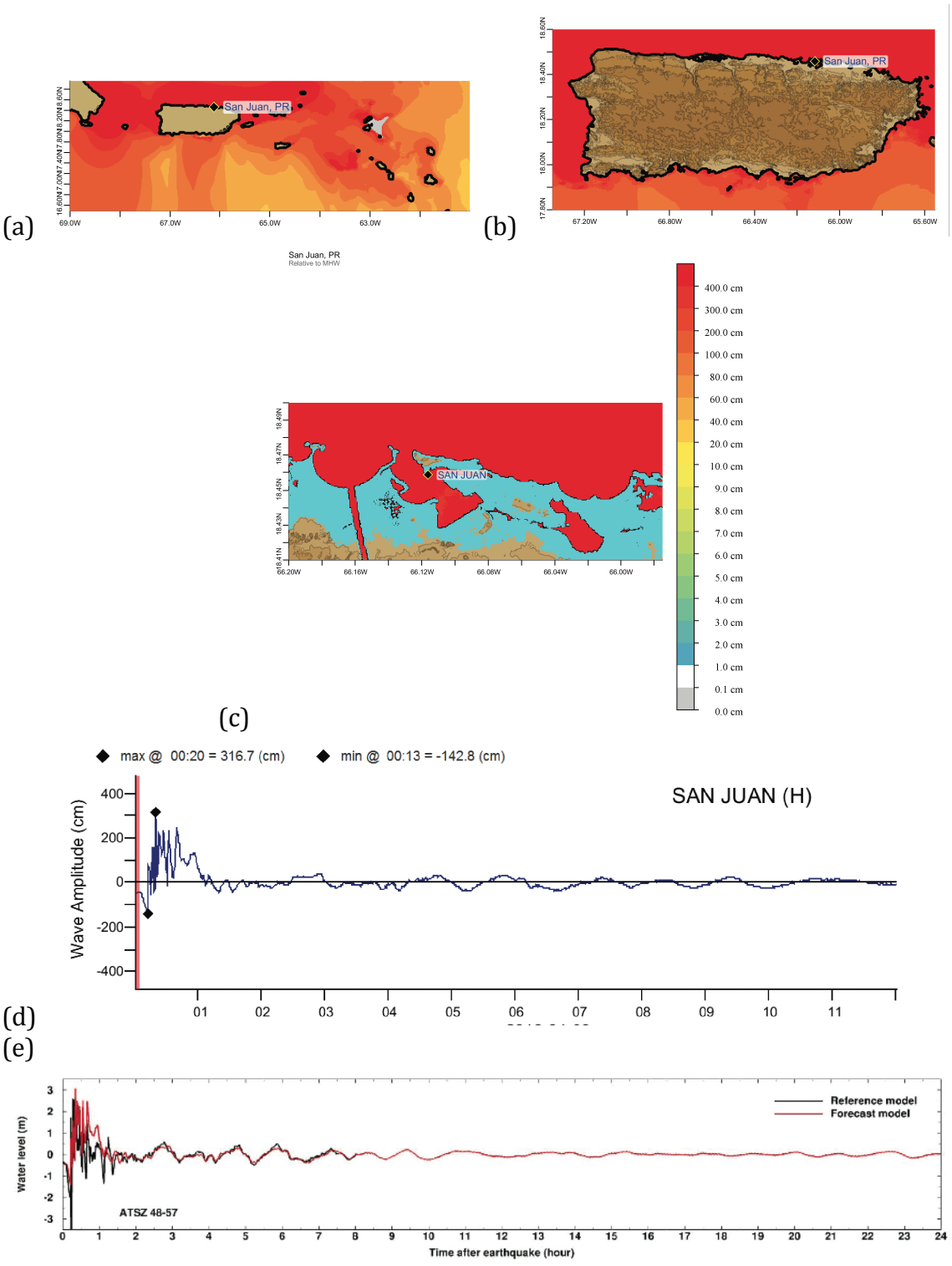

Figure 2: Response of the San Juan forecast model to synthetic scenario ATSZ 48-57 (alpha=25). Maximum computed wave amplitude for (a) A-grid, b) B-grid, and c) C-grid. (d) Time series of wave amplitude at the C-grid warning point obtained from SIFT (e) Time series obtained during model development and is shown for comparison with SIFT test results.

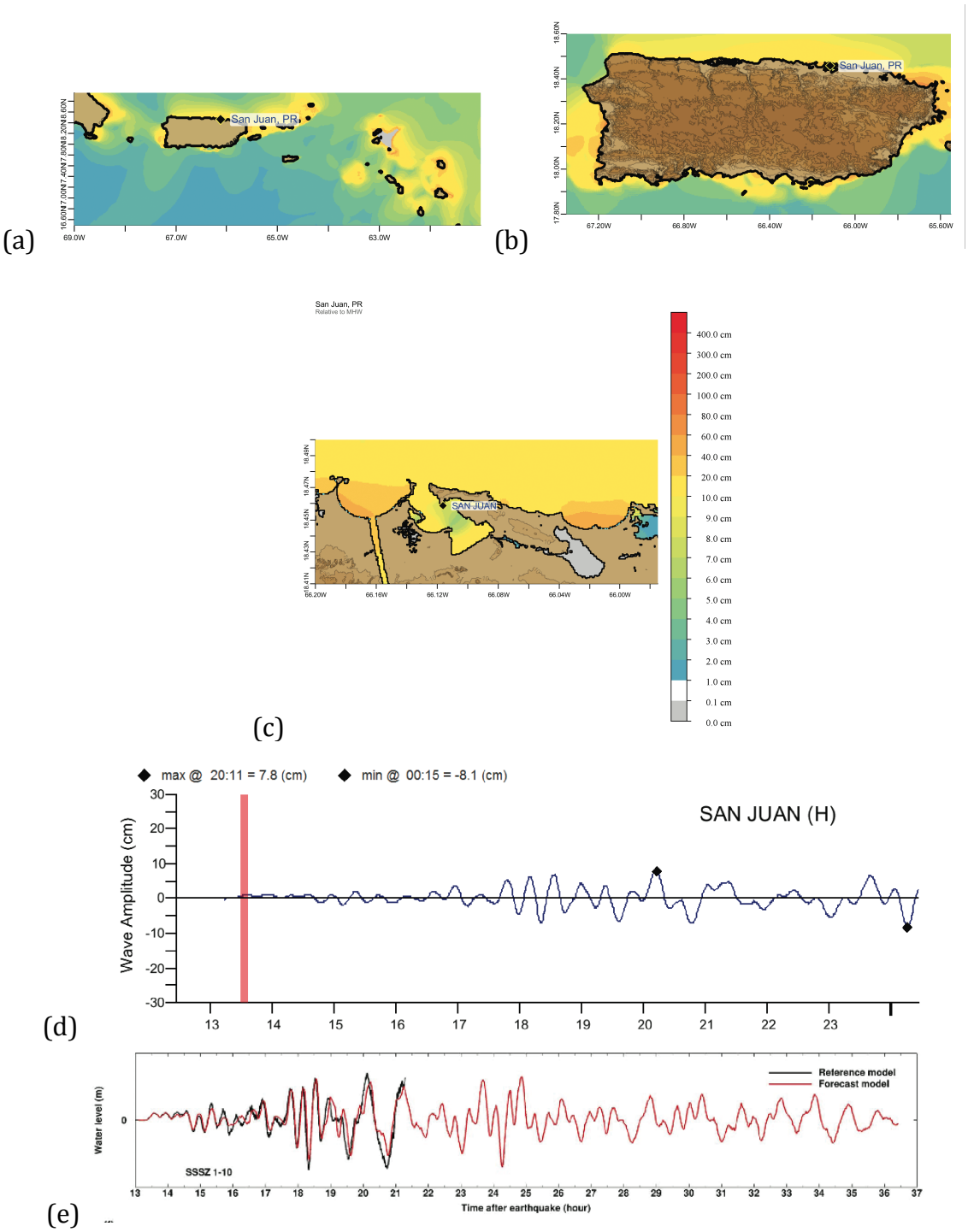

Figure 3: Response of the San Juan forecast model to synthetic scenario SSSZ 1-10 (alpha=25). Maximum computed wave amplitude for (a) A-grid, b) B-grid, and c) C-grid. (d) Time series of wave amplitude at the C-grid warning point obtained from SIFT (e) Time series obtained during model development and is shown for comparison with SIFT test results.